NASA CR-112,237

NASA Contractor Report 172239

Inlet Flowfield Investigation
Part I —Transonic Flowfield Survey

J. A. Yetter
V. Salemann
M. B. Sussman

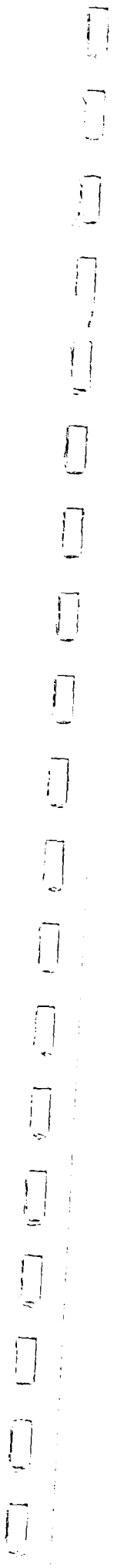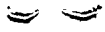Boeing Military Airplane Company
Seattle, Washington 98124

NASA

National Aeronautics and
Space Administration

Langley Research Center
Hampton, Virginia 23665

$N84-15123$

Inlet Flowfield Investigation
Part I—Transonic Flowfield Survey

TABLE OF CONTENTS

LIST OF FIGURES

1.0 SUMMARY

A study was undertaken to establish a data base for the development and validation of analytical codes directed at the analysis of inlet flowfields for advanced supersonic airplanes.

An advanced tactical supercruise fighter study configuration was selected as the vehicle for this program. A model of this configuration, which has been extensively tested for aerodynamic performance and propulsion/aerodynamic interactions was used for transonic flow field surveys and supersonic flow field calculations. A boundary layer survey at supersonic conditions was planned for a propulsion integration test at NASA-Lewis. This report cover the transonic flow field survey. Supersonic flow field computations are reported in Reference 1.

Potential inlet locations were selected in a conceptual design study. A wind tunnel investigation has been conducted to determine the flowfield characteristics in the selected locations. Testing was conducted at the NASA-Langley 16-foot Transonic Tunnel at freestream Mach numbers of 0.6 to 1.20 and angles of attack from 0° to 10°. Inlet flowfield surveys were made at locations representative of wing (upper and lower surface) and forebody mounted inlet concepts. Results are presented in the form of local inlet flowfield angle of attack, sideflow angle, and Mach number contours. Wing surface pressure distributions supplement the flowfield data.

Results showed local angles of attack generally above freestream above the wing and below freestream below the wing. There were large spanwise gradients above the wing at higher angles of attack. For instance, at a Mach number of 0.9 and 10° angle of attack, the local angle of attack over the wing varied from 0° inboard to 20° outboard, while under the wing it varied from 3° inboard to 6° outboard. Sidewash angles varied from $+10^O$ to -20° over the wing due to a leading edge vortex. Wing static pressure measurements confirmed the existence of a leading edge vortex at 10° angle of attack. Below the wing, the sidewash variation was from 5° to 11°. Local Mach numbers varied from .85 to 1.05 over the wing and were near .85 under the wing.

At the forward survey station ahead of the wing, the local angle of attack was about twice the freestream value close to the fuselage, decreasing to near the freestream value at the outboard edge. Sidewash was generally outboard, 2 to 4 degrees. Local Mach number varied from .9 to .94 at a freestream Mach number of .9.

2.0 INTRODUCTION

New and sometimes radically different inlet concepts are continually being proposed for advanced tactical airplanes. The great number of concepts, with numerous perturbations, makes concept evaluation through wind tunnel testing very time consuming as well as expensive. A great effort is being expended throughout the industry to develop new and improved analytical methods to analyze the inlet-forebody problem. With these analytical tools a great number of inlet concepts can be evaluated quickly with wind tunnel testing reserved for only the most likely candidates. To support future code development and validation a comprehensive data base for the inlet flowfield characteristics of an advanced tactical configuration is required.

The Boeing Military Airplane Company (BMAC)[1] and the NASA-Langley Propulsion Aerodynamics Branch have undertaken a multi-task program directed at this problem. Program objectives are:

o Identify inlet concepts and locations which have potential for application on tactical supersonic cruise airplanes
o Determine, through wind tunnel testing, the transonic wing/body flowfield characteristics at the representative inlet locations established in Task I.
o Apply existing codes to compute flowfield characteristics measured in the wind tunnel.

All design work, test data analysis and supersonic flow calculations were to be performed by BMAC with the wind tunnel testing and transonic flow computations conducted by the Propulsion Aerodynamics Branch.

---

1. Work performed under NASA Contract Number NAS1-16612

3.0 CONCEPTUAL DESIGN STUDY

3.1 INLET CONCEPTS

A conceptual study was conducted in which seven inlet concepts were defined for an Advanced Tactical Supercruiser. Schematics of each concept are presented in Figure 1. The baseline configuration (Figure 1a) represents an underwing half-axisymmetric inlet with short diffuser. Concept 1 (Figure 1b) is a 2-D high aspect ratio underwing inlet with short diffuser also. Concepts 2, 3, and 4 consist of body mounted inlets with long diffusers. A half-axisymmetric inlet (Figure 1b) is used in concept 2 and 2-D low and high aspect ratio inlets are used on concepts 3 and 4, respectively (Figure 1c). Wing upper surface mounted inlets with short diffusers are used on concepts 5 and 6 (Figure 1d) with quarter and half-axisymmetric inlets.

3.2 SURVEY AREAS

The inlet concepts presented above established the flowfield survey areas depicted in Figure 2. Survey areas 1 and 2 correspond to the lower and upper wing mounted inlet locations and area 3 is a representative of the body mounted inlet locations. In addition to the flowfield surveys, wing static pressure was measured over the forward portion of the wing.

4

4.0 TEST APPARATUS AND INSTRUMENTATION

4.1 TEST FACILITY

The experimental investigation was conducted in the NASA-Langley 16-foot Transonic Wind Tunnel. The facility is a continuous flow, single return, atmospheric tunnel. Mach numbers from 0.4 to 1.3 are achieved with two counter rotating drive fans and test section air removal. Typical tunnel operating conditions encountered during testing are shown in Figure 3. A detailed discussion of the test facility is available in Reference 2.

4.2 WIND TUNNEL MODEL

The inlet flowfield investigation was conducted with the Boeing Advanced Tactical Supercruiser Wind Tunnel Model (Reference 3). The model is a 10.5 percent scale adaptation of a concept developed by Boeing in conjunction with Air Force sponsored Air-to-Surface (ATS) concept studies. The general arrangement of the advanced supercruiser airplane is presented in Figure 4. The twin engine airplane has an aspect ratio 1.5 delta wing with a leading edge sweep of 68^0. The airplane is configured with close coupled canards having similar planforms as the wings.

The model has a wing span of 37.8 inches and an overall length of 100.8 inches. Flowfield testing was conducted with the clean wing/body configuration without canards and nacelles. A photograph of the model installed in the NASA-Langley 16-foot Tunnel is presented in Figure 5.

Testing was conducted with the model mounted on a dummy force balance (required for mounting purposes). No aerodynamic force data were obtained. Static pressure measurements were taken on the forward portion of the upper and lower wing surfaces. Locations of the 19 static pressure orifices are shown in Figure 6. Coordinates of the wing pressure taps are also tabulated. The wing surface pressures were measured with a low pressure scanivalve located in the nose of the model. Model angle of attack was measured with an electrical analog attitude indicator (Keistler Gauge) also located in the model nose cone.

5

Boundary layer trip strips were applied to the leading edges of the wing and body to produce representative fully developed flows over the instrumented and surveyed portions of the model.

4.3 FLOWFIELD SURVEY MECHANISM

A survey probe was used to obtain the local flowfield characteristics. Positioning of the probe at the desired locations was achieved with a remotely controlled survey mechanism provided by NASA-Langley. A schematic of the strut mounted survey mechanism is shown in Figure 7. The main support shaft, mounted atop and parallel to the strut head, provides longitudinal translation through the test section. The blade of the survey mechanism rotates about the axis of the support shaft to provide angular variations in the probe position. A small translating sting (0.75 inch diameter) attached to the roll blade provides radial movement along the blade. The survey probe itself is mounted on the tip of the translating sting. Servomechanisms on each component of the survey mechanism enable independent actuation and 3 degrees of freedom. The survey mechanism is capable of surveying a cylindrical volume approximately 4 feet in diameter and 4 feet long. The nominal position of the survey probe is established by the longitudinal position (X) of the support shaft, the radial position (R) of the sting, and the blade roll angle (O). A photograph of the survey mechanism installed in the 16-foot tunnel is shown in Figure 8.

As shown in Figure 7, the survey probe is positioned parallel to the strut centerline. A 4° angle of attack offset, built into the supercruise model support sting to increase the maximum angle of attack capability, produces a 4° bias between the model angle of attack and the flow angle sensed by the probe. This discrepancy was accounted for in the test data reduction.

The flowfield surveys were conducted with a wedge shaped survey probe. A schematic of the probe is shown in Figure 9. The probe consists of a 45° half-angle wedge with a single total pressure orifice at the center of the probe and one quasi-total orifice on each side. The probe is small enough to minimize the flowfield interference yet strong enough to minimize deflections and vibrations. The survey probe is attached directly to the 0.75 inch diameter support sting mounted in the blade of the survey mechanism (Figure 7).

6

4.4   SURVEY PROBE CALIBRATIONS AND DATA REDUCTION

Survey probe calibrations were conducted before and after the inlet flowfield survey runs. Pretest calibrations were made with the probe mounted on the survey mechanism. The maximum angle of attack obtained during these calibrations was limited by the survey mechanism to 10° at M < 1.0 and 7.5^O at M > 1.0. Post-test calibrations were made with the probe sting-mounted on the nose of the tunnel strut head (survey mechanism removed). Angles of attack of up to 15° were obtained for the final calibrations. Results of the final calibration were subsequently used for the test data reduction.

Calibration procedures consisted of first running the probe in the upright position and then rolling the probe 180° and repeating the calibration. Inverting the probe provided a combined angle of attack calibration of $\pm15^O$. The calibrations were done at a series of freestream Mach numbers from 0.4 to 1.28.[1] Tunnel upflow angles were determined from the calibration results and the data was adjusted accordingly.

Two nondimensional parameters are used to compute the local flowfield angles and local mach numbers. The flow angle parameter (QP) is defined as the difference in pressure measured by two outer orifices normalized by difference in pressure between the center orifice and the average of the outer two:

$$QP = \frac{PT3 - PT1}{(PT2 - \frac{PT1+PT3}{2})}$$

QP is directly proportional to the flow angle formed by the local relative wind and the survey probe axis. QP was used to compute both the local flowfield angle of attack and the local sideflow angle (the probe was rolled 90° for the sideflow surveys).

The local Mach number parameter (PM) is defined as the average of the outer pressures normalized by the pressure measured with the center orifice:

---

1. Calibration data was obtained at the following freestream Mach numbers:
    0.4, 0.6, 0.8, 0.9, 0.95, 1.00, 1.05, 1.10, 1.20, and 1.28

$$PM = \frac{PT1 + PT3}{2 * PT2}$$

PM is proportional to the local flowfield Mach number.

A typical set of calibration results showing the variation in QP and PM with Mach number and angle of attack are shown in Figures 13 and 14, respectively. Data for the flow angle parameter (QP) were curve fit as a function of angle of attack and the coefficients tabulated for each Mach number. Data for the Mach parameter (PM) were tabulated and a 2-way interpolation routine was used to determine a local flow angle and Mach number simultaneously until a value for the flow angle was converged upon. An additional 4.0° was added to the computed flow angle to account for the 4.0° bias existing between the probe and the model (see Section 2.3).

The runs made with the probe rolled 90° were used to compute the local sideflow angles (measurements of local sideflow and angle of attack were made in separate tunnel runs). To compute the sideflows at positions coincident with the local angle of attack locations (probe in the upright position), the measured QP values were tabulated as a function of Mach number ($M_{c\partial}$), angle of attack (α), survey blade roll position (0), and radial sting position (R). Values of QP were then interpolated for the same locations and the local sideflow angles computed using the previously computed local Mach number.

Accuracy of the local flowfield angles are expected to be better than 1 degree. Local flow angles above 15° are based on extrapolations and are therefore subject to uncertainty. Local Mach numbers are accurate to within 0.005.

4.5   TEST PROCEDURES AND CONDITIONS

The flowfield survey areas were established by the inlet concepts formulted in Task I. Local flowfield surveys were made for each area in separate tunnel runs. The survey probe was positioned at the desired model station prior to tunnel start-up. Flowfield surveys were then performed by systematically varying the support blade roll angle (0) and survey sting radial position (R). The nominal positions at which the flowfield survey measurements were

made for Areas 1 and 2 are shown in Figure 10. Area 3 survey positions are shown in Figure 11. Typically, a total of 20 flowfield measurements were made over Area 1 at three radial positions. A total of 34 measurements were made over Area 2 at seven radial positions. Ten measurements were made at 2 radial positions for Area 3. Flowfield surveys closer to the model body and wing surfaces were not possible because of obstructions from either the model support sting or the model itself. A photograph of the model and survey mechanism surveying Area 2 is shown in Figure 12.

Flowfield surveys were conducted at freestream Mach numbers of 0.6, 0.9, and 1.2. Model angle of attack was set at 0, 5, and 10 degrees at subsonic speeds. At M = 1.2 the maximum angle of attack was limited to 7.5 degrees by stress limitations of the survey mechanism. Typical unit Reynolds numbers obtained during testing are presented in Figure 3.

5.0 TEST RESULTS

At each test condition (M_∞, α), the local flowfield angle of attack, sideflow, and Mach number were obtained. The results of the flowfield survey are presented in Figures 16 through 33. The following directory of Figure numbers is presented to simplify discussion of the test results:

Figure Numbers

Survey Area	M_∞	$\alpha=0^\circ$	$\alpha=5^\circ$	$\alpha=7.5^\circ$	10°
1 and 2	0.6	16	17	--	18
	0.9	19	20	--	21
	1.20	22	23	24	--
3	0.6	25	26	--	27
	0.9	28	29	--	30
	1.2	31	32	33	--

In each figure the following results are presented:
    a. local flowfield characteristics
    b. local angle of attack
    c. local sideflow angle
    d. local Mach number
    e. wing surface pressure distributions (Areas 1 and 2 only)

In the subsequent sections general observations and trends in the data base are discussed. No attempt has been made to direct the reader to particular figures. Local angle of attack, sideflow angle, and Mach number contours were plotted directly from the reduced test data. The summary of local flowfield characteristics is a composite vector plot visualizing the direction of local flow in the survey plane perpendicular to the airplane longitudinal axis. The magnitude of each vector represents the resultant of the local sideflow and

11

upflow angle (the scale factor may differ among survey areas and test conditions). Wing surface pressure distributions are presented to supplement the flowfield data.

A preview of what may be observed in the wing flowfield data may be obtained by reviewing available force data for the supercruise model. Clean-wing lift characteristics obtained from previous wind tunnel test are presented in Figure 15. The data indicate that the zero-lift angle of attack is about 1.5 degrees. The lift curve slope is linear up to an angle of attack of about 7 degrees. Above this angle the lift curve shows a non-linear increase in lift (shaded area). This trend is indicative of the occurrence of leading edge vortex flows. Vortices of this sort are common on highly swept wings (supersonic planforms) with sharp leading edges when operated at moderate and high angles of attack.

5.1   AREA 1 FLOWFIELD CHARACTERISTICS

Area 1 is the flowfield around the inlet concepts located on the lower wing surface. The general characteristics of the inlet flowfield, in the plane perpendicular to the wing chord, is a spanwise flow moving outboard and up towards the wing leading edge at conditions of positive lift. At $\alpha = 0^0$ the inlet flowfield is directed primarily downward with little spanwise flow. In all instances the surveyed flowfield appears to be consistent and well ordered.

Local angle of attack (α_L) measurements indicate an increase in local alpha in the spanwise direction at conditions of positive lift. The magnitude of α_L increases with increasing angle of attack. The variation in α_L across the survey area ranges from about 3^0 at $\alpha = 5^0$ to 6^0 at $\alpha = 10^0$. At $\alpha = 0^0$ the variation in local alpha is within the accuracy of the measurements.

Local angles of attack are in all cases less than the freestream angle of attack. The wing acts to shield the inlet from potentially high freestream flow angles. The most effective shielding appears to occur inboard and close to the wing surface.

The local sideflows (β) are generally spanwise directed away from the body and increase in magnitude as the wing leading edge is approached. An increase in angle of attack causes an increase in the local sideflow angles. The sideflow gradients across the flow area also increase with α. The variations in sideflow angle at high angles of attack are comparable to the levels observed for local angles of attack. Mach number appears to have little effect on the measured sideflow angles.

The local Mach number (M_L) may be thought of as representative of the chordwise flowfield characteristics. Results show that at a positive lift condition the local Mach number is indeed less than the freestream, indicating a region of positive pressure as would be expected. At $\alpha = 0^0$ the local Mach numbers are typically greater than freestream (low pressure and no lift). In the spanwise direction, when $\alpha > 0^0$, the inboard Mach numbers are typically higher than those near the edge of the wing. An increase in Mach number is also obtained as wing surface is approached. However, the Mach gradient across the survey area is generally small. The variation in local Mach number across the inlet face is less than 5 percent of the freestream value.

5.2 AREA 2 FLOWFIELD CHARACTERISTICS

Area 2 represents potential locations of inlet concepts mounted on the upper wing surface. The flowfield is typically characterized by an inwardly directly spanwise flow. At conditions of positive lift the flowfield is directed upward at the wing leading edge and rotates inward at inboard positions. At an angle of attack of 10^0 a rotating flow is evident indicating the existence of a leading edge vortex. The core of the vortex is located inboard of the wing leading edge and slightly above the wing surface. The core appears to move slightly inboard with increasing Mach number.

Maximum values of the local flowfield angle of attack are obtained in the vicinity of the wing leading edge with a subsequent decrease in local flow angle inboard across the wing. The magnitude of local alpha is dependent on angle of attack. An increase in alpha increases the local flow angle as well

as the flow angle gradient across the survey area. The most significant change in local flow angle due to angle of attack occurs near the wing surface. The effects of freestream Mach number on the local flowfield angle of attack is small.

The local sideflow component of the upper wing flowfield typically increases inboard in the spanwise direction. At the leading edge the local flows are directed primarily upward; inboard and near the wing surface the sideflows become the major component of flow in the survey plane. The magnitude of the local sideflow typically decreases in the direction away from the wing. The magnitude of the sideflows and the sideflow gradients across the flow area increase with angle of attack. Mach number has only a small effect on the local sideflow angles.

At $\alpha = 10^O$ the local sideflows and local angles of attack combine to establish the rotating flowfield of the leading edge vortex. Flow reversal along the wing surface inboard of the vortex core is apparent in both the sideflow and local angle of attack flowfields.

At conditions of positive lift the maximum local Mach numbers are obtained in the inboard portion of the wing near the wing surface. At subsonic Mach numbers an increase in angle of attack produces the expected increase in local Mach number. Sonic conditions are indicated on the upper wing surface at $\alpha = 10^O$ for the M = 0.9 test condition. At M = 1.2 an increase in angle of attack from 5° to 7.5^O produces a drop in the local Mach number indicating the presence of an upstream shock. The Mach gradient across the survey area typically increases with angle of attack. The major contributor to large Mach gradients, however, appear to be the formation of vortices and upstream shocks.

A survey of the wing static pressure distributions provide insight into the characteristics of the surveyed flowfields. At conditions of positive lift, the upper surface pressures show a sharp drop in pressure at wing leading edge indicating an increase in the local flowfield velocity. This trend was not

14

evident in the local flowfield data. At $\alpha = 10^o$, the minimum pressure point moves inboard from the wing leading edge indicating the presence of a higher speed flow. The position of the leading edge vortex can be inferred from this data. Based on the flowfield data, the location of the vortex core is actually inboard from that inferred from the surface pressure data.

The survey data along the first and second survey arcs from the axis of the probe often displays unexpected characteristics, see Figure 16a, 17a and 23a. The raw data and data reduction were reviewed for these and other isolated questionable points. In some cases, it was found that the iterations in flow angle and Mach number did not converge, and those points were eliminated. However, no explanation was found for the sudden changes in flow direction in the first two arcs.

5.3   AREA 3 FLOWFIELD CHARACTERISTICS

Area 3 represents the survey location for the body mounted inlet concepts. In general, the flowfield is directed upward and outboard away from the body at positive lift conditions. At $\alpha = 0^o$ the flows are predominately outward and irregular.

Local angle of attack measurements show an increase in local angle of attack at inboard locations near the body. The local flows angles in this area are dominated by the flows passing around the body. Outboard values are nearly freestream. An increase in angle of attack causes increase in local conditions as well as an increase in the flow angle gradient across the survey area. The variations in local angle of attack due to changes in freestream Mach number are small.

The magnitude of the local sideflow angles decrease as the body is approached. At outboard locations the flow is primarily directed outward. At inboard locations the flow tends to change direction and flow inwards towards the body. This tendency occurs at a position above the maximum body half-breadth. The local flow, having been forced around the blunt body, tries to fill the low pressure region above it. At $\alpha = 0^o$ the sideflows are primarily directed outboard away from the body.

15

Increasing angle of attack results in a significant increase in local sideflow gradients due to an increase in both the outwardly directed outboard flow angles and the inboard body directed flows. A change in Mach number has little effect on the magnitude of the local sideflows.

At $\alpha = 0^O$ the local Mach numbers are comparable to the freestream value. Increasing angle of attack to 5° produces local Mach numbers greater than the freestream condition at the inboard locations. A further increase in alpha ($M \geq .9$) results in a decrease in local inboard Mach number possibly due to the presence of a shock wave of the forebody (nose).

6.0 CONCLUSIONS

A substantial data base has been obtained for the inlet flowfield characteristics of an advanced tactical supersonic cruise airplane. Local flowfield characteristics were obtained for overwing, underwing, and forebody mounted inlet concepts. The flowfield data include local angles of attack, local sideflow angles, and local Mach numbers. Data are available for freestream Mach numbers of 0.6, 0.9, and 1.20 at angles of attack from 0 to 10 degrees. Based on a study of these data the following conclusions are made:

o   From an aerodynamic standpoint the optimum inlet location is under the wing. In this position the wing effectively shields the inlet from high flow angles, local flowfield Mach numbers are reduced, and the local flow angle gradients are a minimum.

o   A forebody side-mounted inlet location, though less favorable than the underwing concept, has potential for application to the supercruise airplane.

o   Locating the inlet on the wing upper surface appears to be in the least likely location of the 3 concepts considered. The existence of higher flow velocities (greater than freestream), shocks, and leading edge vortex flows only act to complicate the inlet design and compromises performance.

The acquired data base, though incomplete on some areas, should provide a sufficient base to support analytical code developments directed at the analysis of the inlet flowfield problem.

7.0 REFERENCES

1. Paynter, G., Salemann, V., "Inlet Flow Field Investigation - Part II, Computation of the Flow about a Supercruise Forebody at Supersonic Speeds," Boeing Document D180-27939-1, December 1983.

2. Corson, B. W., Runckel, J. L., Igoe, W. B., "Calibration of the Langley 16-Foot Transonic Tunnel with Test Section Air Removal," NASA TR R-423, August 1974.

3. Hutchison, R. A., Banken, G. J., "Model 987-350 2-D Nozzle Jet Effects Program - Model Description," Boeing Document D180-25257-1, December 1979.
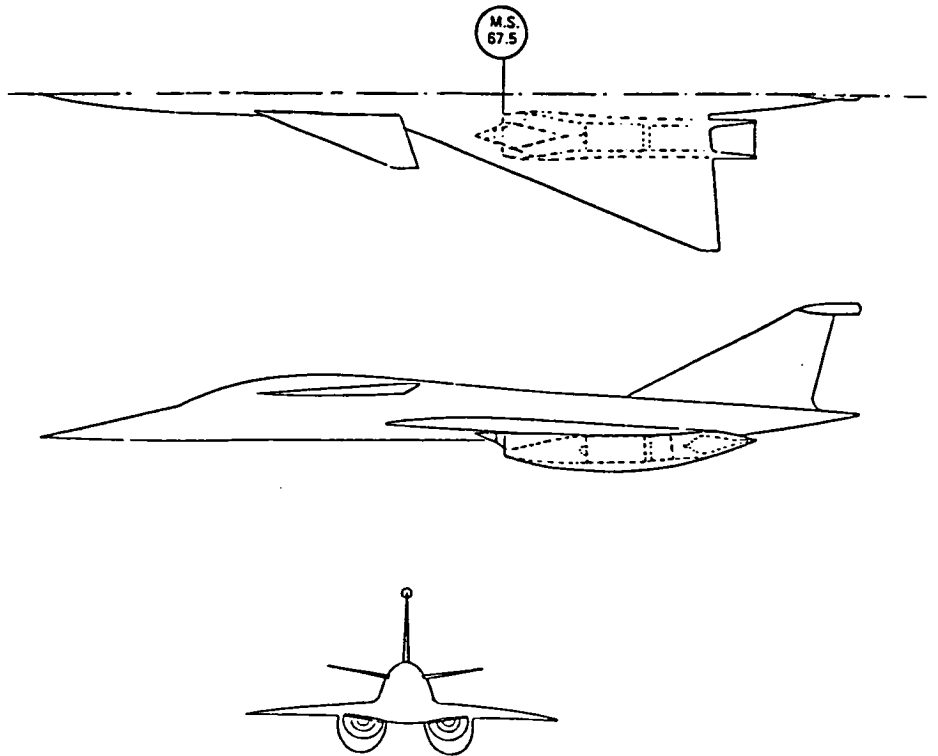
BASELINE CONFIGURATION

Under-Wing Half-Axisymmetric Inlet, Short Diffuser

Figure 1a. Inlet Concepts for the Advanced Tactical Supercruiser

19

CONCEPT NO. 1

Under-Wing 2-D High-Aspect-Ratio Inlet, Short Diffuser

CONCEPT NO. 2

Side-Mounted Half-Axisymmetric Inlet, Long Diffuser

Figure 1b. Inlet Concepts

20
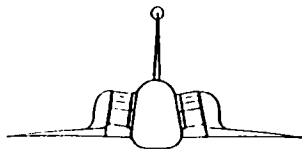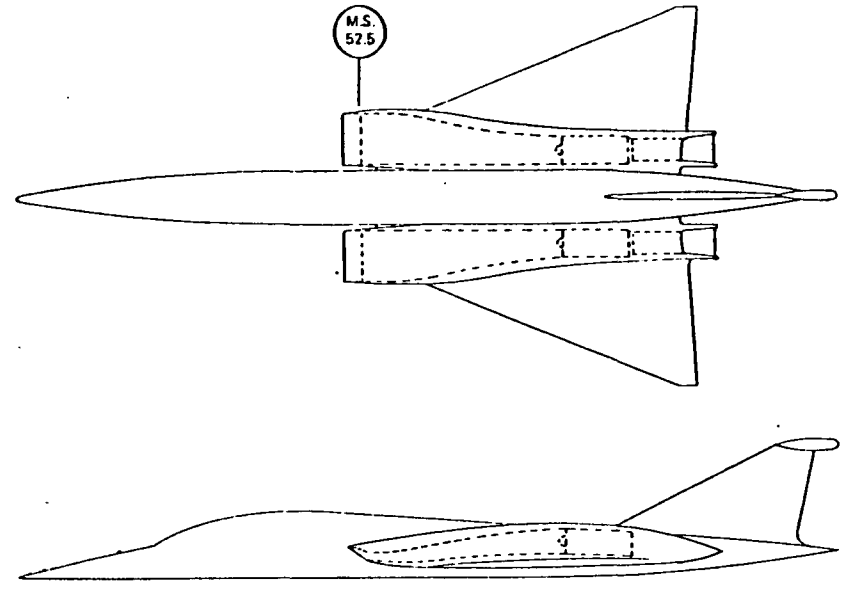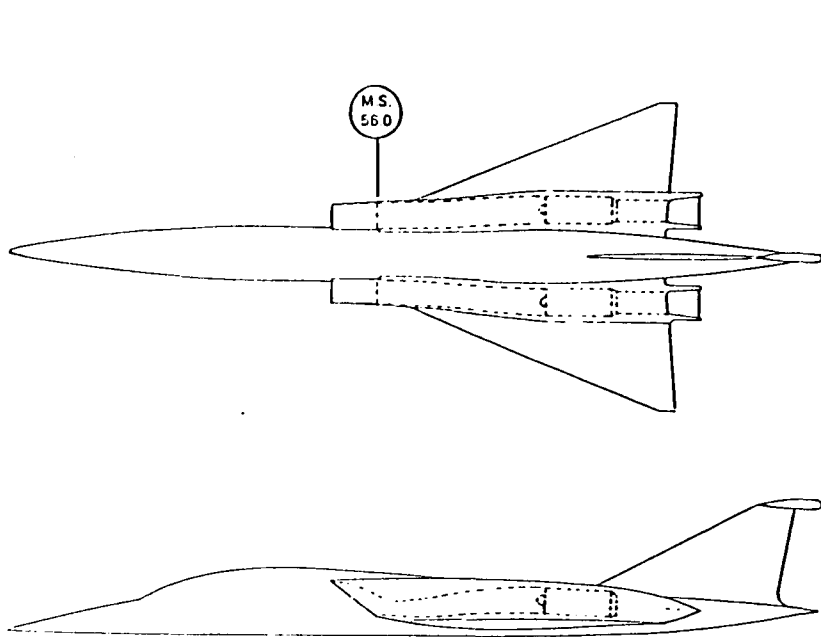
CONCEPT NO. 3

Side-Mounted 2-D Low-Aspect-Ratio Inlet, Long Diffuser
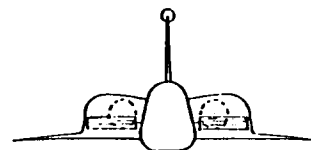
CONCEPT NO. 4

Side-Mounted 2-D High-Aspect-Ratio Inlet, Long Diffuser

Figure 1c. Inlet Concepts
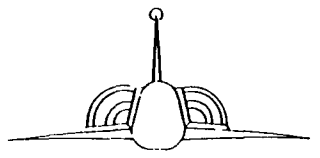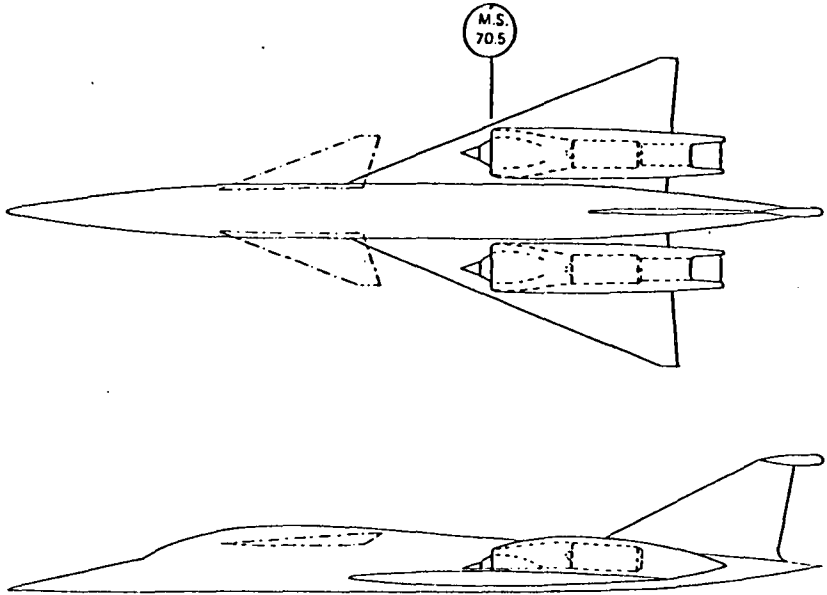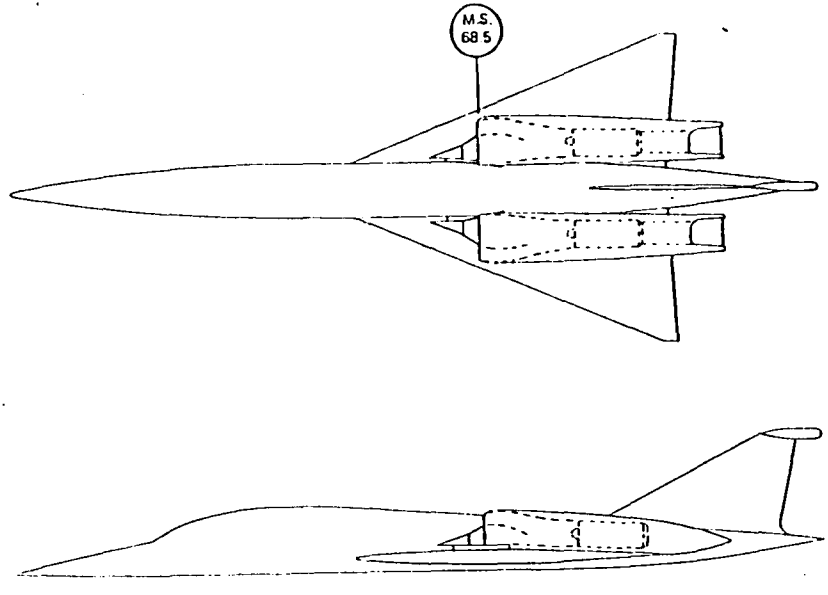
CONCEPT NO. 5

Top-Mounted 1/4-Axisymmetric Inlet, Short Diffuser
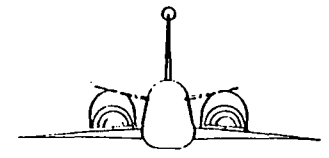
CONCEPT NO. 6

Top-Mounted Half-Axisymmetric Inlet, Short Diffuser

Figure 1d. Inlet Concepts

NO. 2

NO. 1

M.S.
70.5

NO. 3

M.S.
50.5
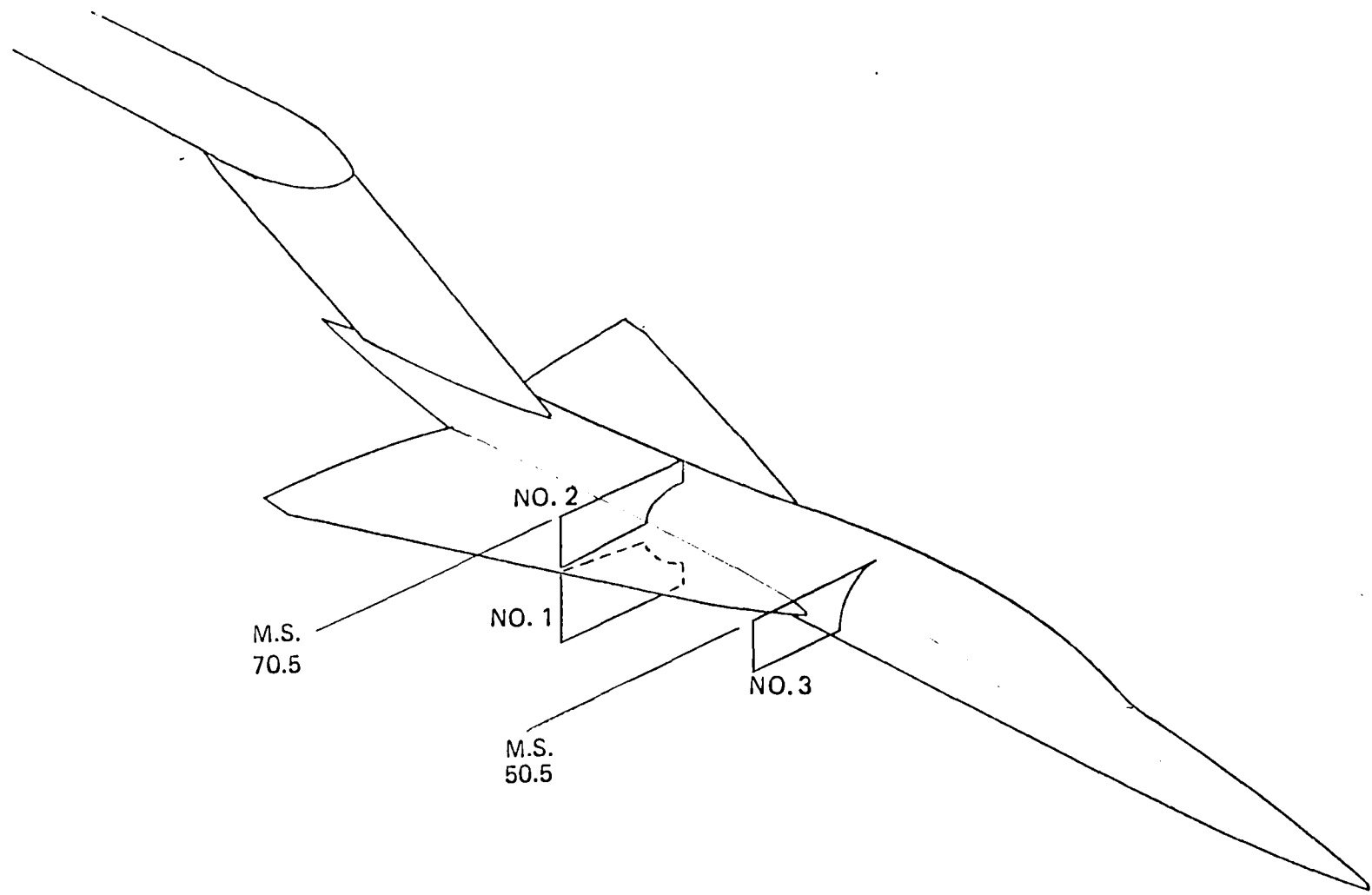
Figure 2. Inlet Flowfield Survey Areas
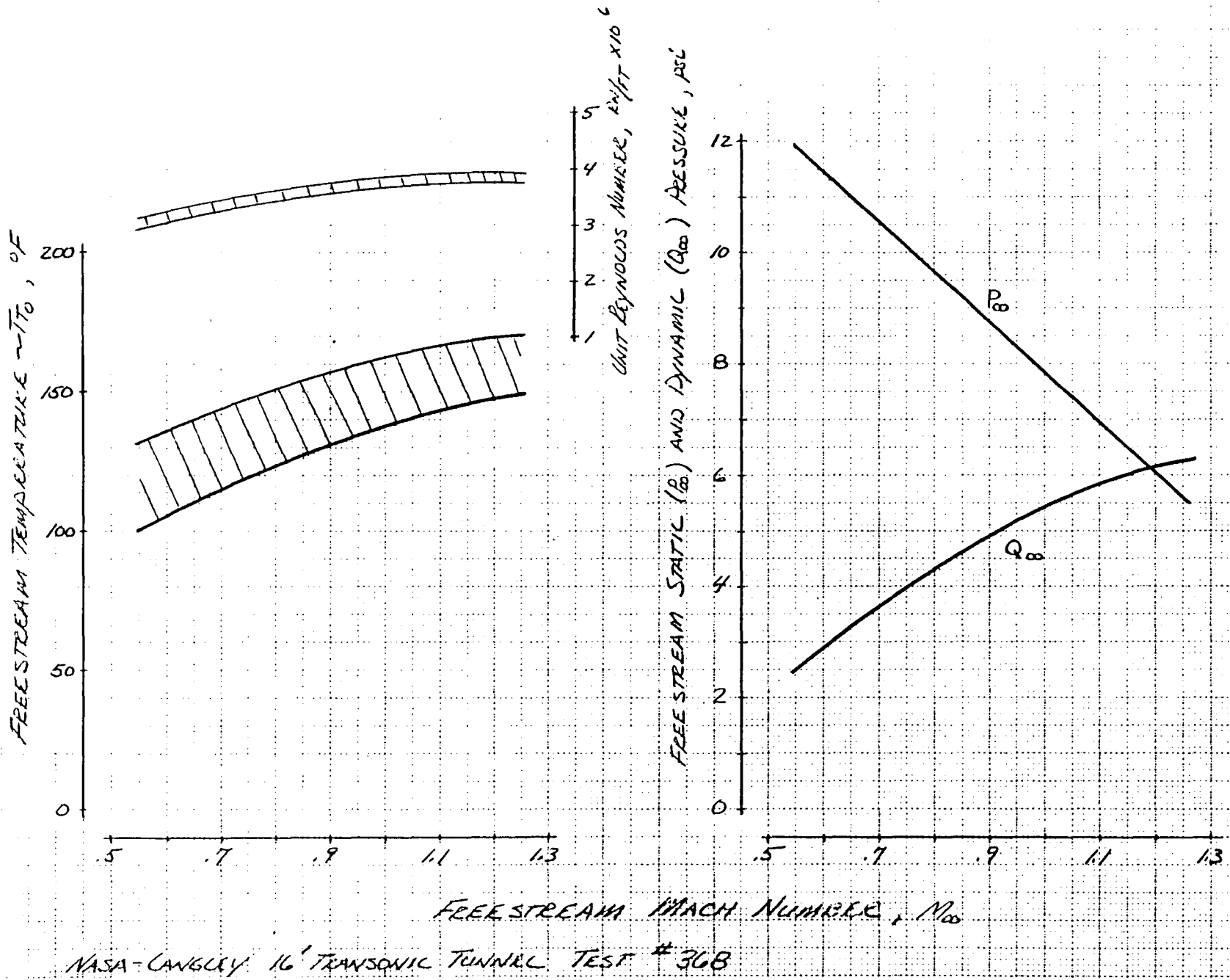
Figure 3. Wind Tunnel Freestream Test Conditions
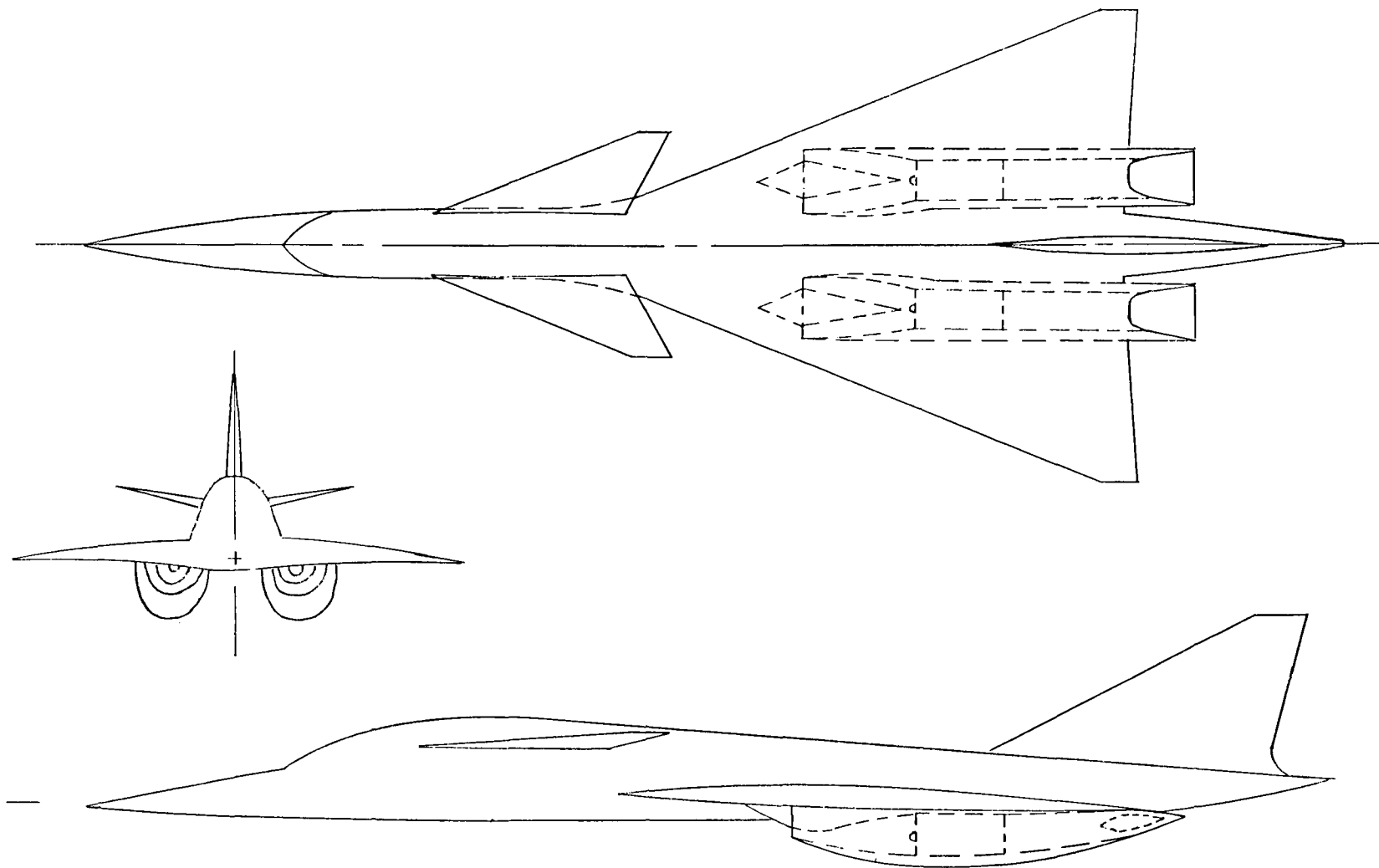
Figure 4. Boeing Advanced Tactical Supercruiser — ATS-350
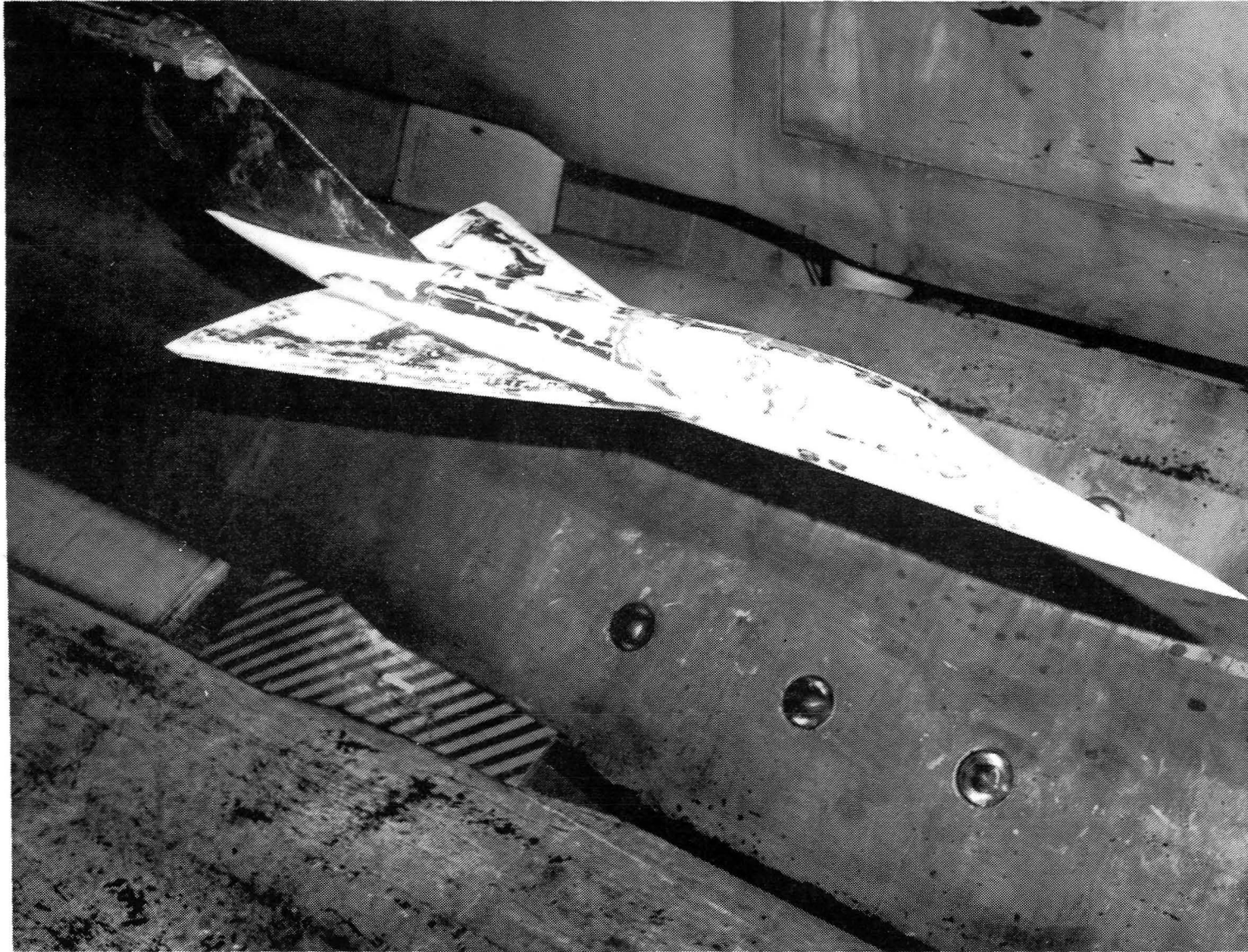
Figure 5. The Boeing Advanced Tactical Supercruiser Model (ATS-350) Installed in the NASA-Langley
16-ft Transonic Tunne
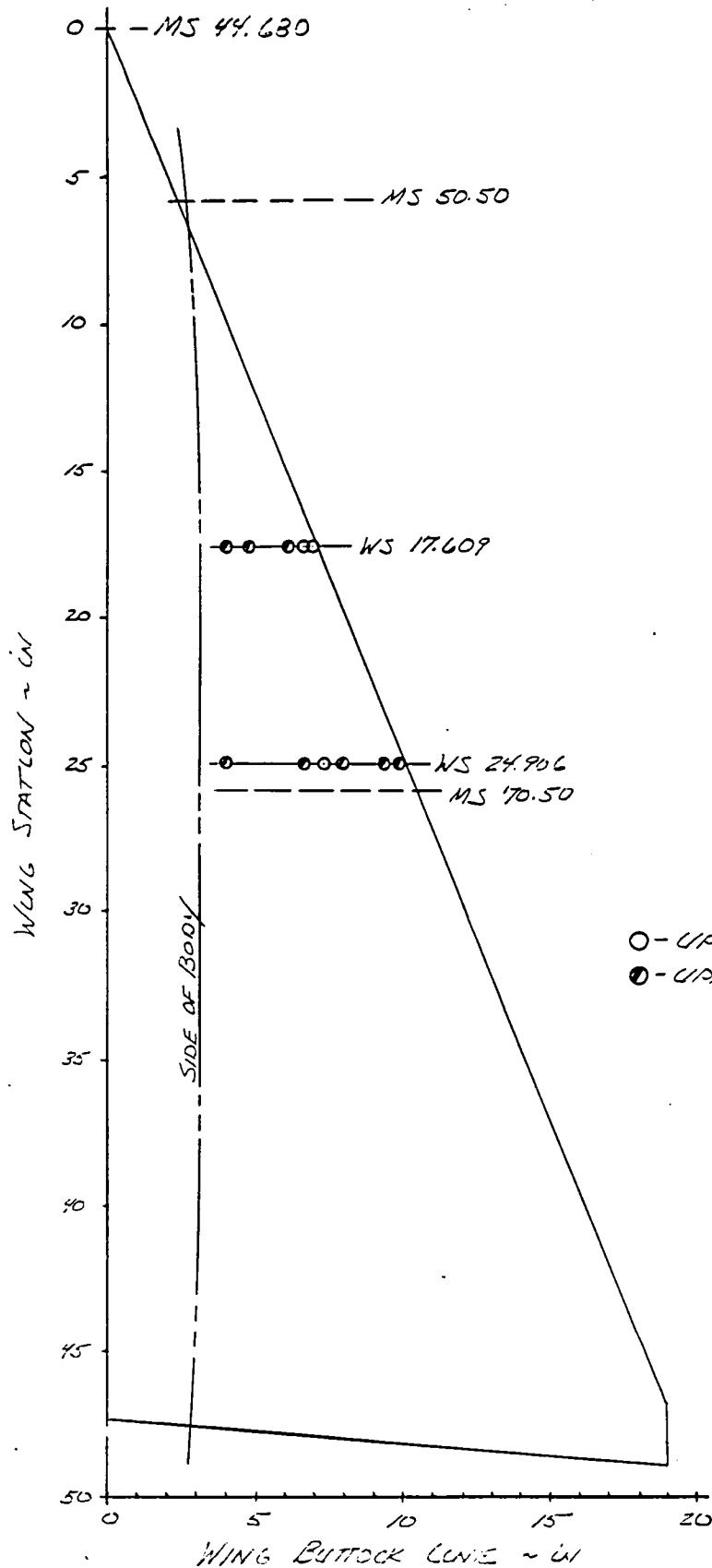
WING STATIC PRESSURE TAPS

SURFACE	WS	BL	
UPPER	17.609	3.997	*
		4.800	
		6.100	
		6.581	
		6.937	
	24.906	3.997	*
		6.600	*
		7.295	
		7.900	
		9.308	*
		9.811	
LOWER	17.609	3.997	
		4.800	
		6.100	
	24.906	3.997	
		6.600	
		7.900	
		9.308	
		9.811	

* DATA NOT AVAILABLE

O – UPPER SURFACE PRESSURES
◑ – UPPER & LOWER SURFACE PRESSURES

— MS 44.630
— MS 50.50
— WS 17.609
— WS 24.906
— MS 70.50

SIDE OF BODY

WING STATION ~ IN

WING BUTTOCK LINE ~ IN

Figure 6. Wing Upper and Lower Surface Pressure Instrumentation

27
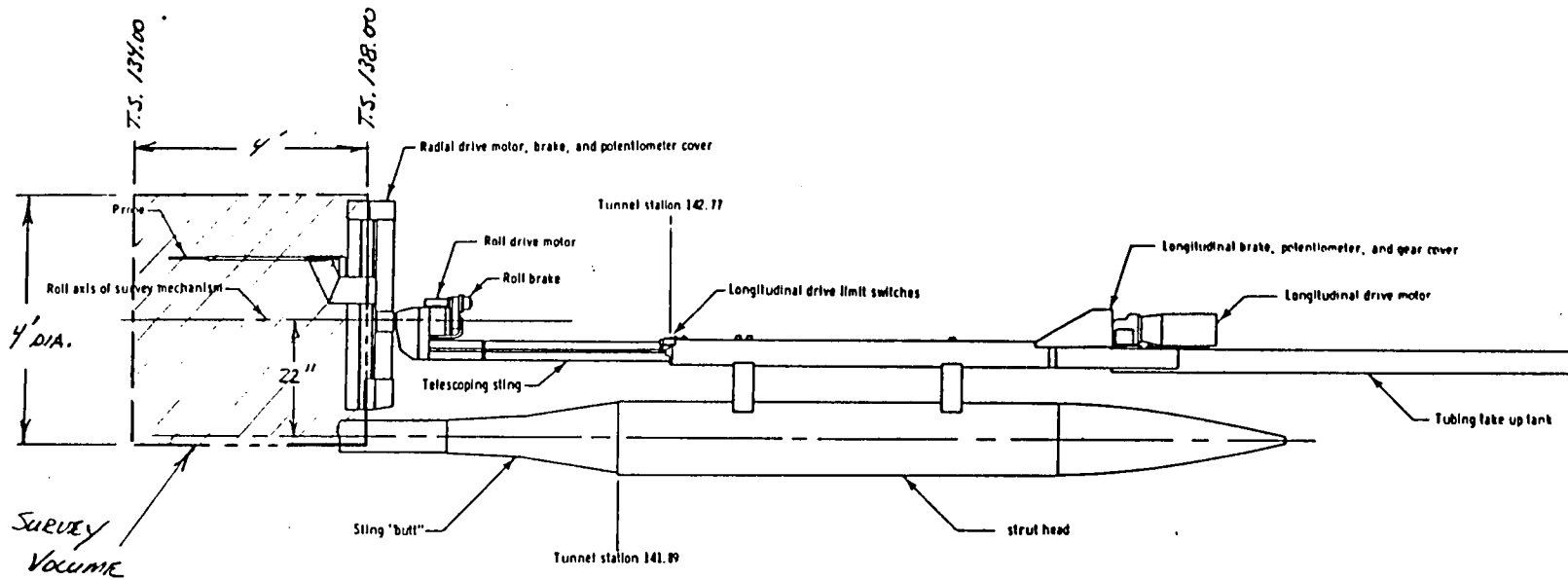
Figure 7. NASA-Langley Flowfield Survey Mechanism
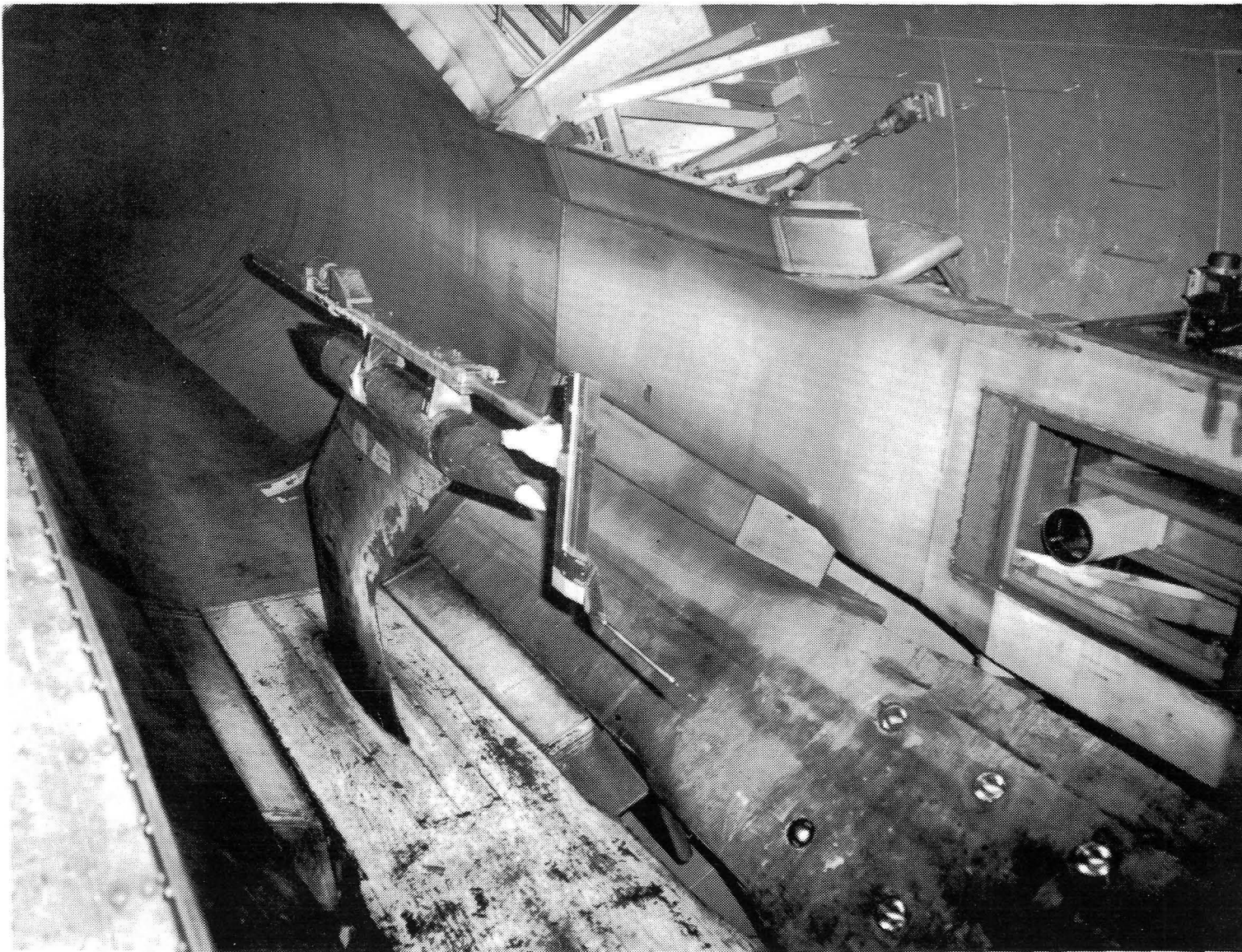
Figure 8. The NASA-Langley Strut Mounted Flowfield Survey Probe

.020 ID TUBING (3)

.250 DIA.

1.95

.20

45°

.10

.90

.05

.033

SURVEY
STING

PROBE

45°

PROBE 1
PROBE 2
PROBE 3

.020 DIA.
(TYP.)

DETAIL A-A'

30
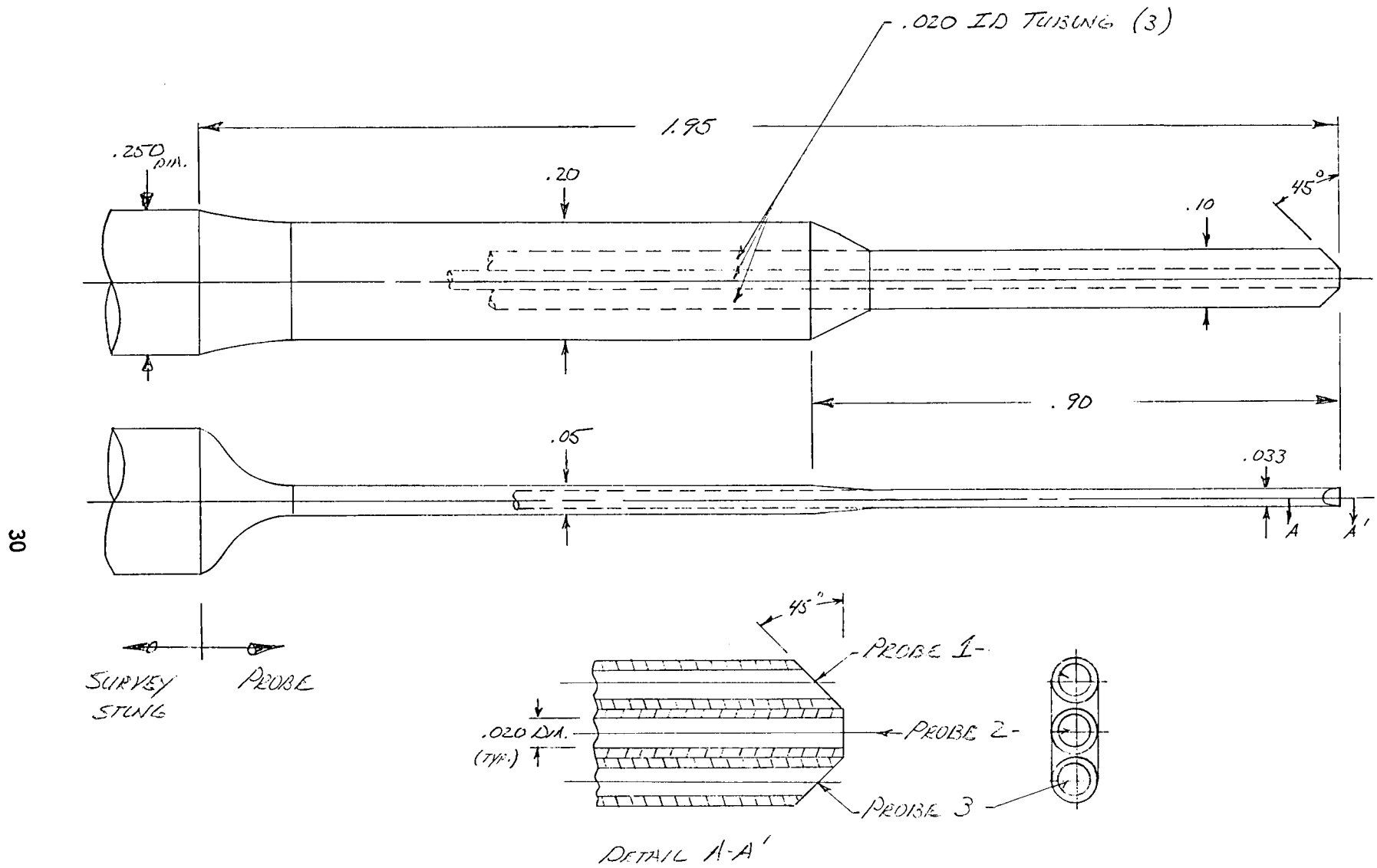
Figure 9. Flowfield Survey Probe (NASA-LARC 16T Prism Probe)
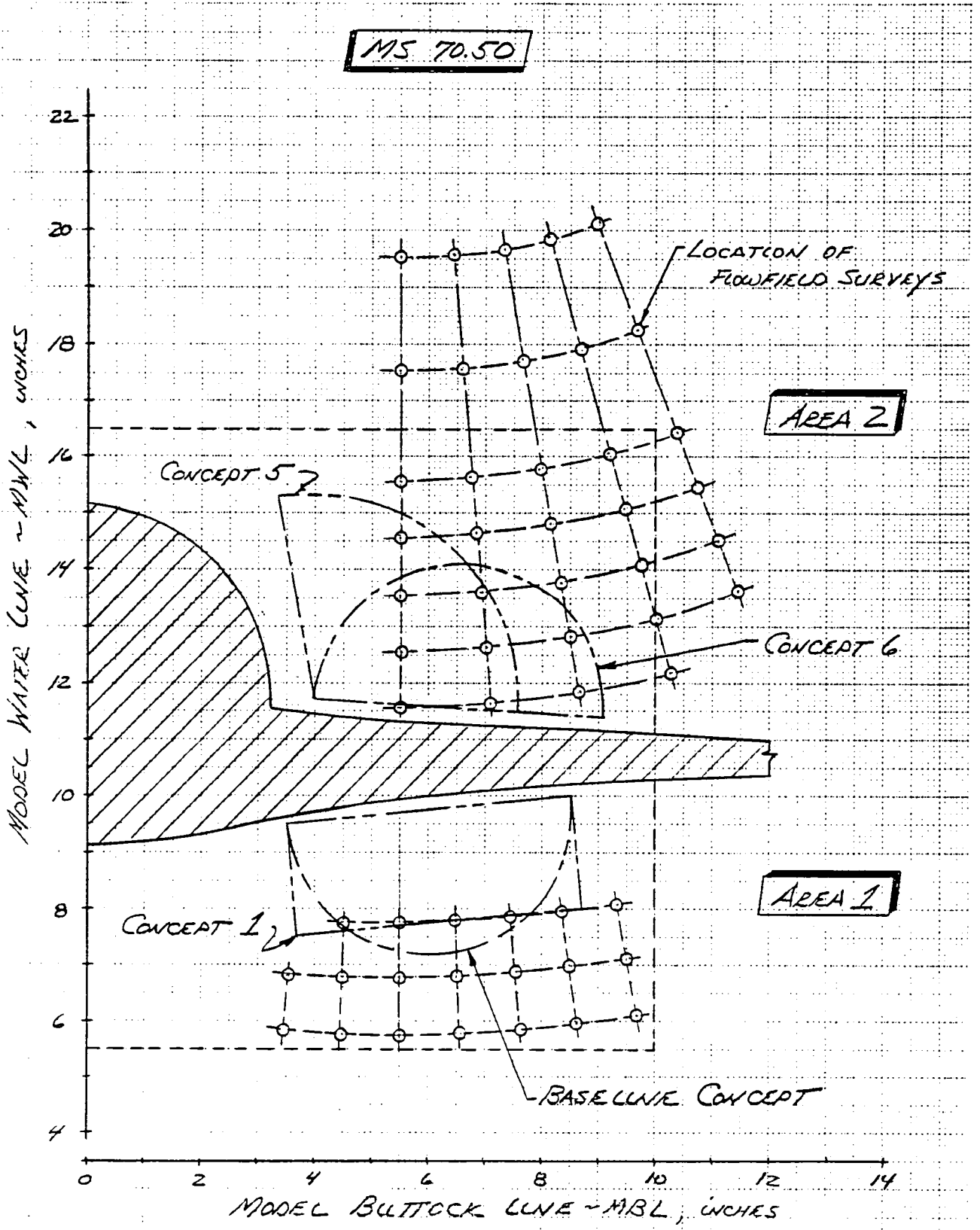
Figure 10. Inlet Flowfield Survey Locations, MS = 70.50

MS 50.50

AREA 3

CONCEPT 3

CONCEPT 2

CONCEPT 4

FLOWFIELD SURVEY
LOCATIONS

MODEL WATER LINE ~ MWL, INCHES

MODEL BUTTOCK LINE ~ MBL, INCHES
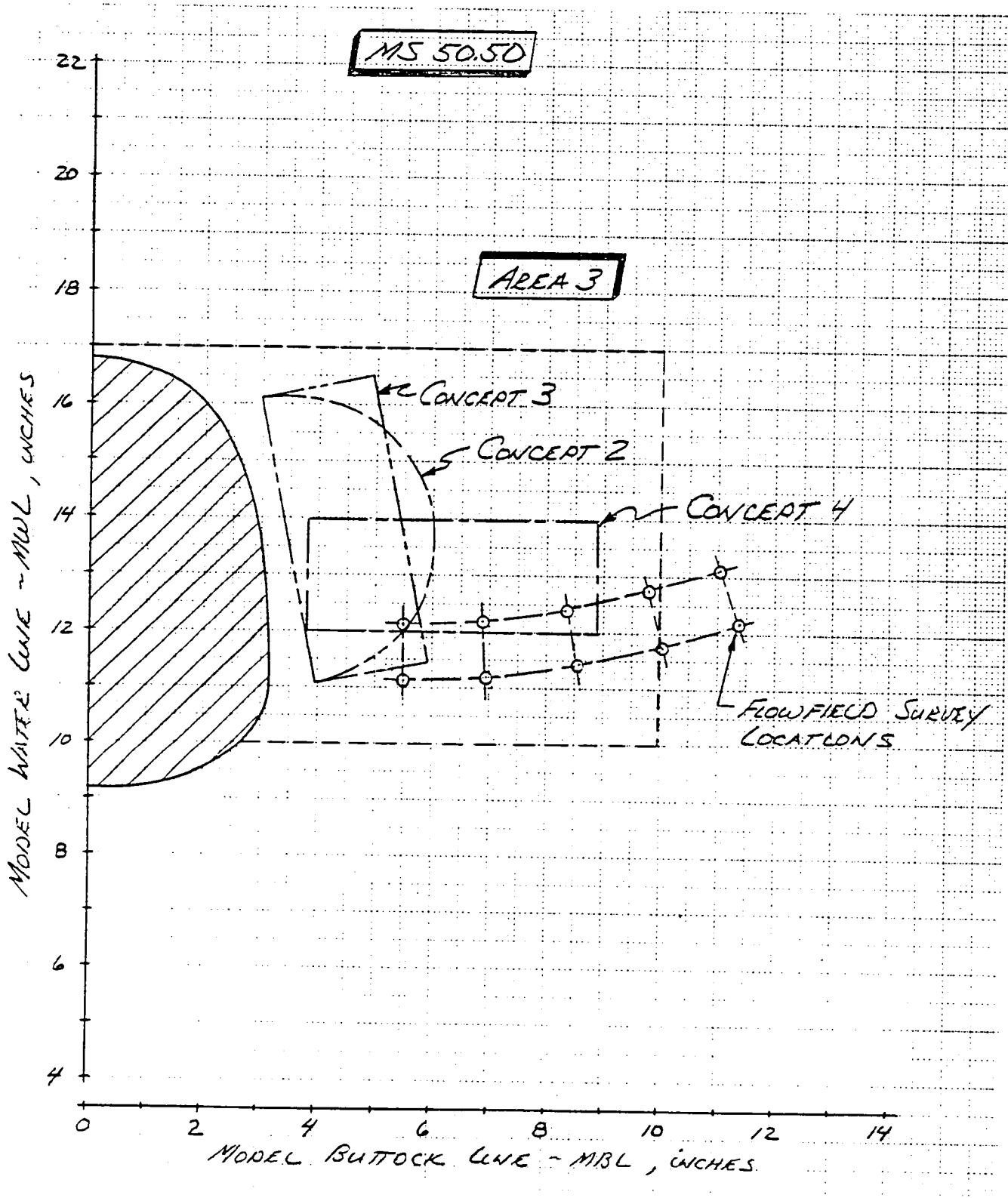
Figure 11. Inlet Flowfield Survey Locations, MS = 50.5

32
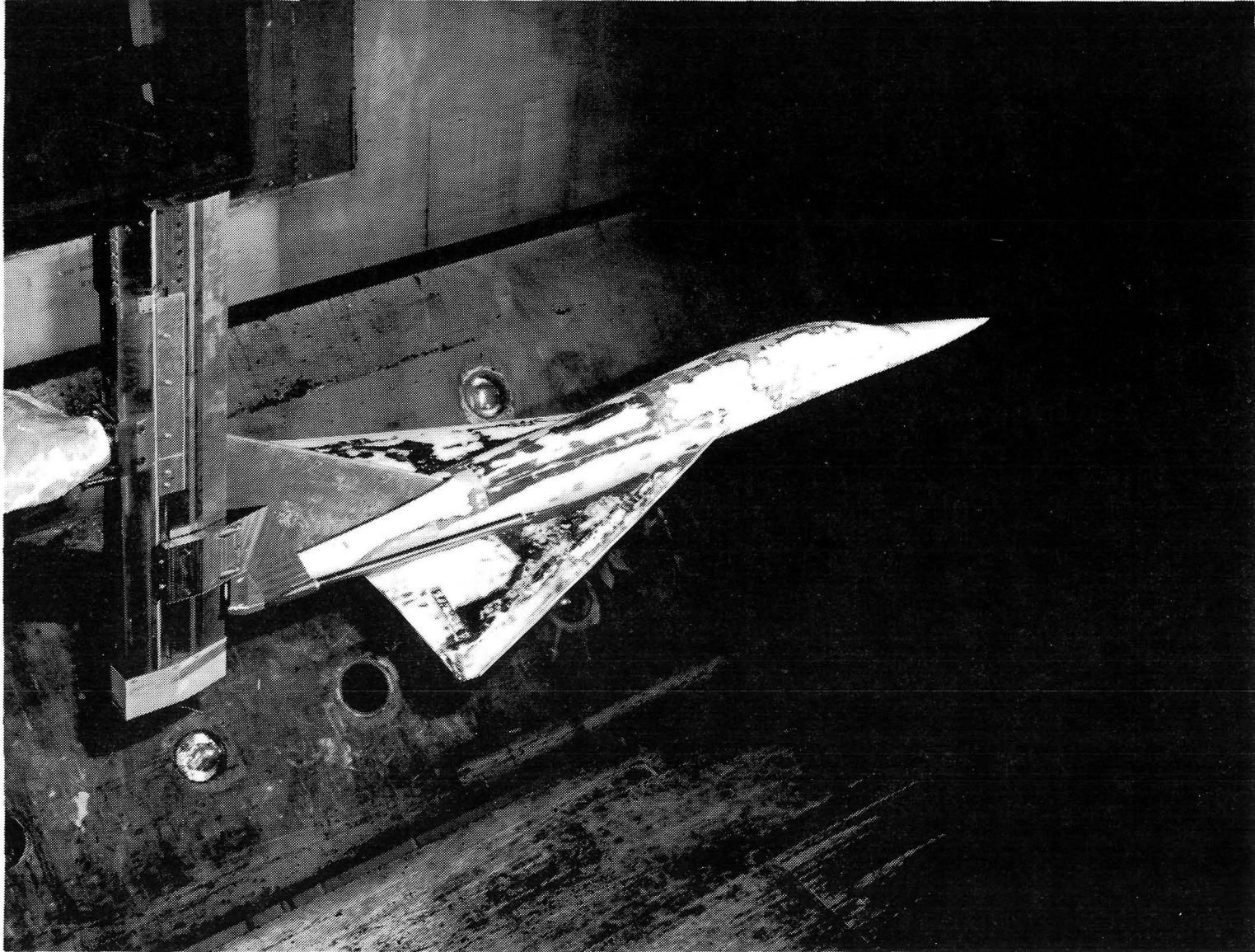
Figure 12. Typical Test Set-Up for the Inlet Flowfield Survey
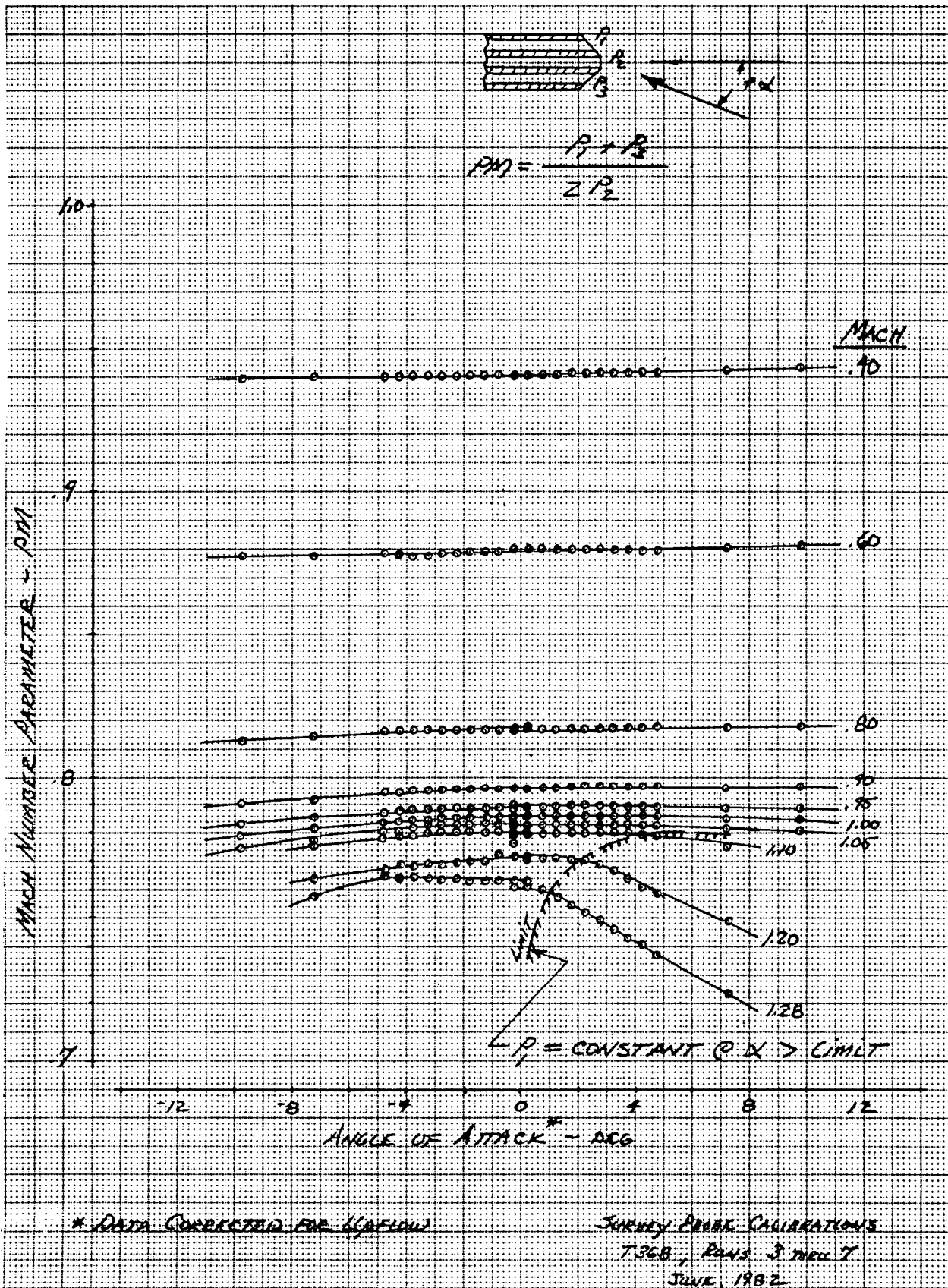
Figure 13. Survey Probe Calibrations — Mach Number Parameter

34
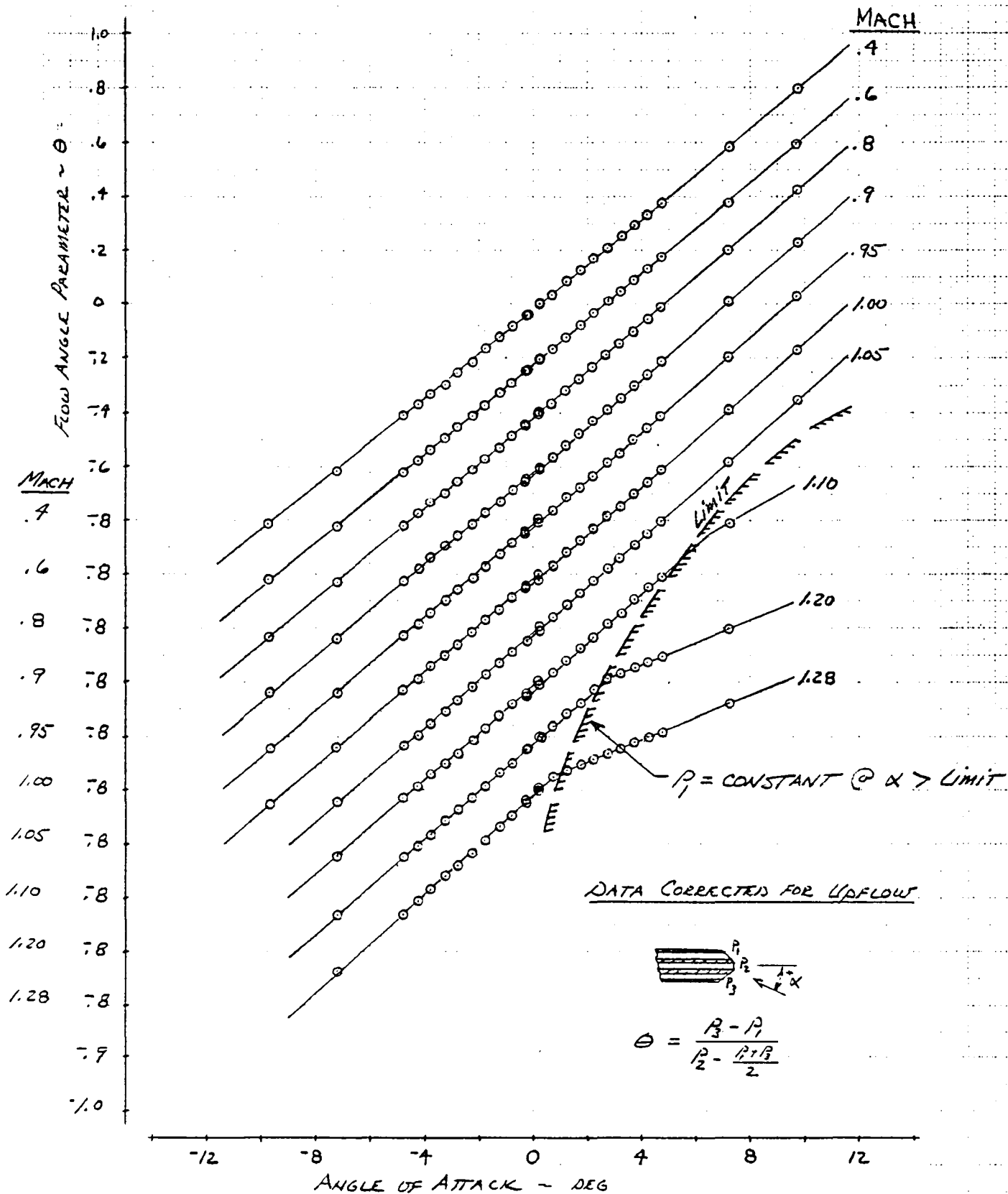
Figure 14. Survey Probe Calibrations—Flow Angle Parameter

35
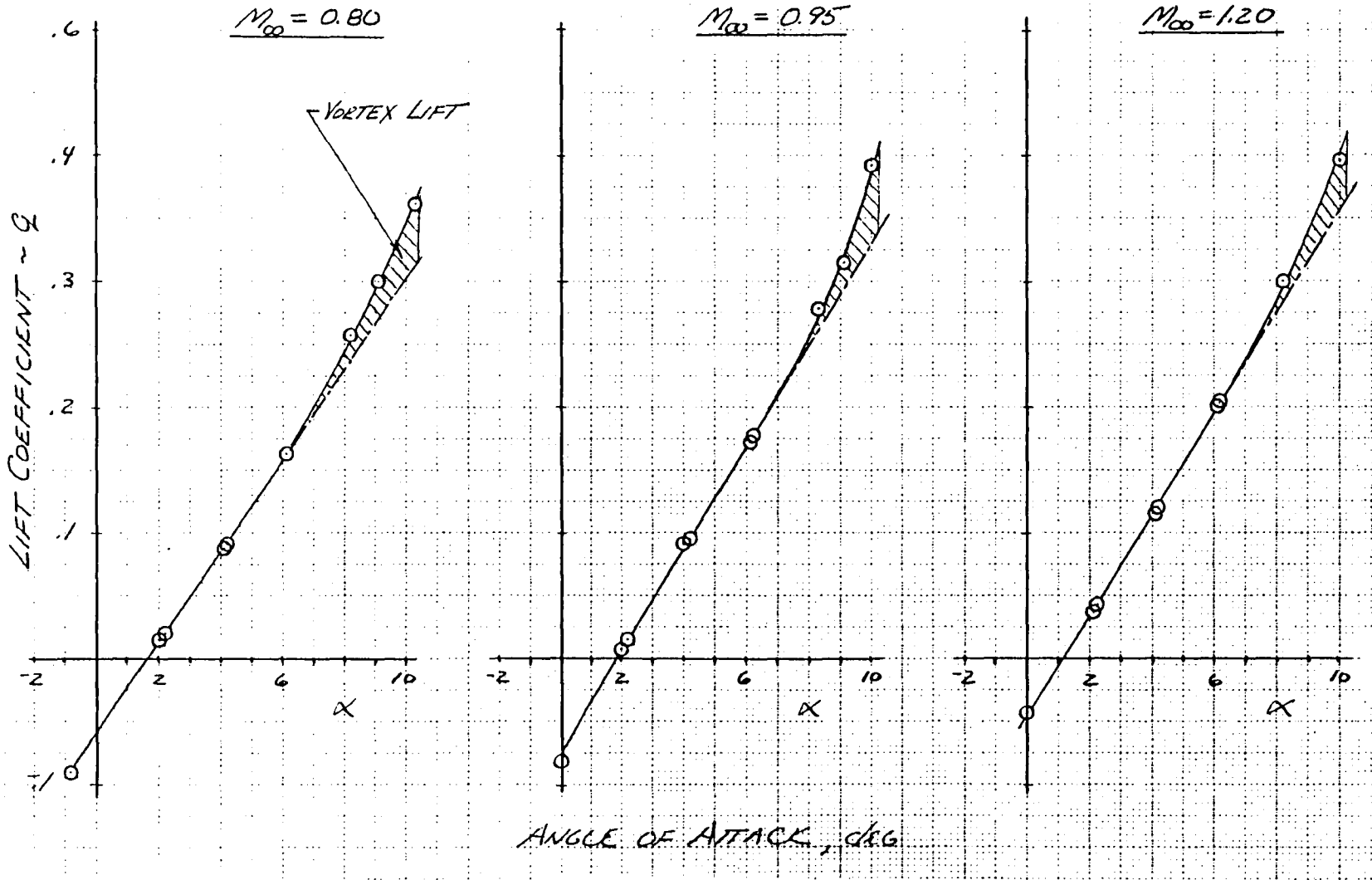
Figure 15. Model 987-350 Clean Wing Lift Characteristics
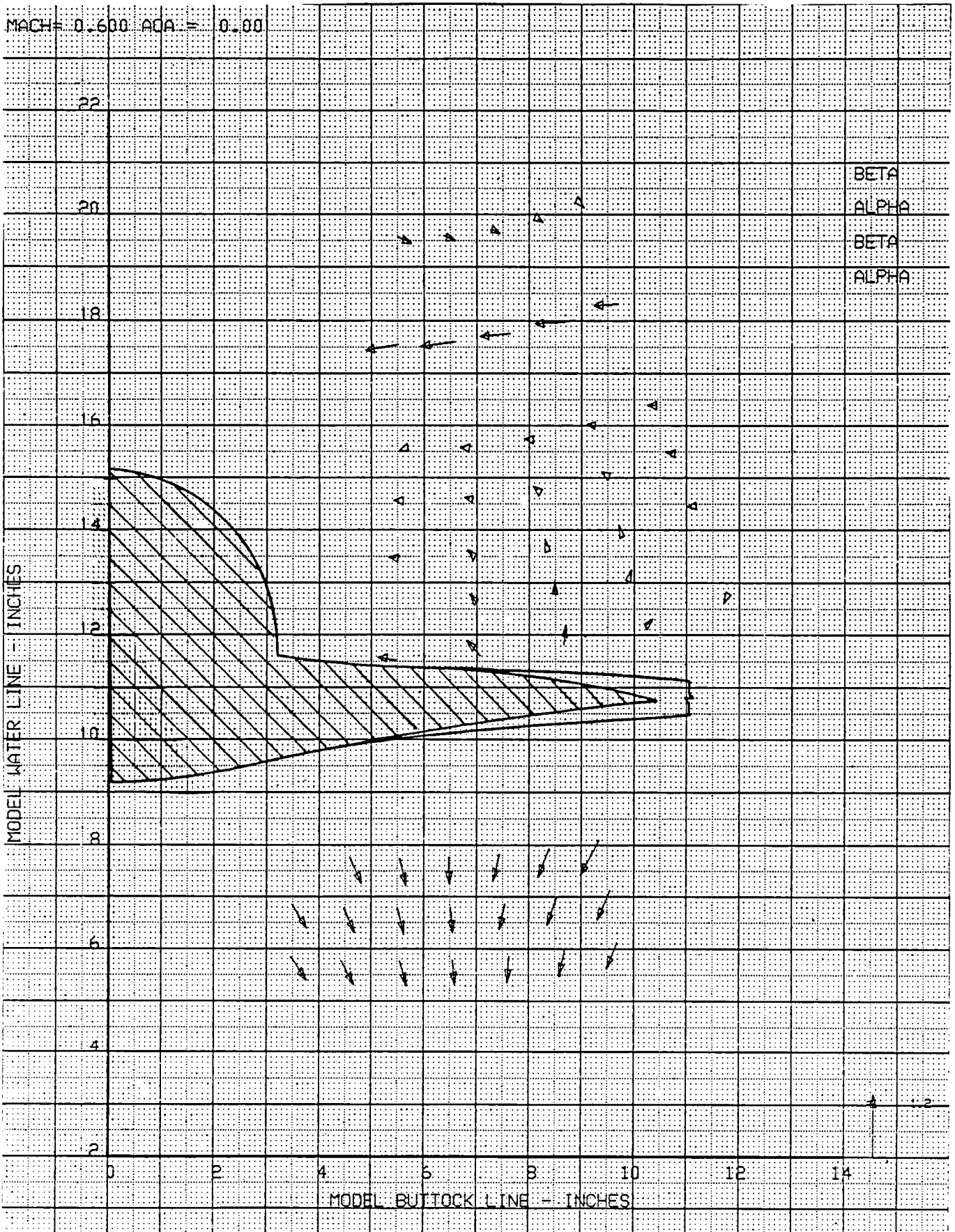
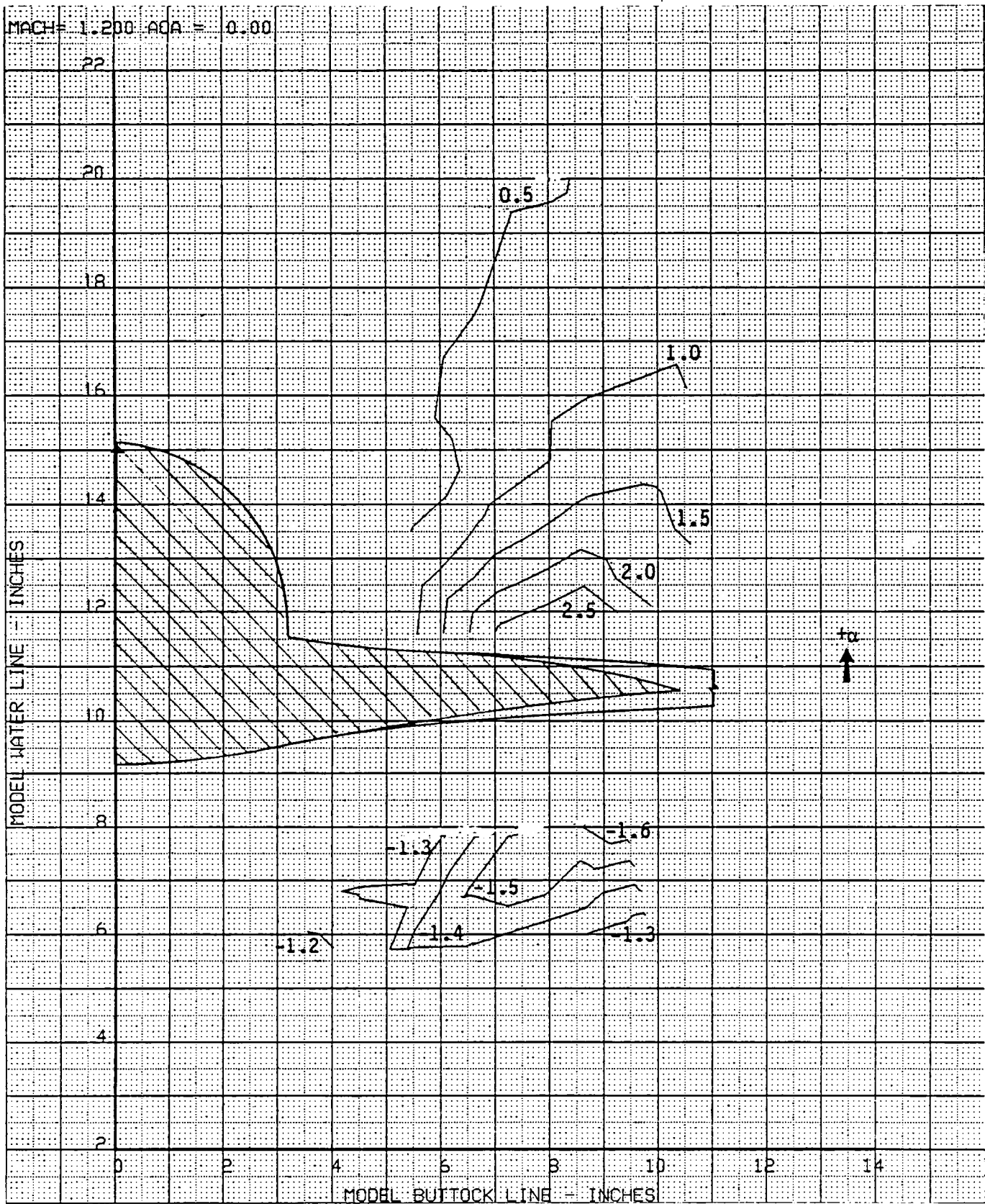*Figure 16a. Local Flowfield, MSTA = 70.50; Mach Number = 0.6; Angle of Attack = 0.0 deg*

37
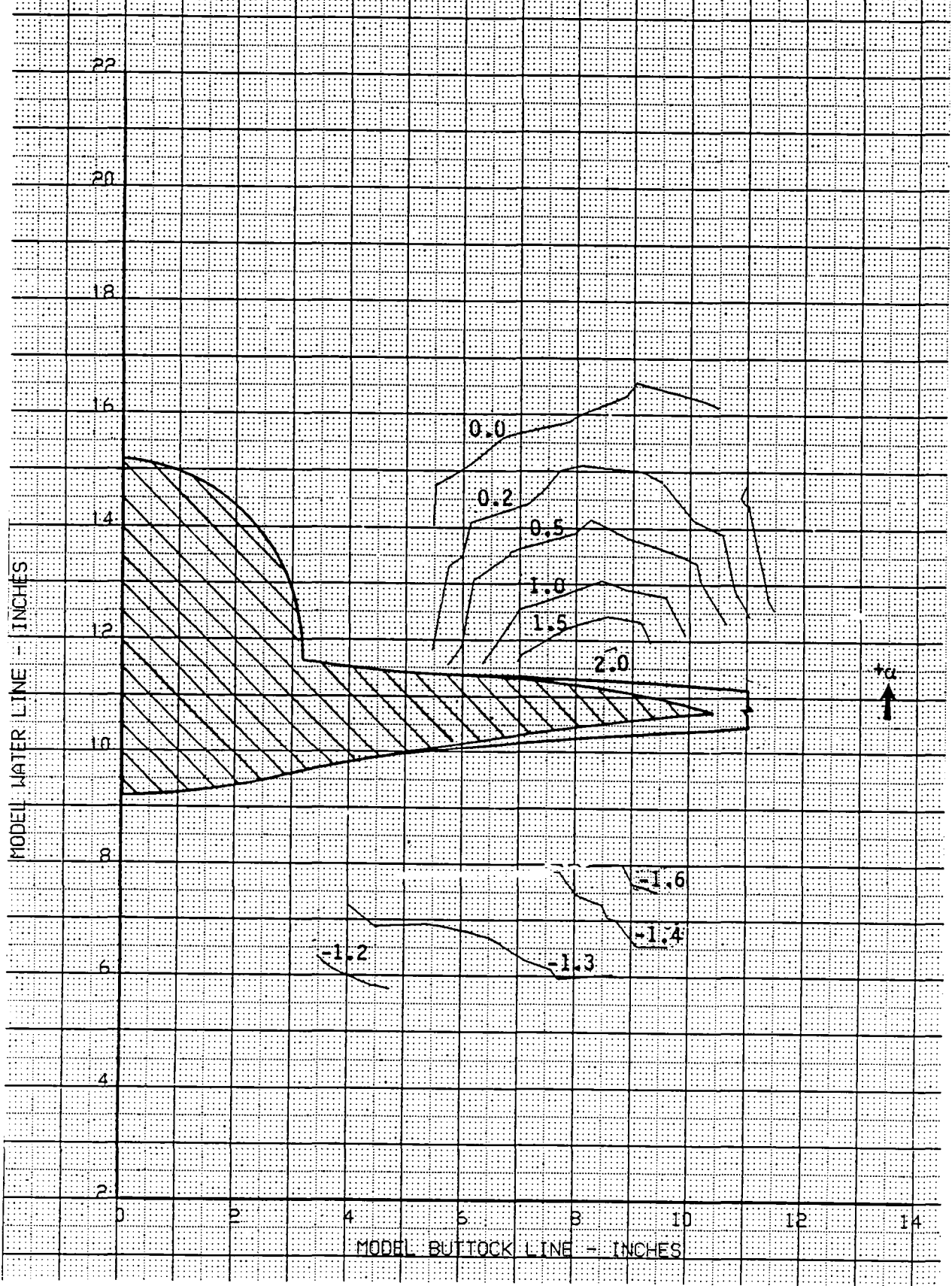
Figure 16b. Local Angle of Attack, Mach Number = 0.6; Angle of Attack = 0.0 deg
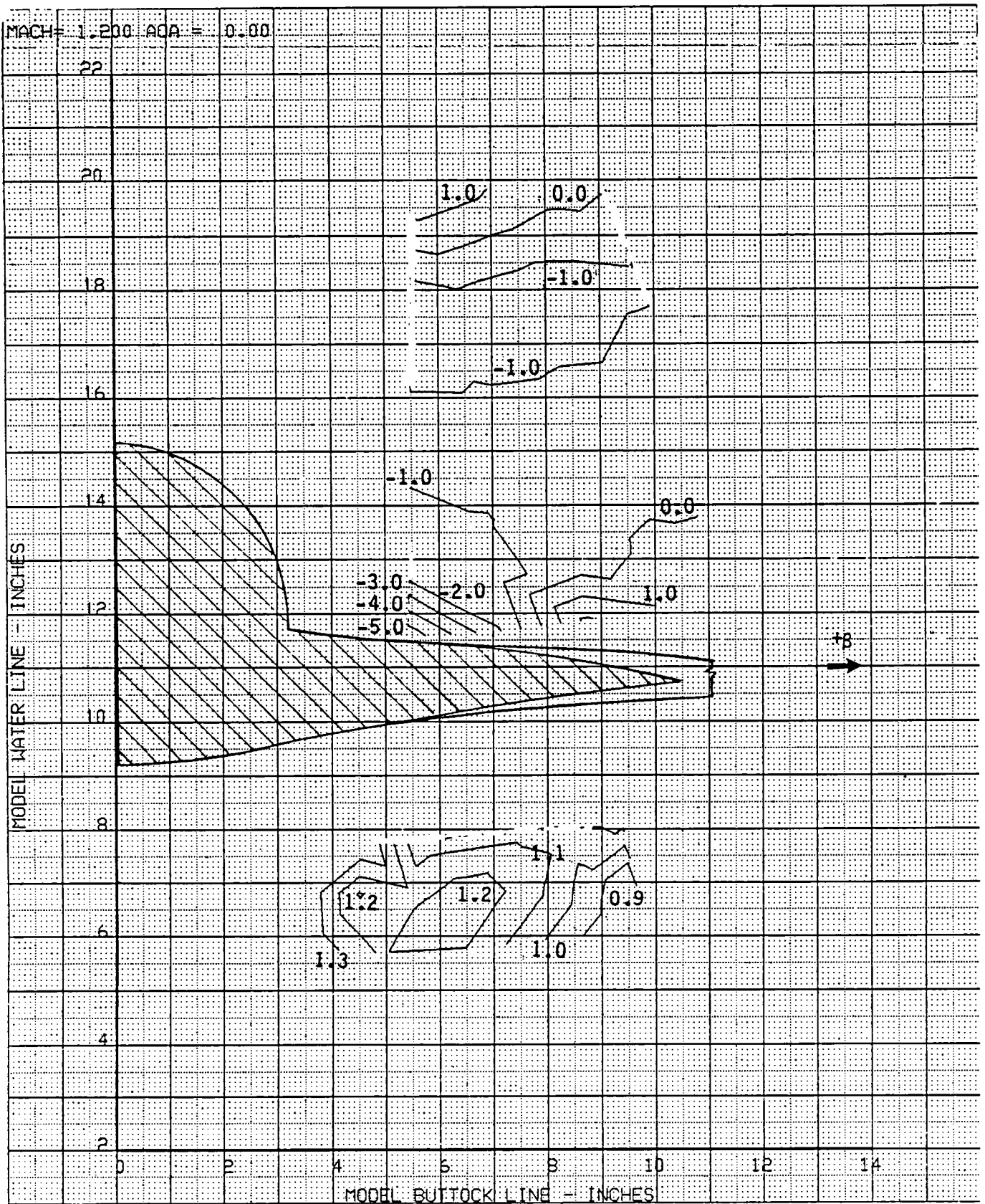
38
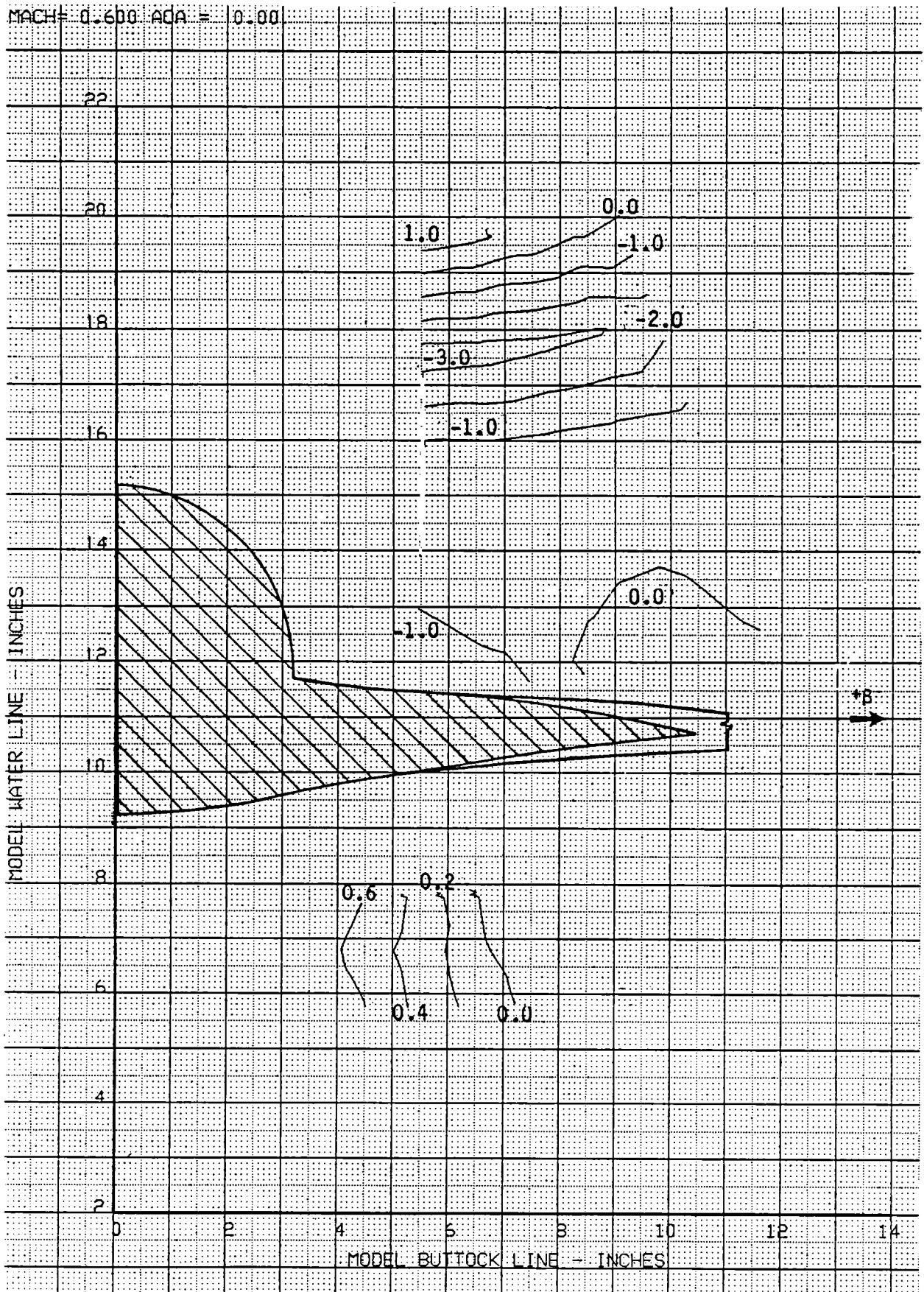
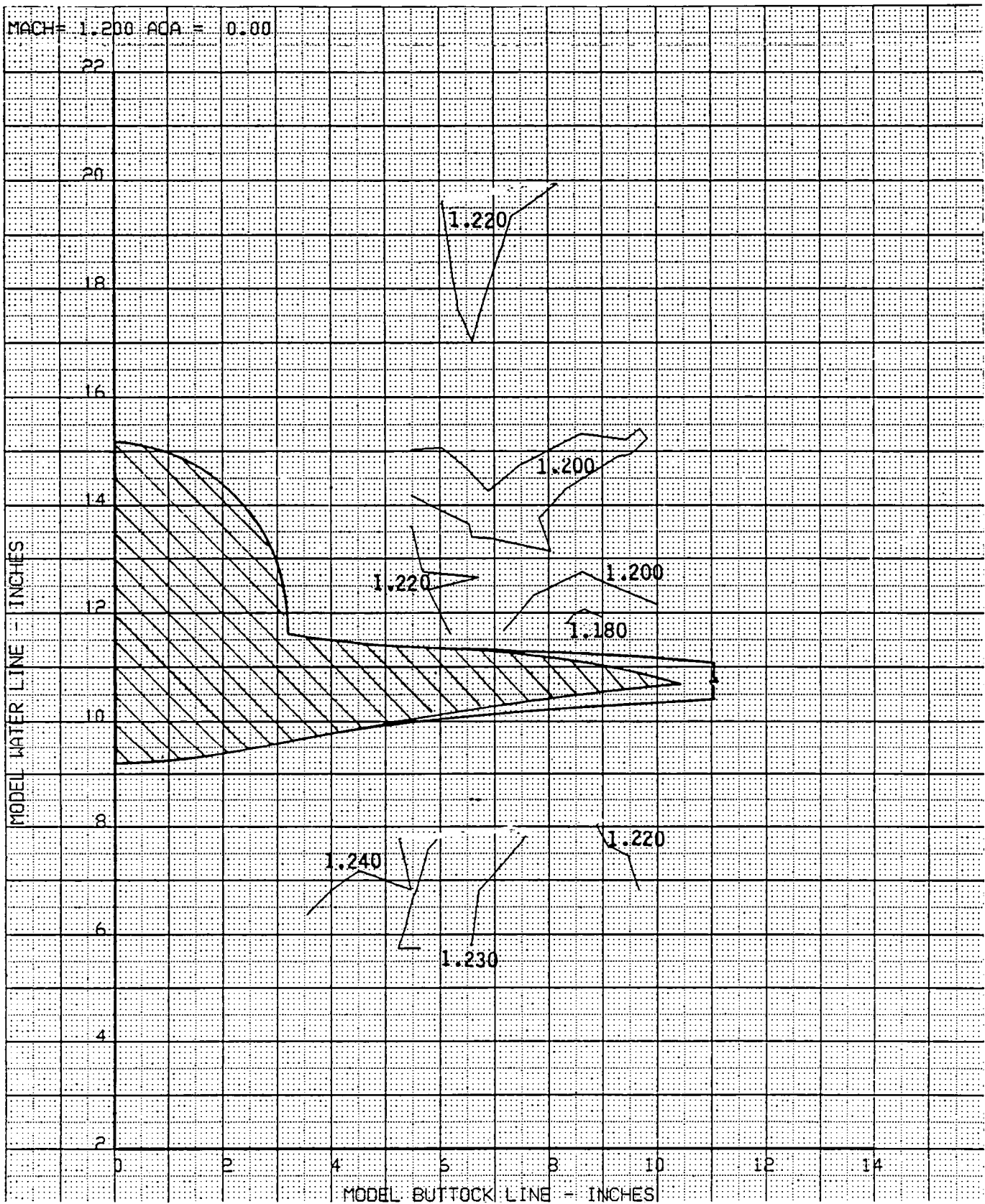*Figure 16c. Local Sideflow Angle, Mach Number = 0.6; Angle of Attack = 0.0 deg*

39
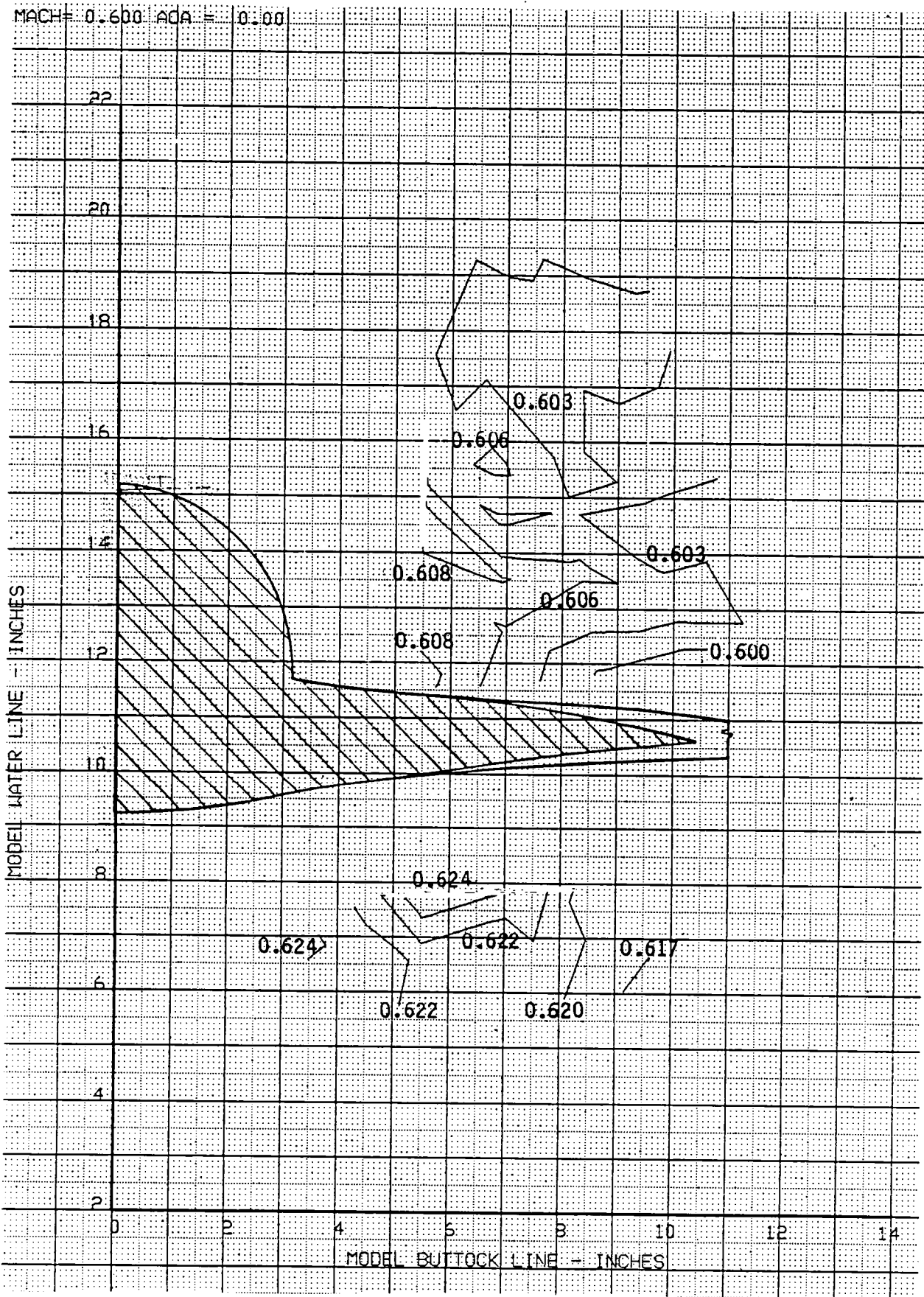
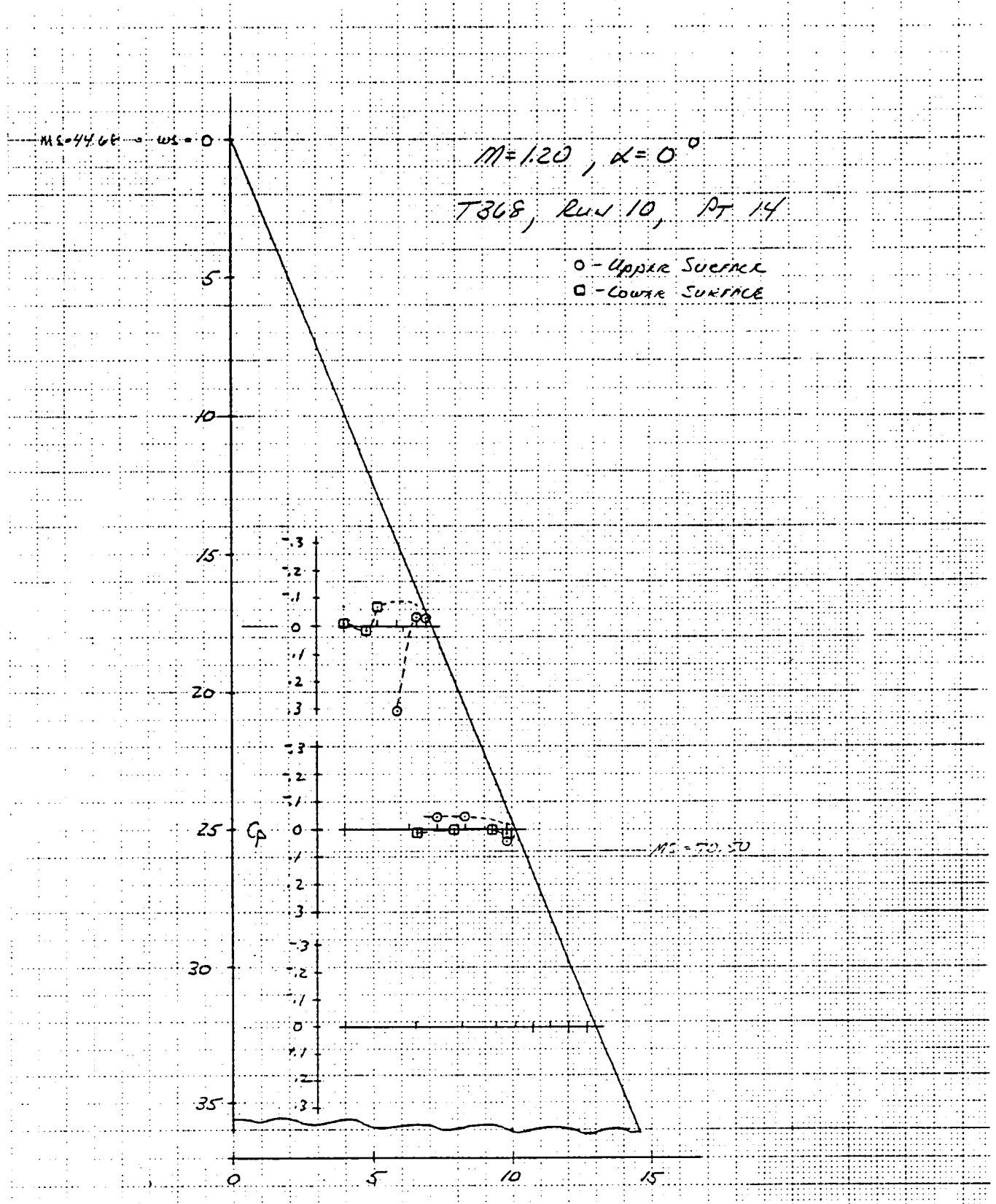Figure 16d. Local Mach Number, Mach Number = 0.6; Angle of Attack = 0.0 deg

40
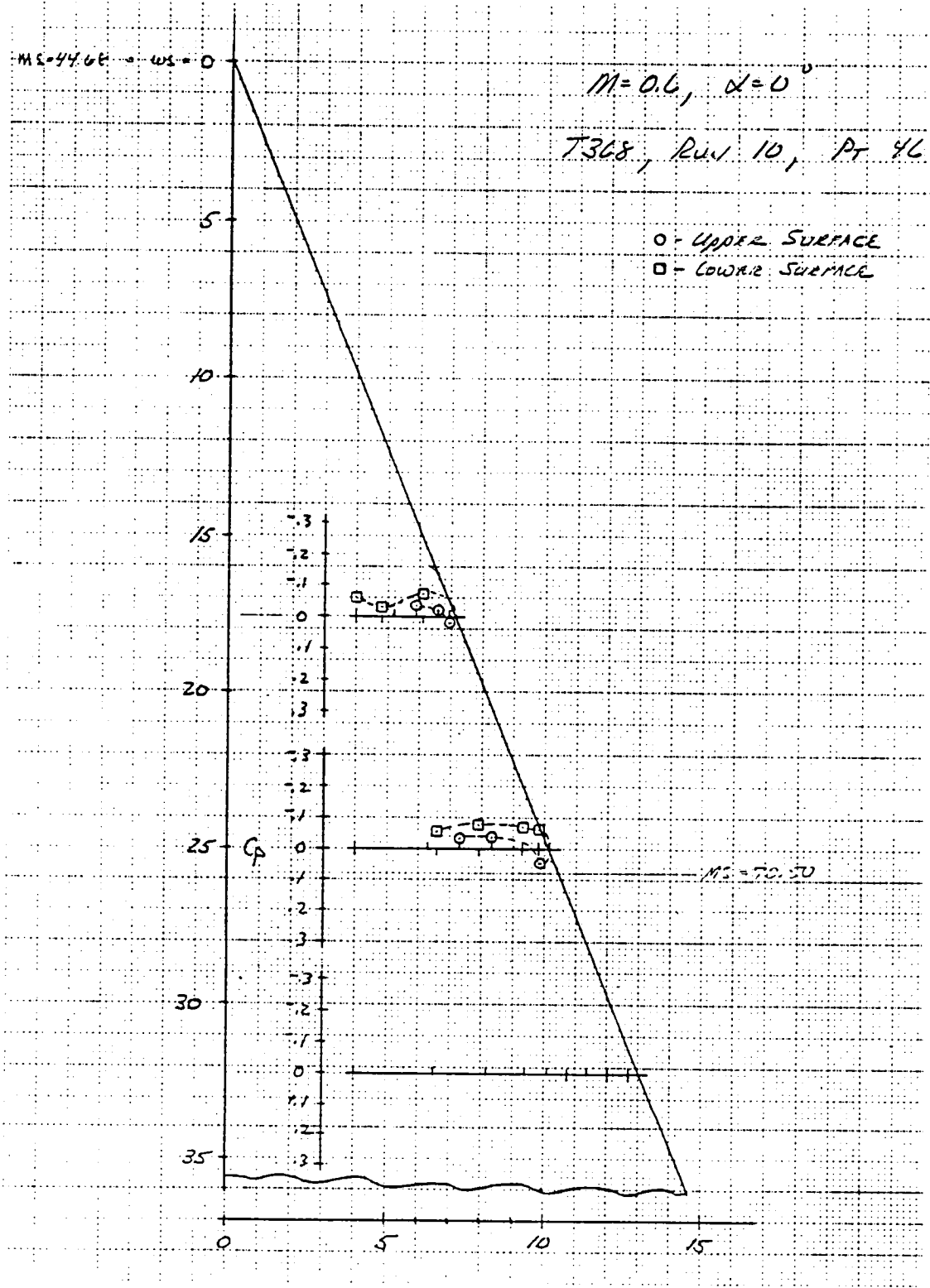
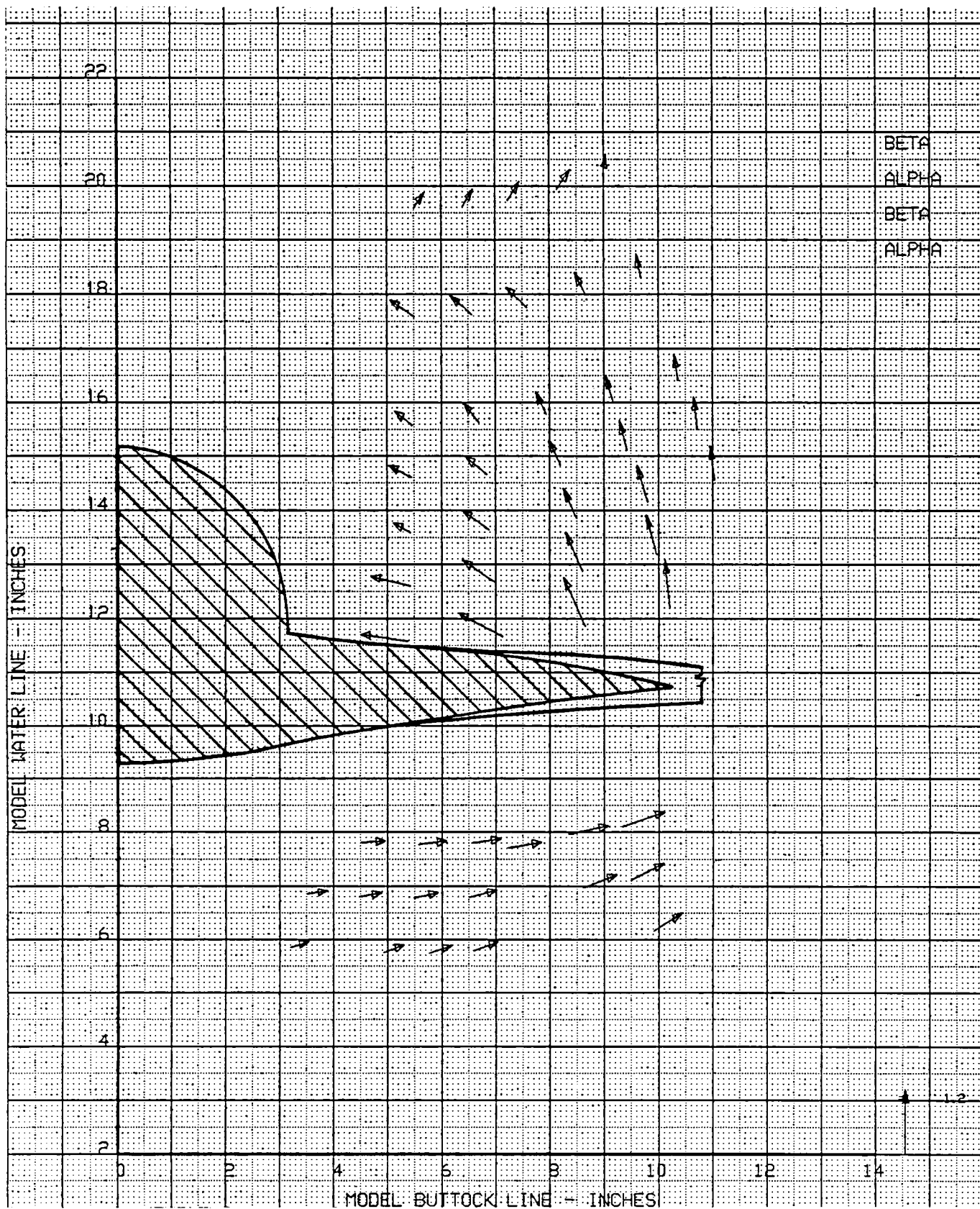Figure 16e. Wing Static Pressure Distributions, M = 0.6, α = 0 deg

41
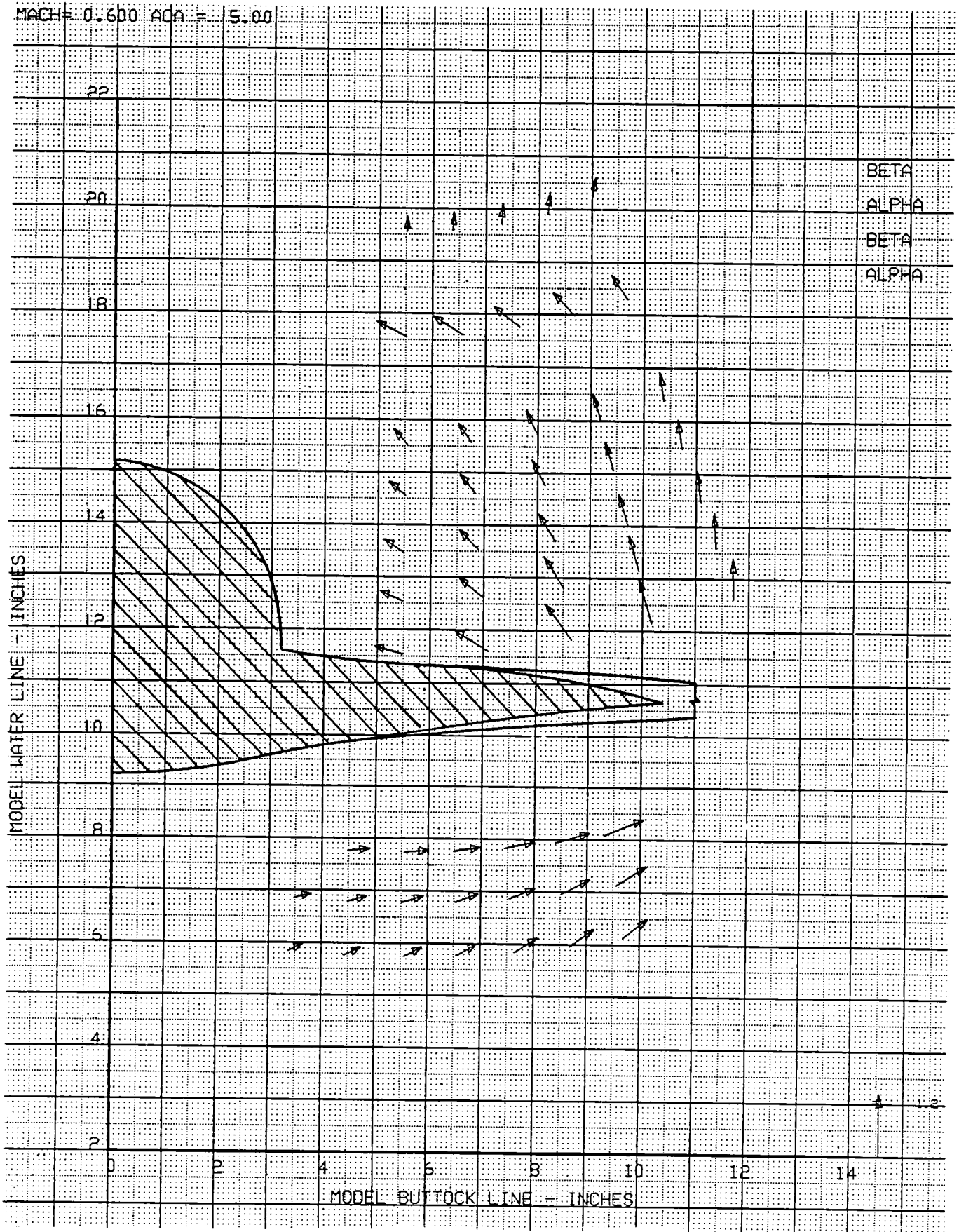
Figure 17a. Local Flowfield, MSTA = 70.50; Mach Number = 0.6; Angle of Attack = 5.0 deg

42
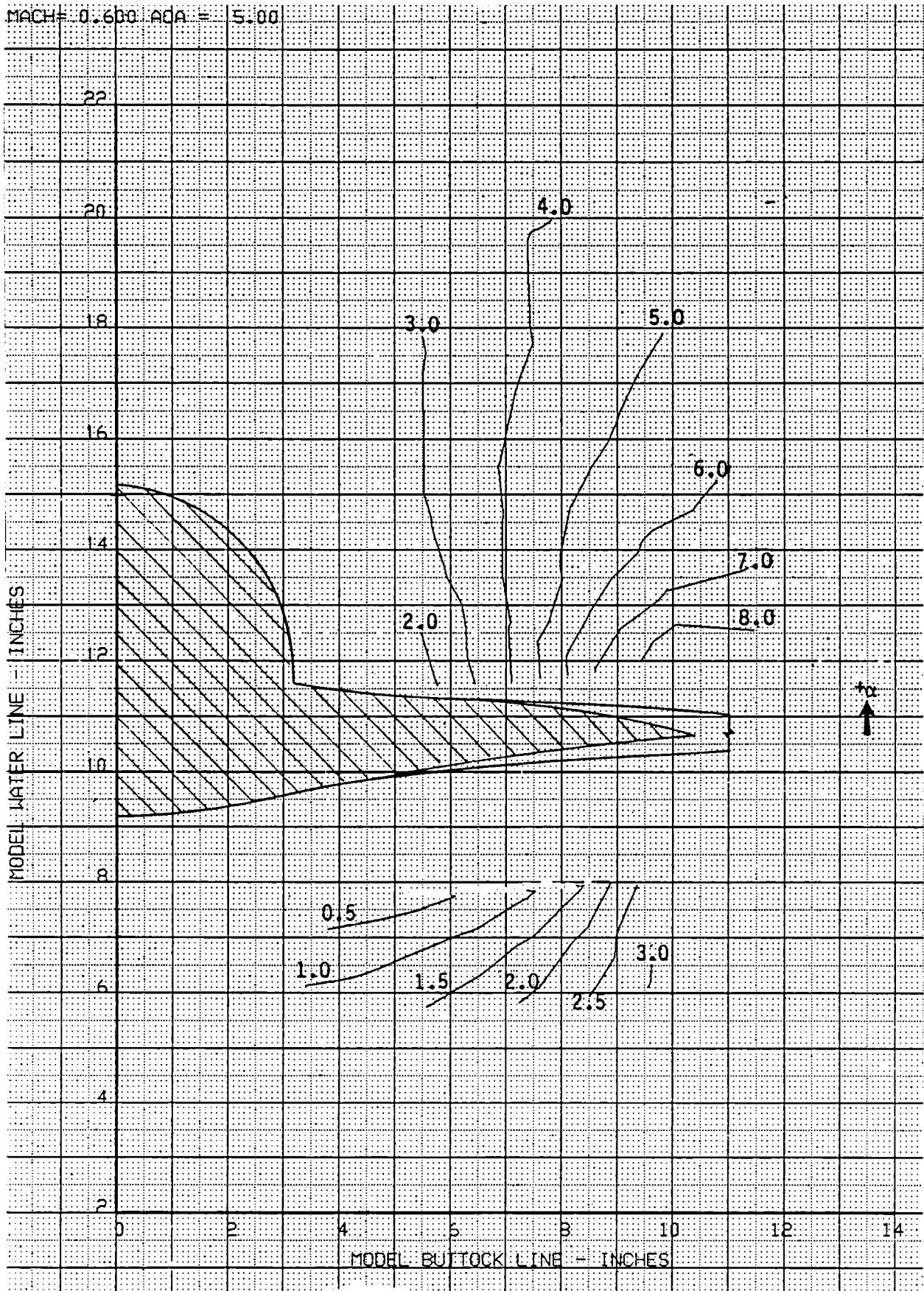
Figure 17b. Local Angle of Attack, Mach Number = 0.6; Angle of Attack = 5.0 deg

43

MACH= 0.600 AOA = 5.00
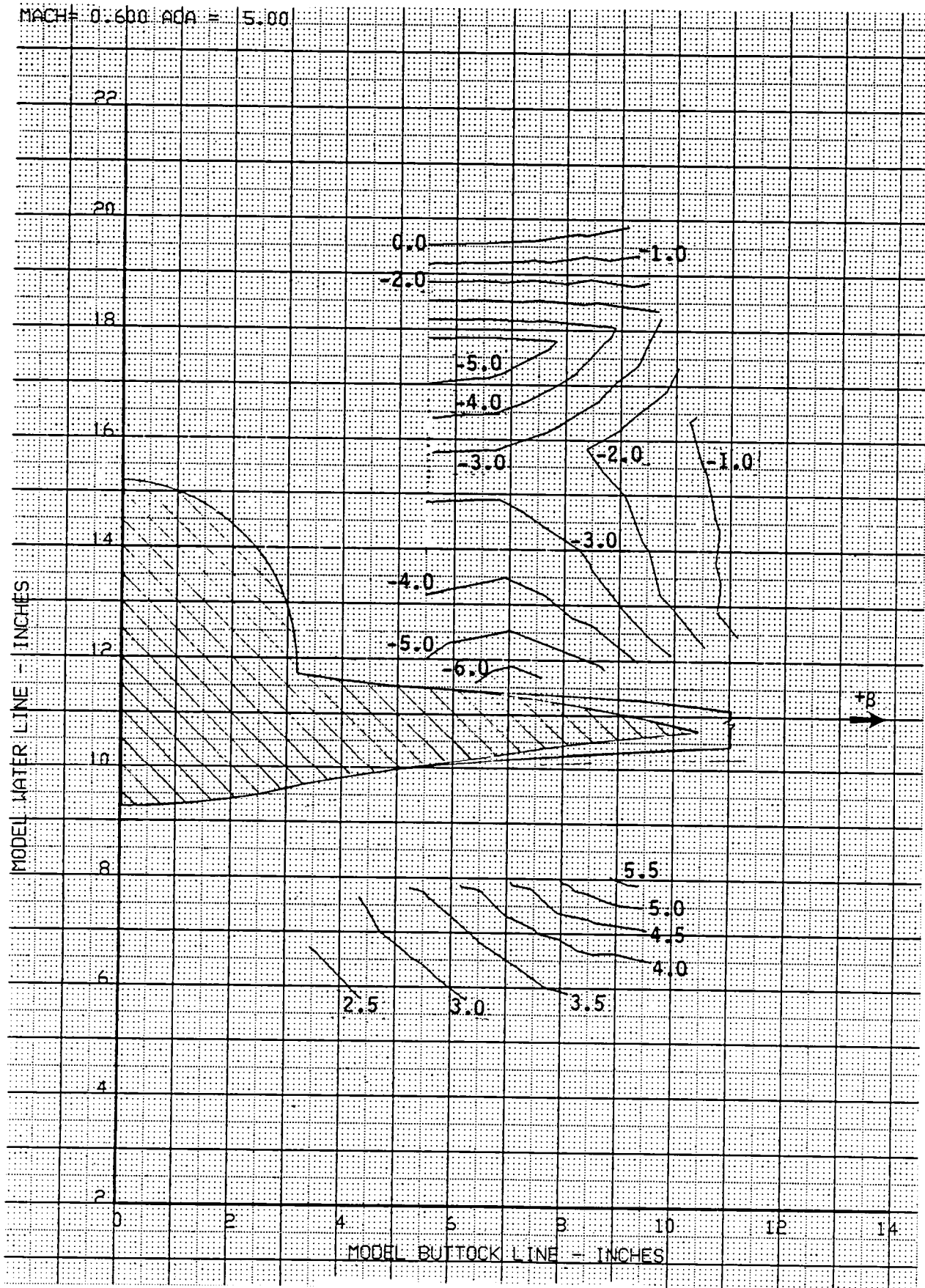
Figure 17c. Local Sideflow Angle, Mach Number = 0.6; Angle of Attack = 5.0 deg

44
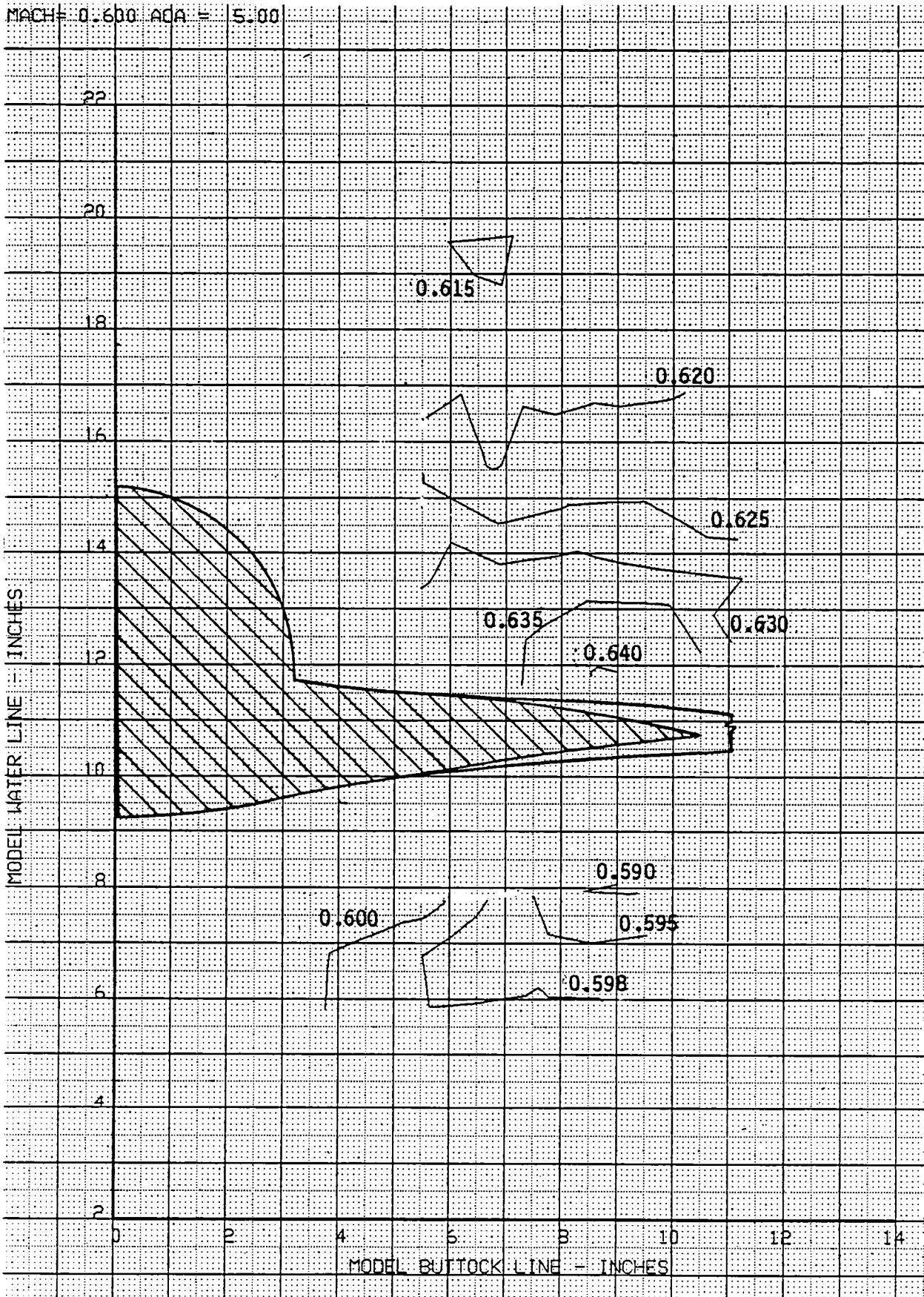
Figure 17d. Local Mach Number, Mach Number = 0.6; Angle of Attack = 5.0 deg

45
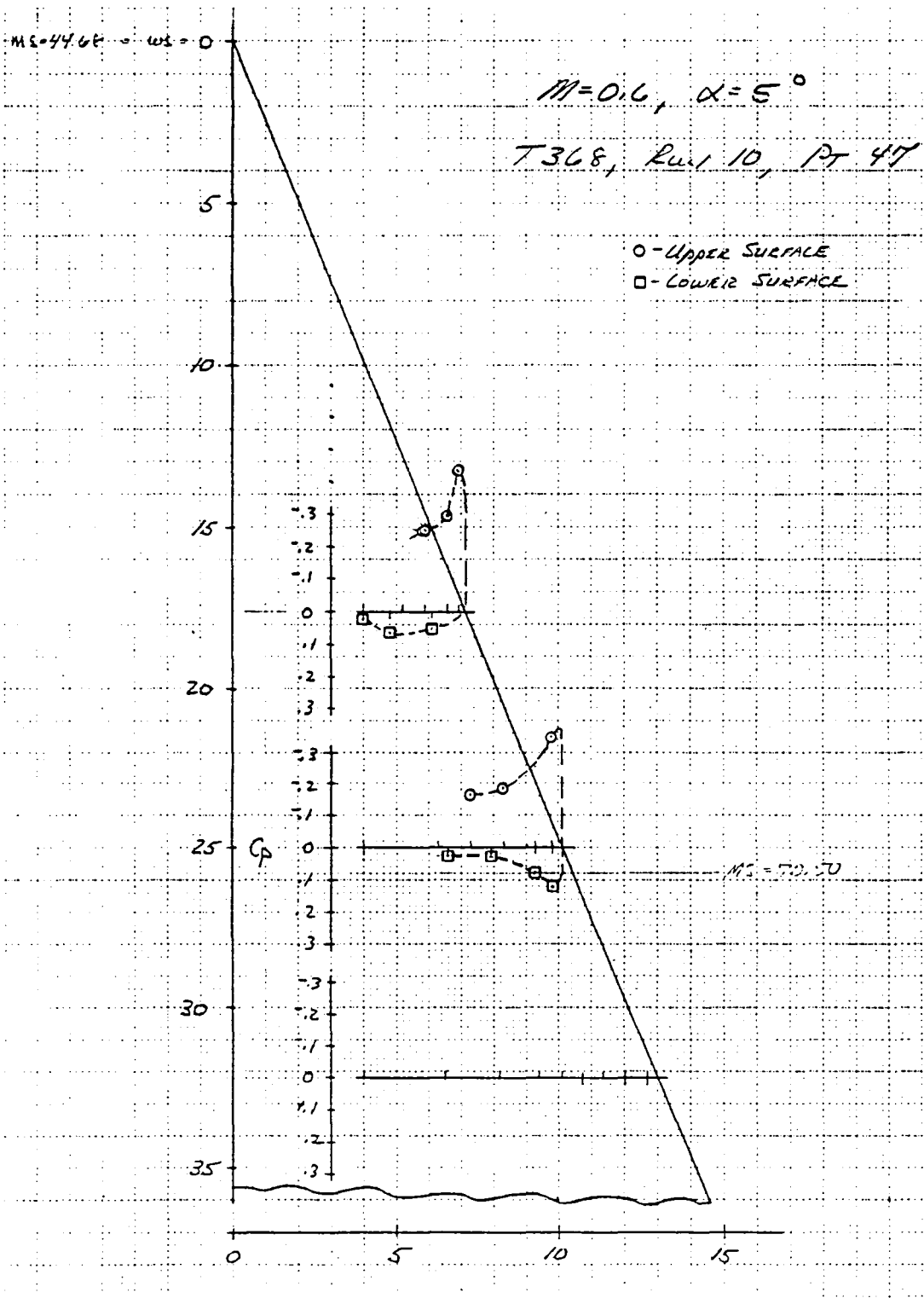
Figure 17e. Wing Static Pressure Distributions, M = 0.6, α = 5.0 deg

46
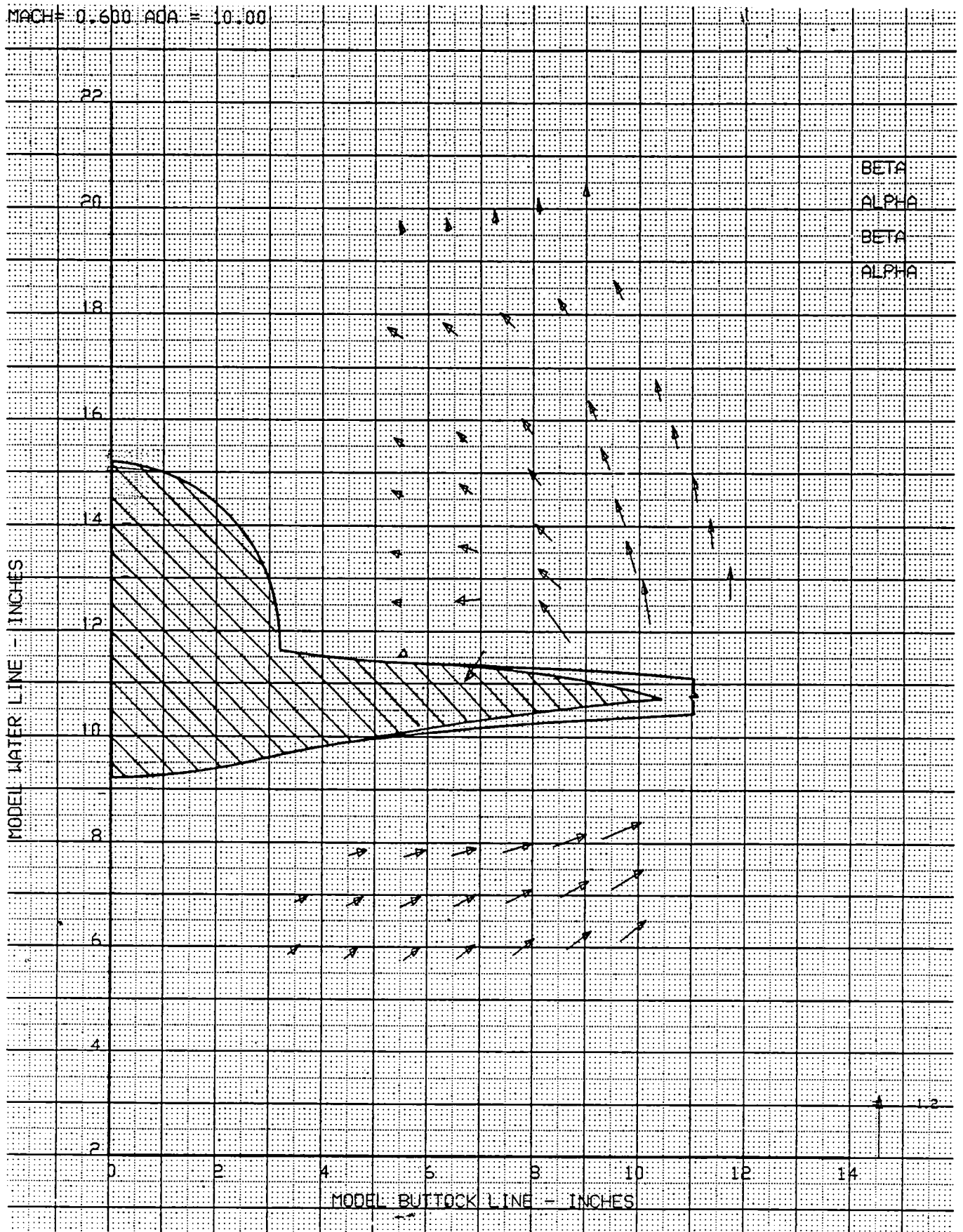
Figure 18a. Local Flowfield, MSTA = 70.50; Mach Number = 0.6; Angle of Attack = 10.0 deg

47
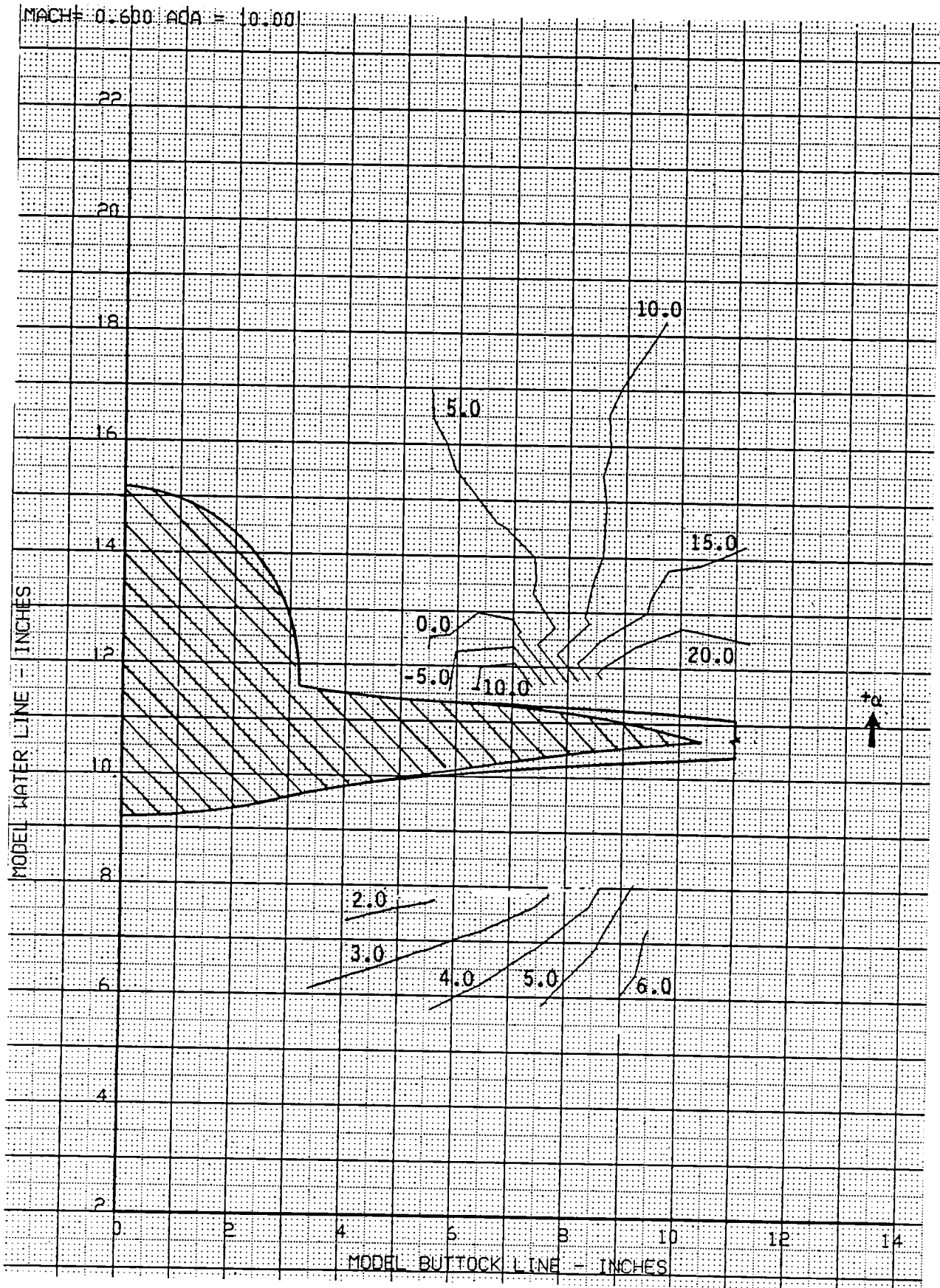
Figure 18b. Local Angle of Attack, Mach Number = 0.6; Angle of Attack = 10.0 deg

48
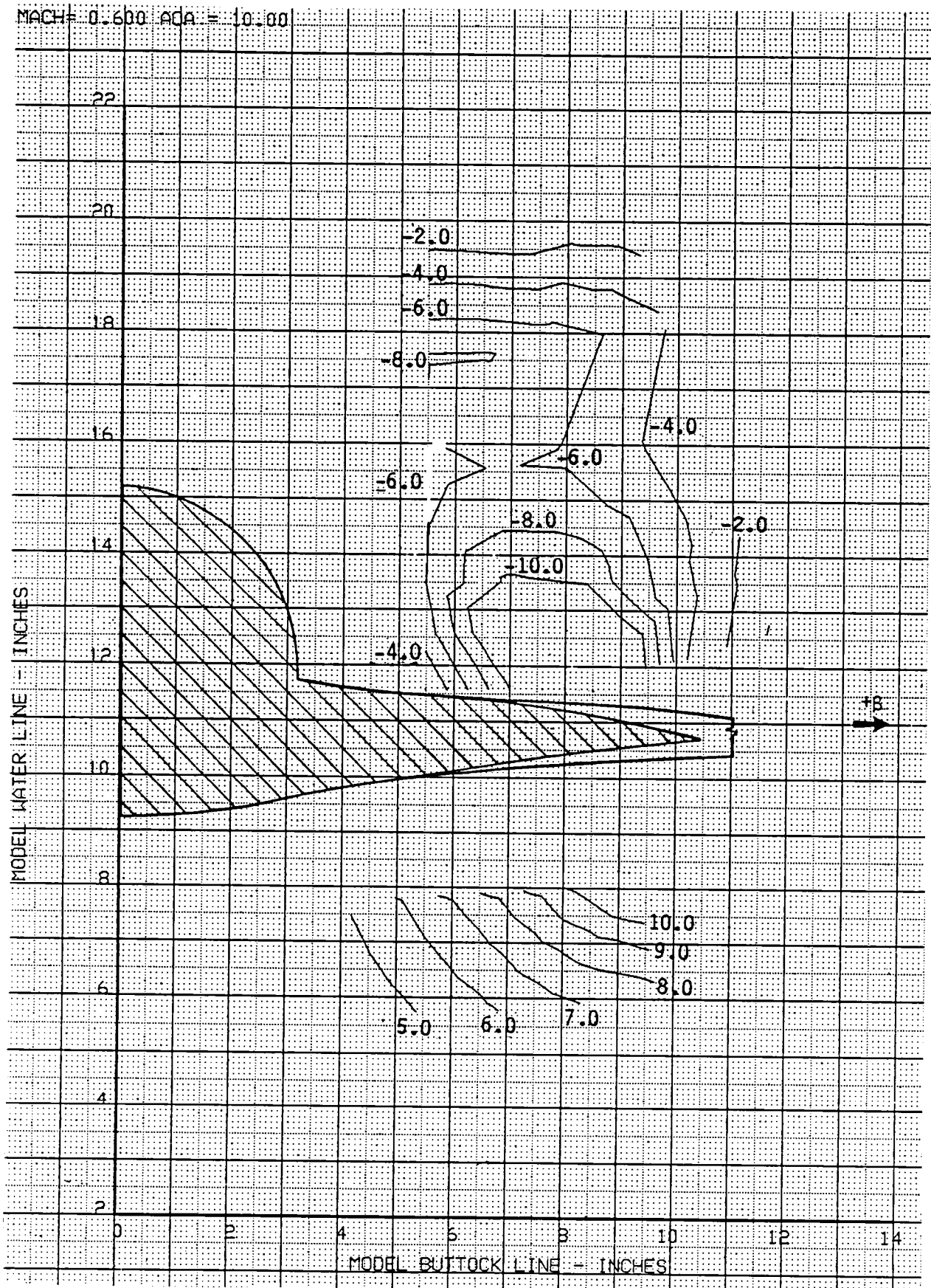
*Figure 18c. Local Sideflow Angle, Mach Number = 0.6; Angle of Attack = 10.0 deg*

49
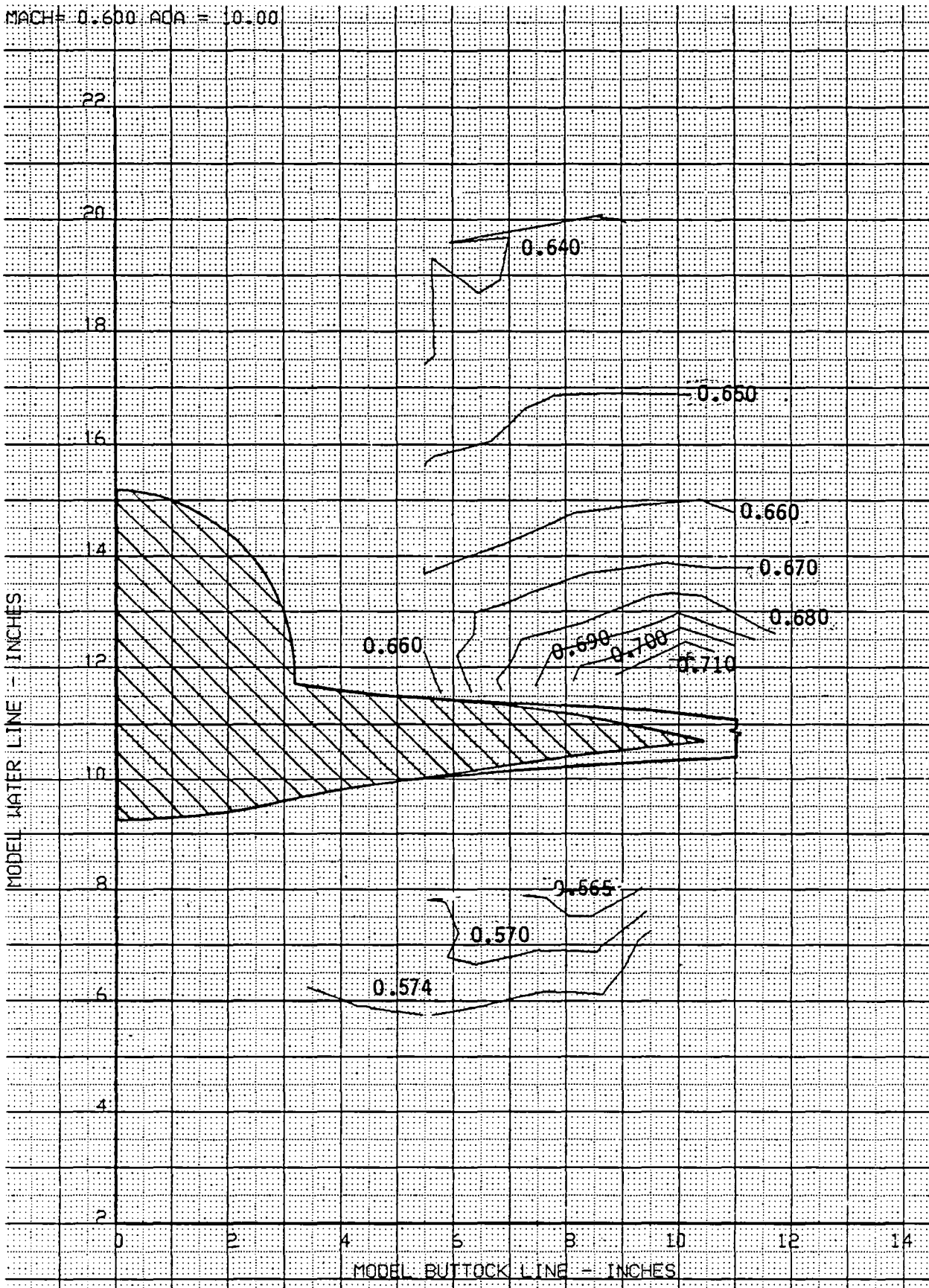
Figure 18d. Local Mach Number, Mach Number = 0.6; Angle of Attack = 10.0 deg

50
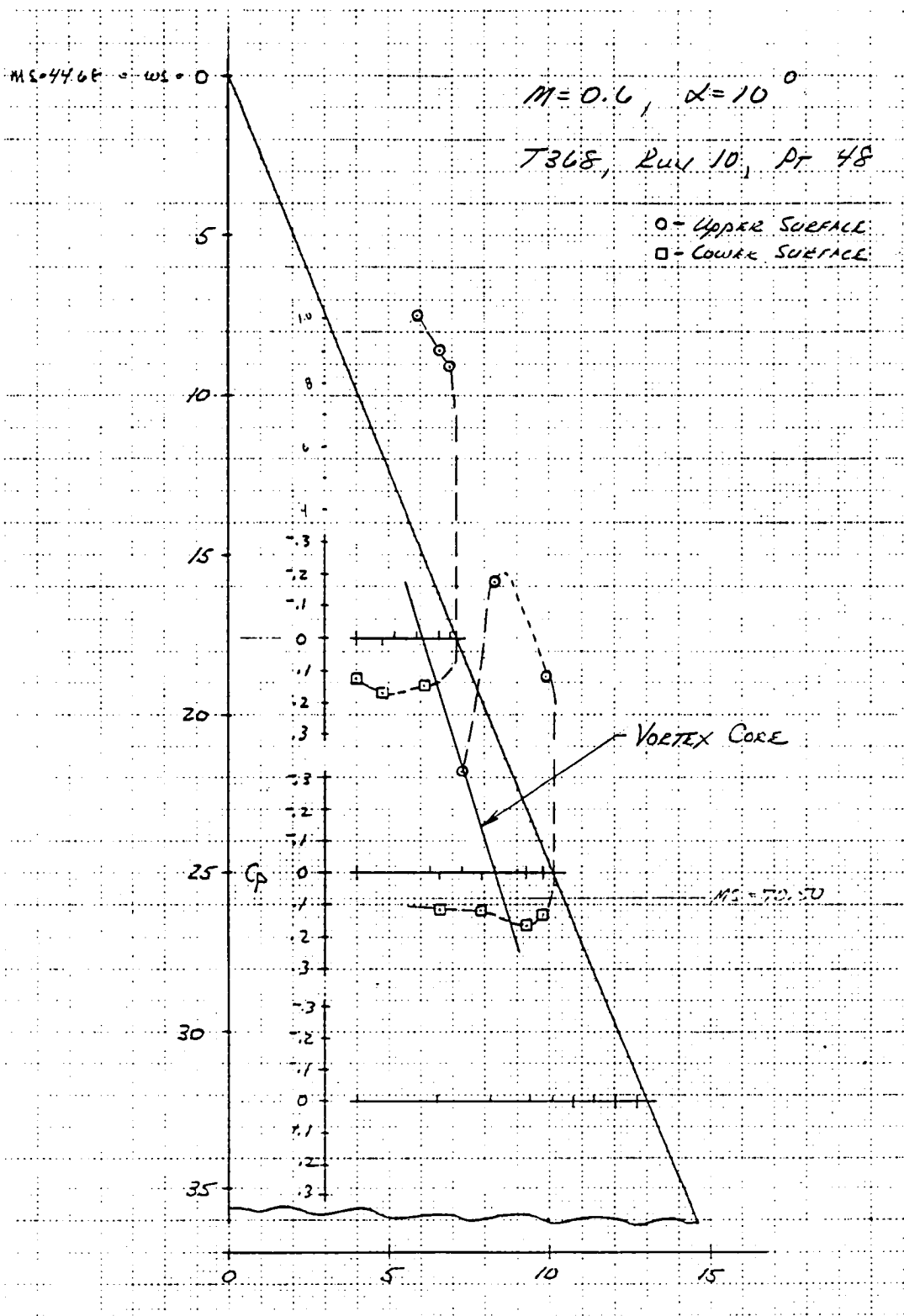
Figure 18e. Wing Static Pressure Distributions, M = 0.6, α = 5.0 deg
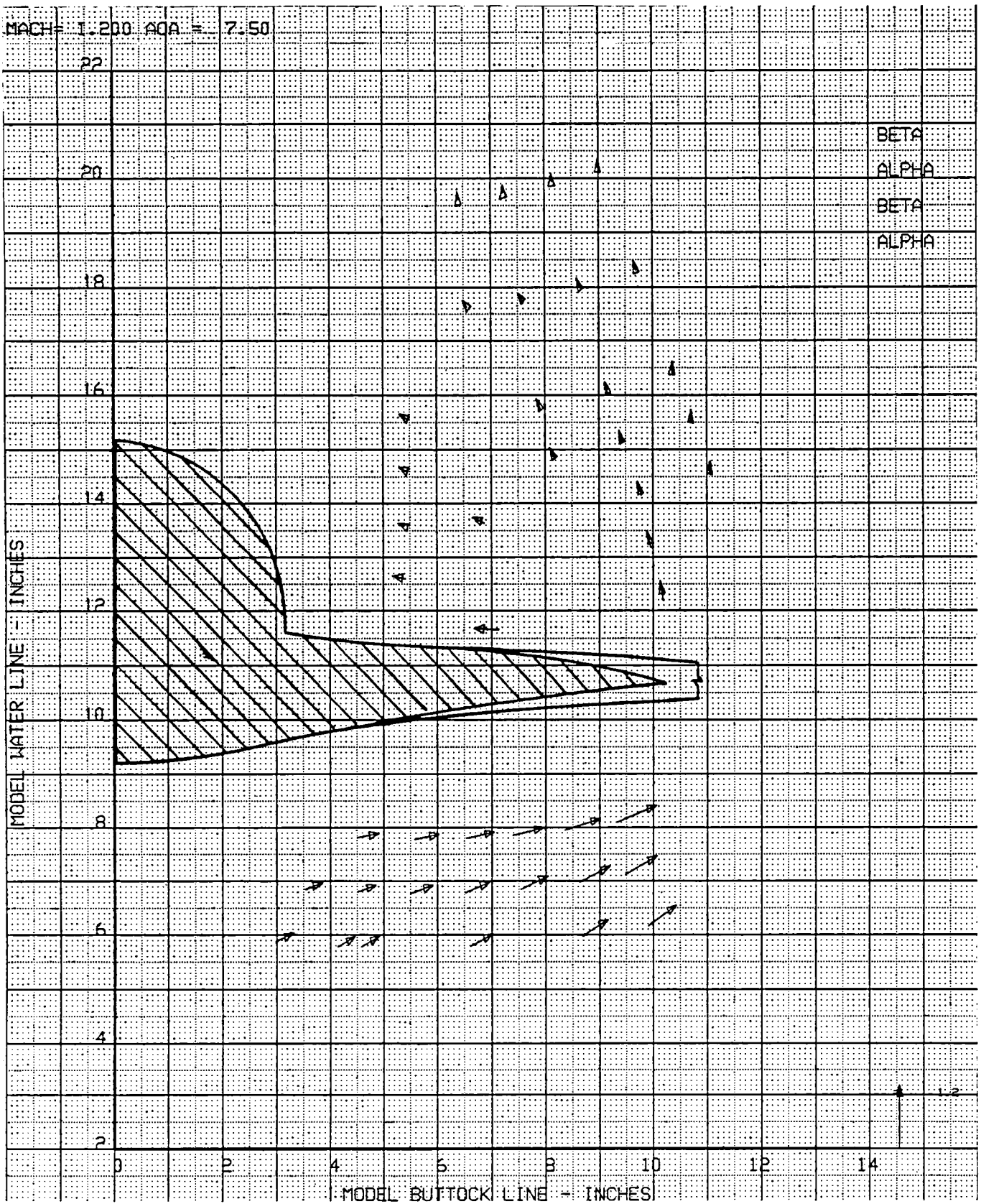
MACH= 0.900 AOA = 0.00
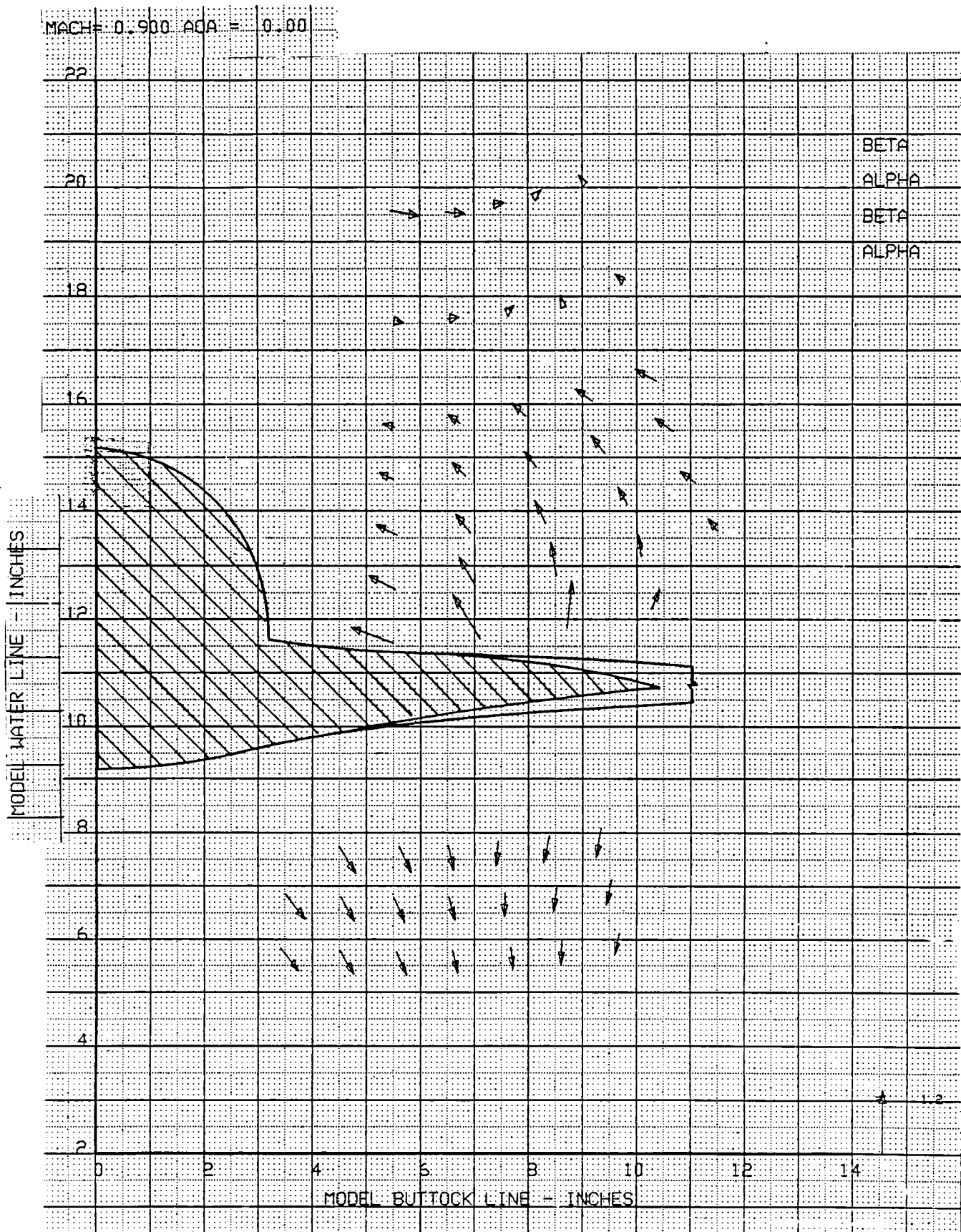
Figure 19a. Local Flowfield, MSTA = 70.50; Mach Number = 0.9; Angle of Attack = 0.0 deg

52
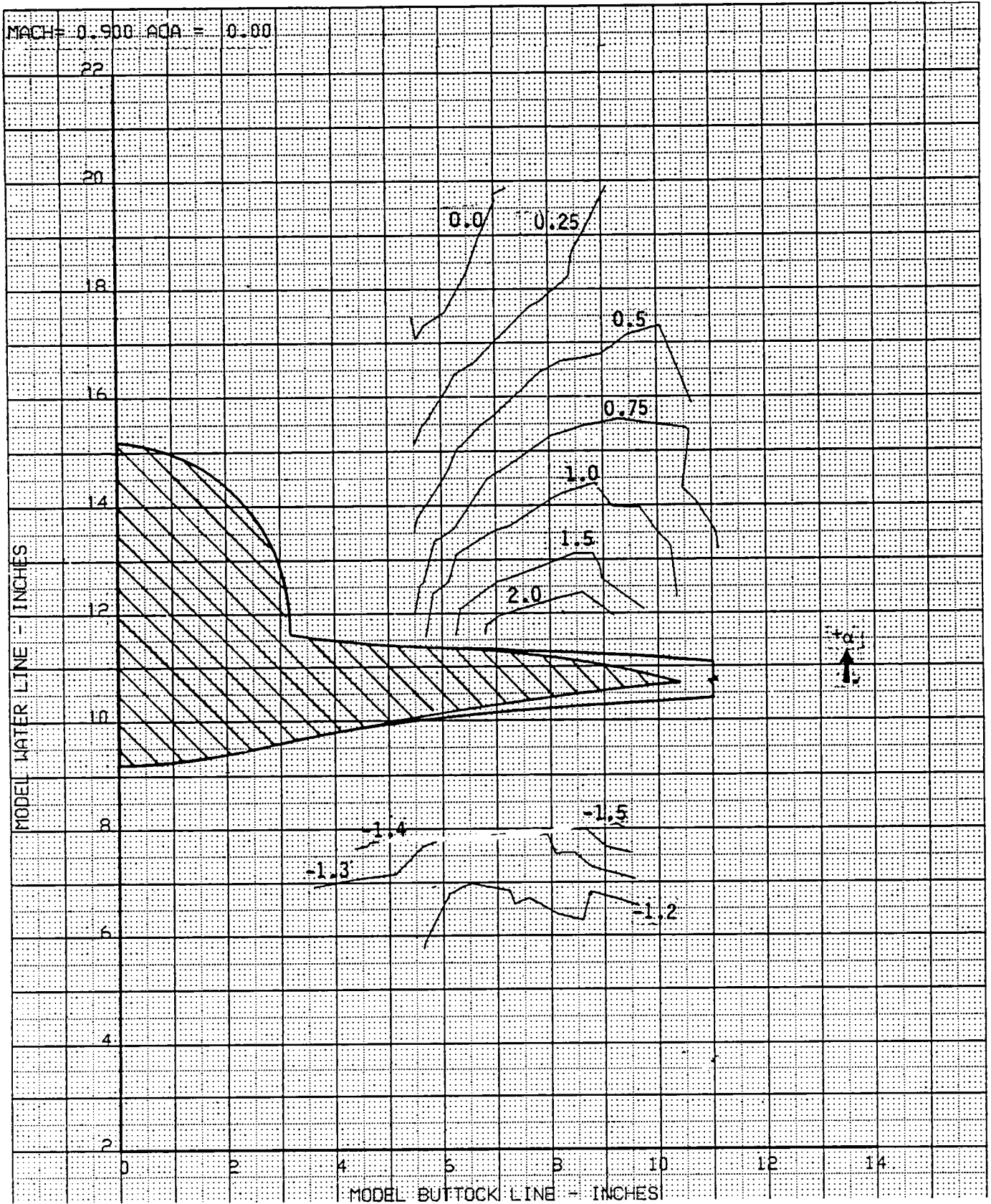
Figure 19b. Local Angle of Attack, Mach Number = 0.9; Angle of Attack = 0.0 deg

53
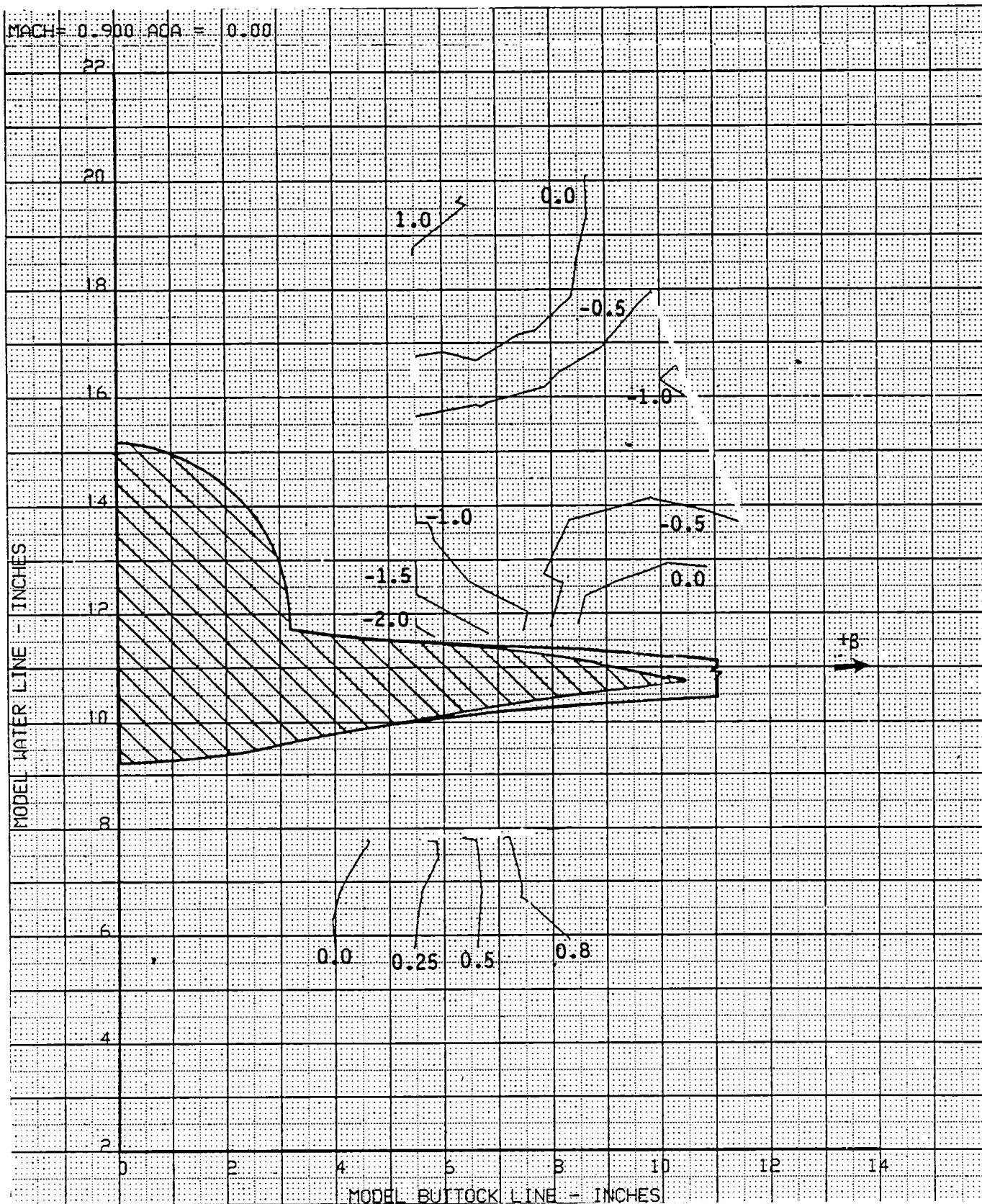
Figure 19c. Local Sideflow Angle, Mach Number = 0.9; Angle of Attack = 0.0 deg

54
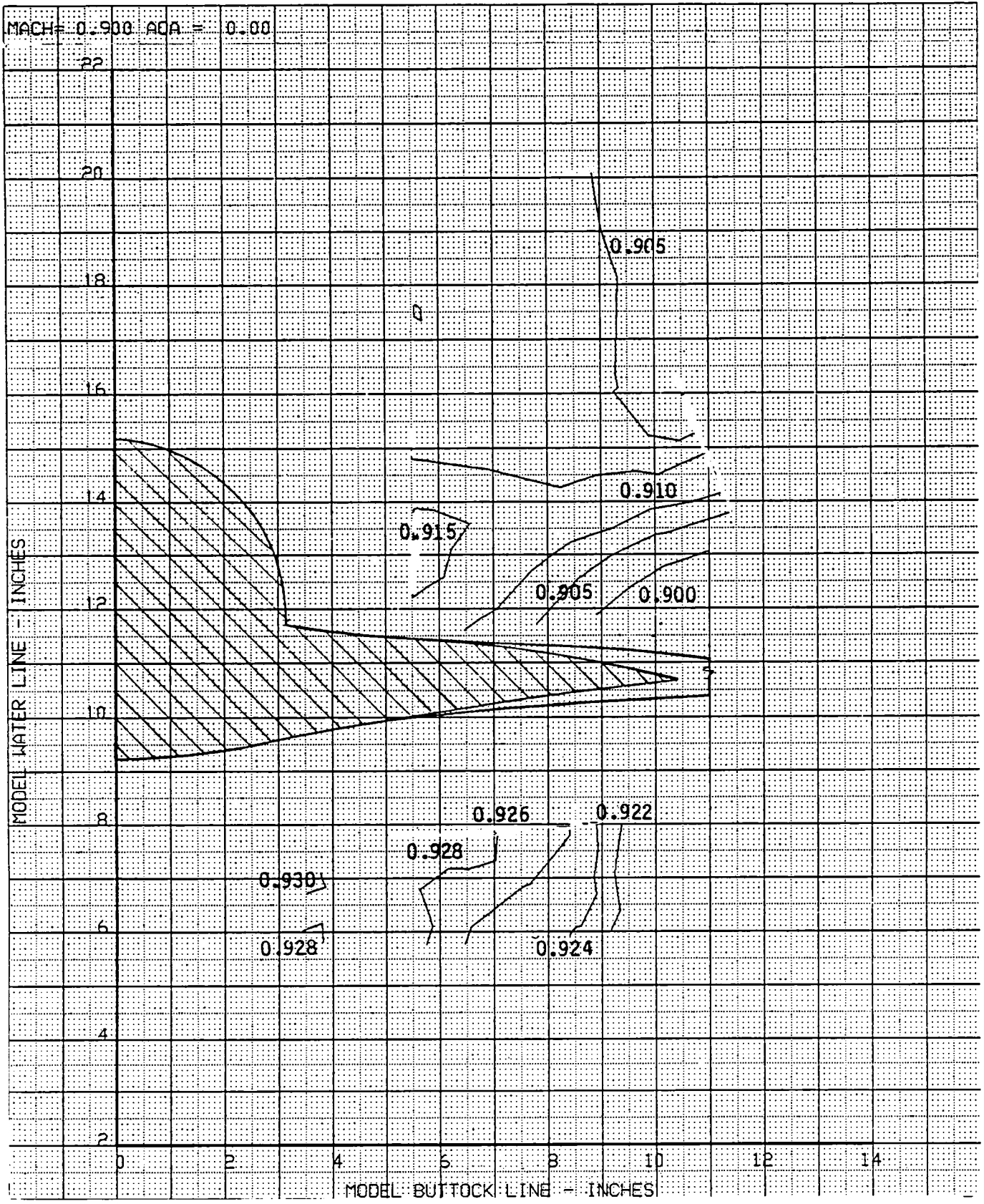
Figure 19d. Local Mach Number; Mach Number = 0.9; Angle of Attack = 0.0 deg

55
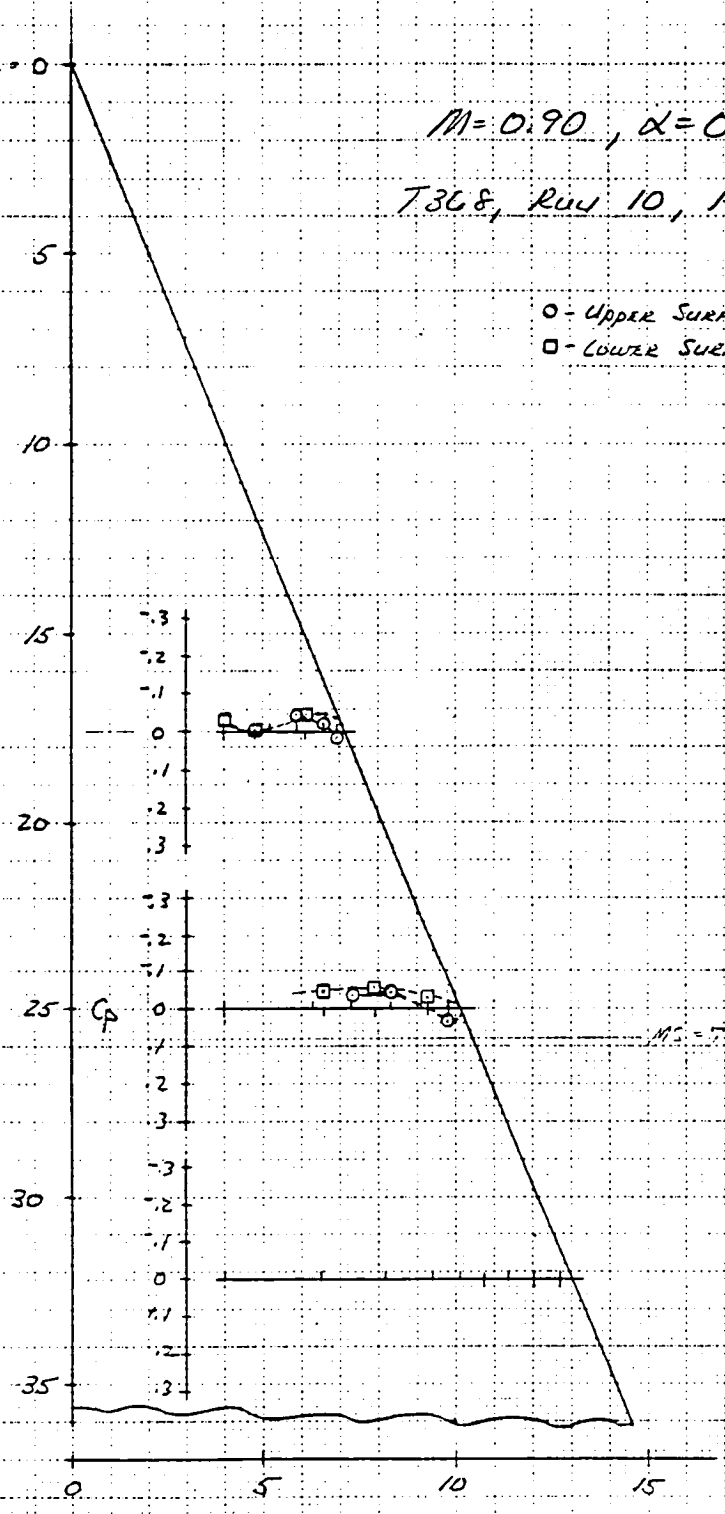
Figure 19e. Wing Static Pressure Distributions, M = 0.9, α = 0.0 deg

56
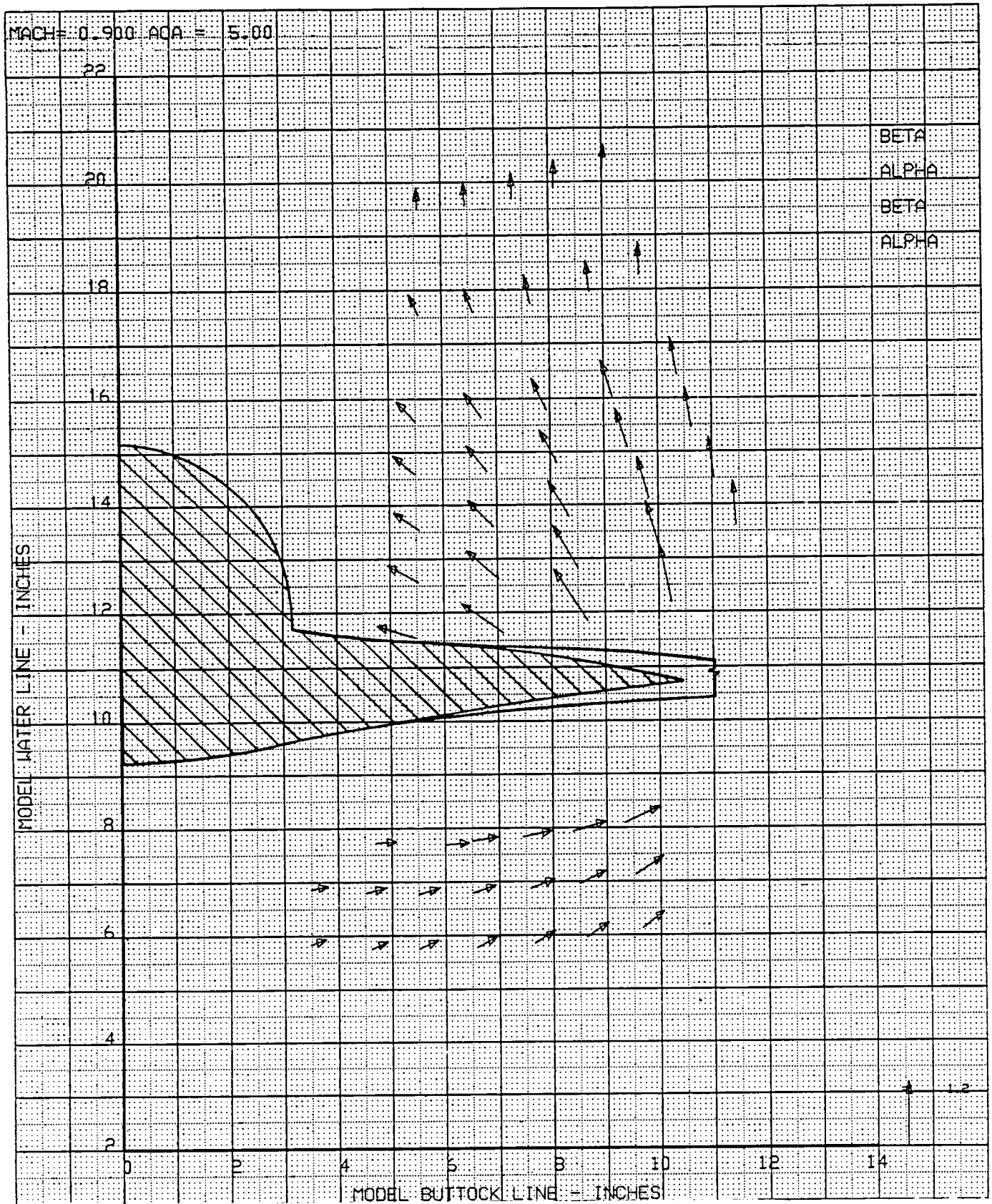
Figure 20a. Local Flowfield, MSTA = 70.50; Mach Number = 0.9; Angle of Attack = 5.0 deg

57
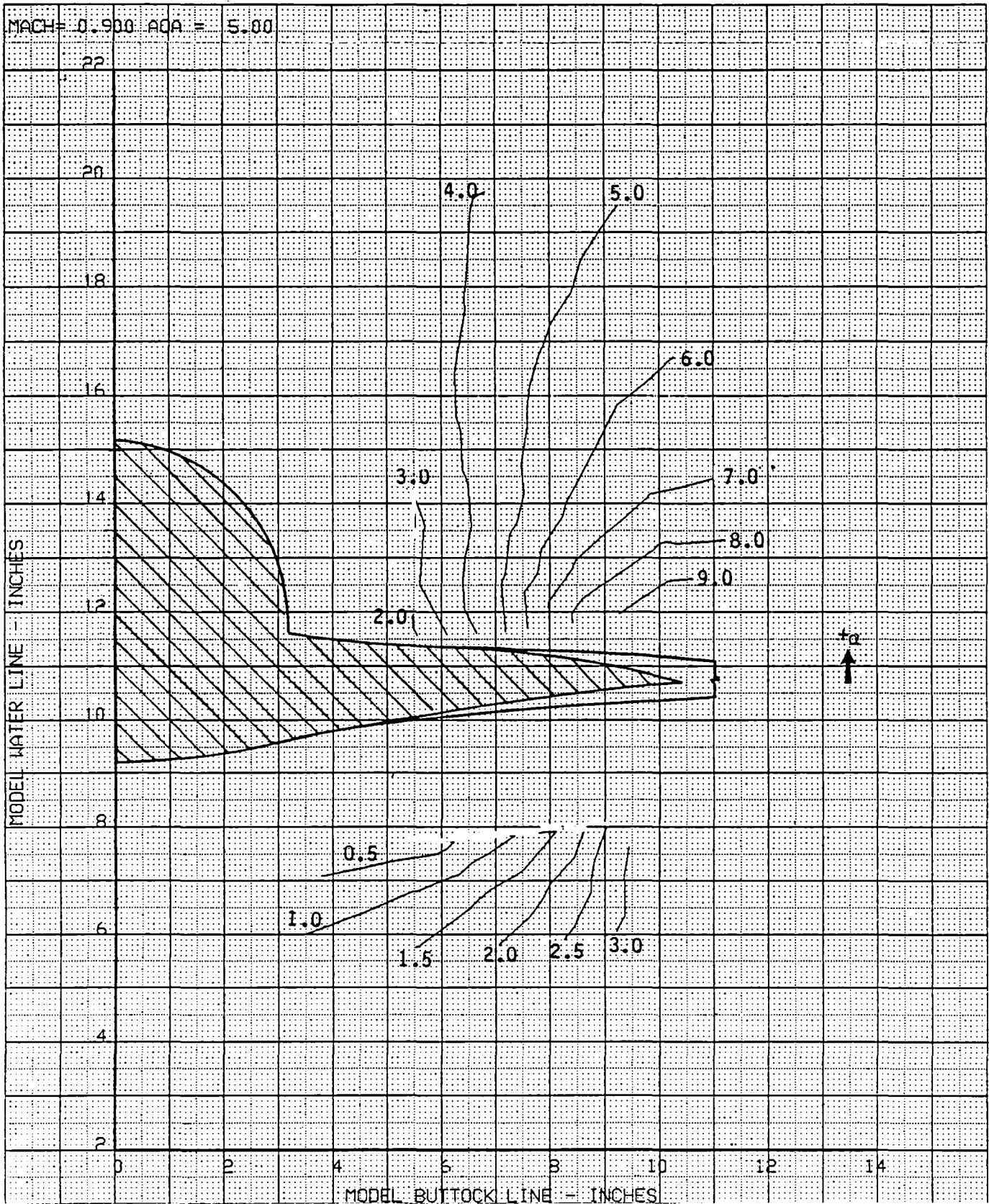
Figure 20b. Local Angle of Attack, Mach Number = 0.9; Angle of Attack = 5.0 deg
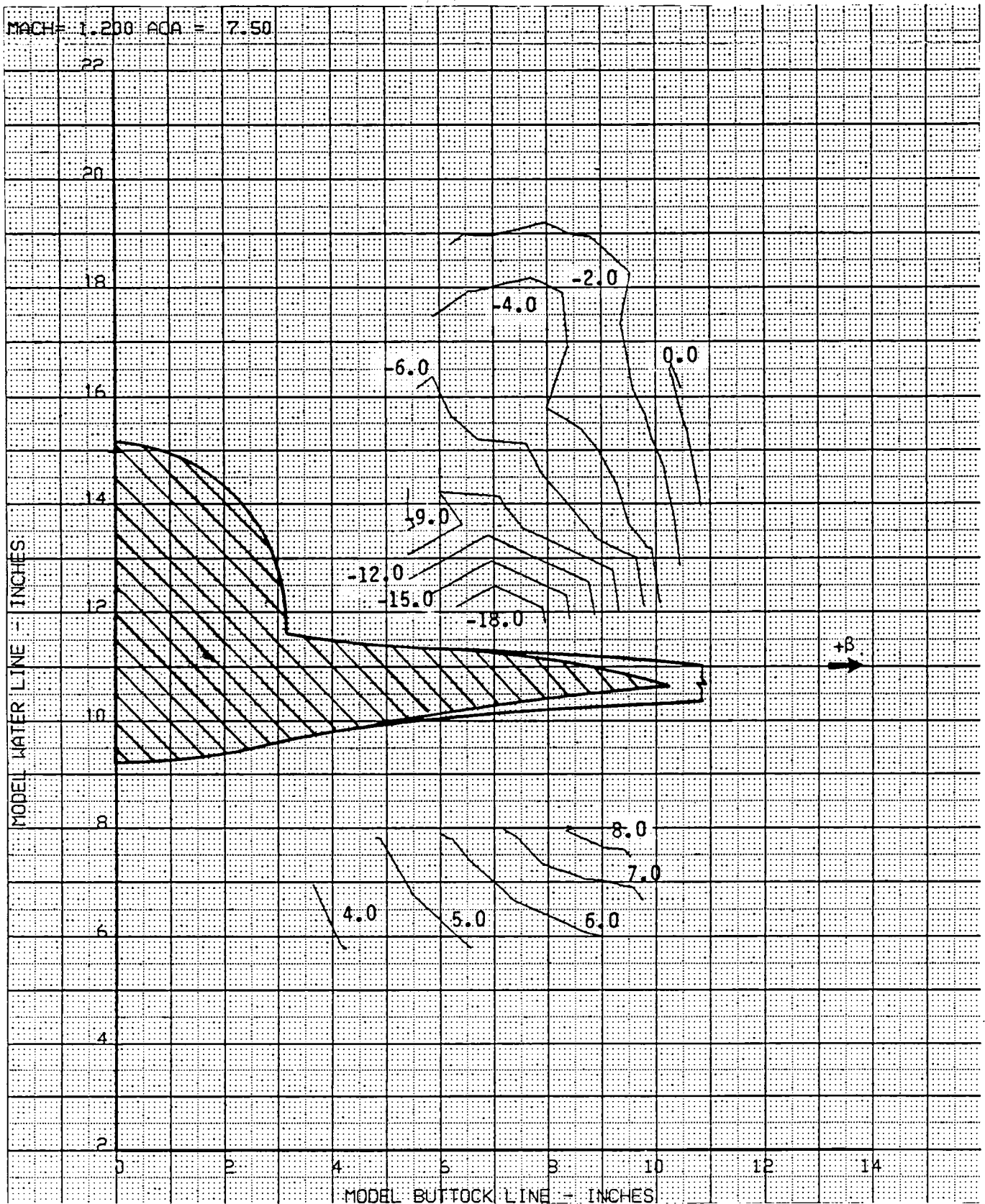
58
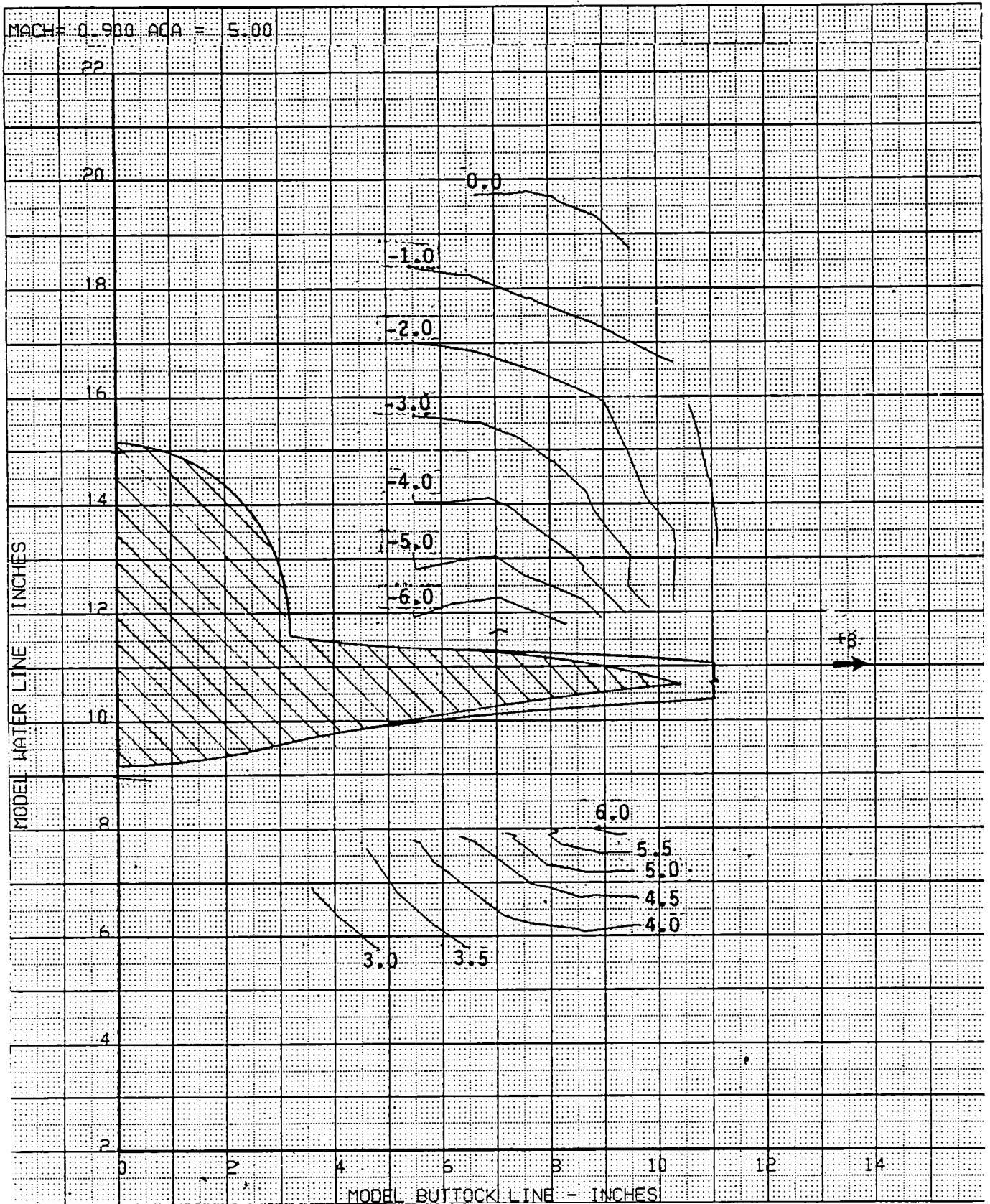
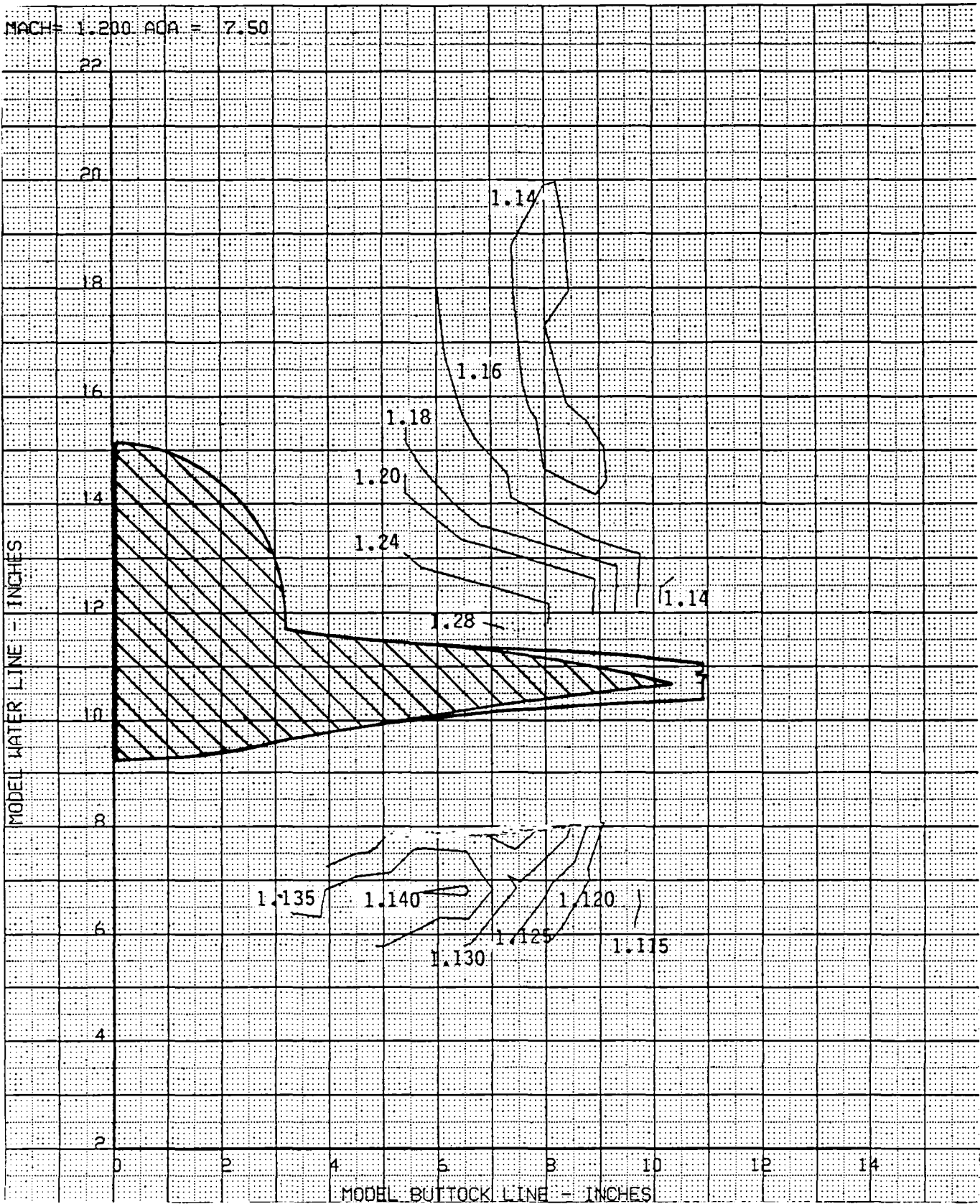Figure 20c. Local Sideflow Angle, Mach Number = 0.9; Angle of Attack = 5.0 deg

59
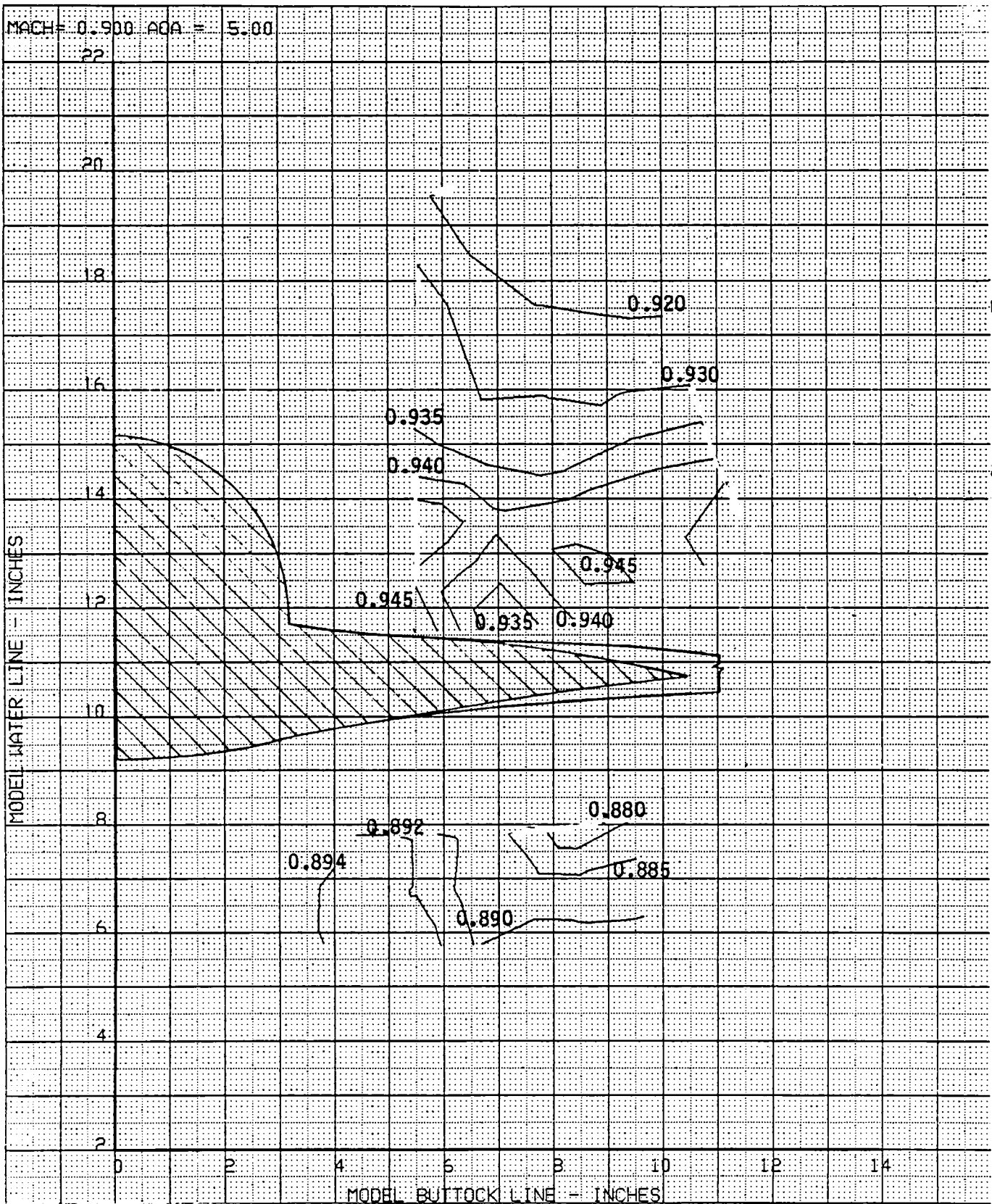
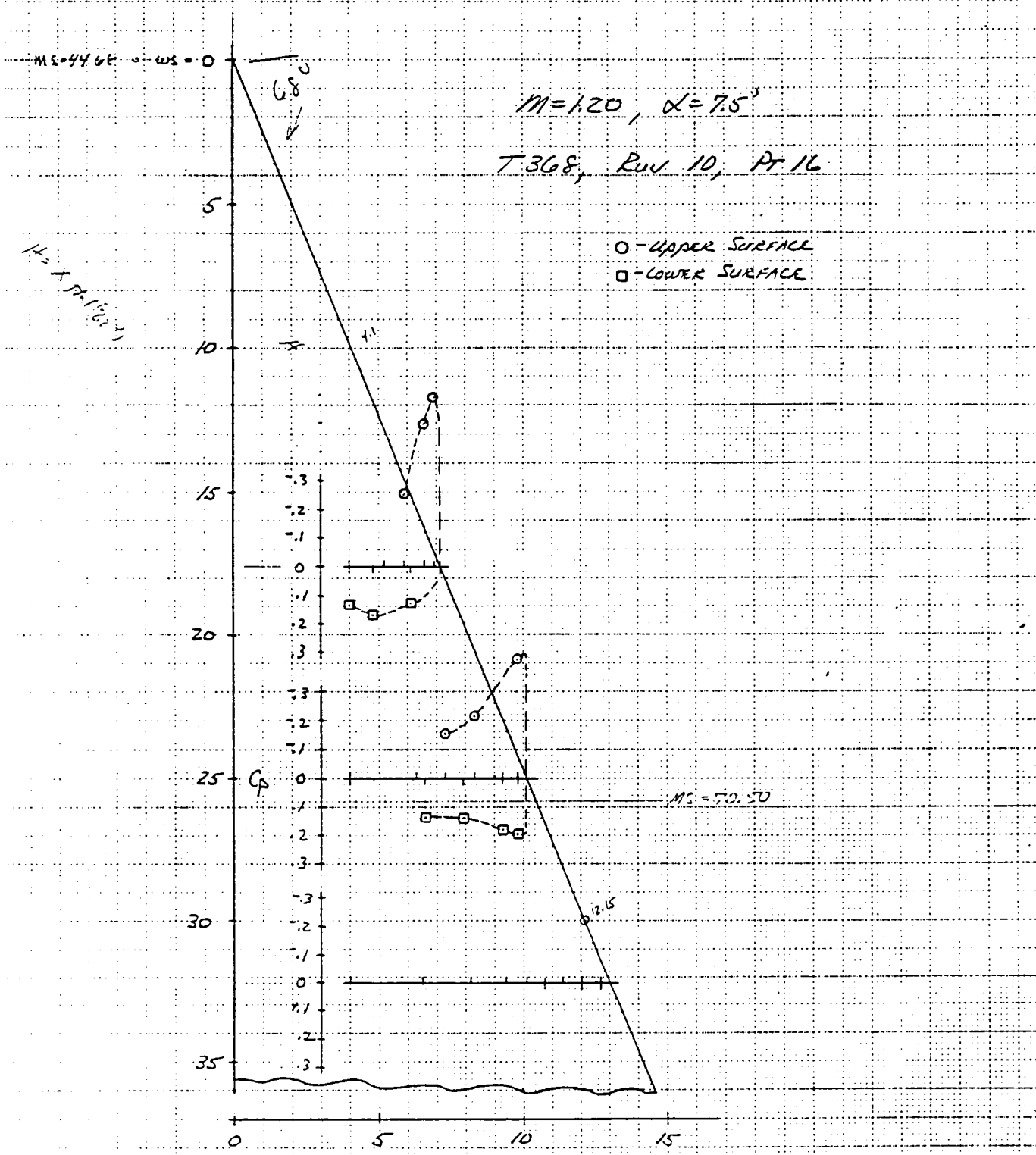*Figure 20d. Local Mach Number, Mach Number = 0.9; Angle of Attack = 5.0 deg*

60
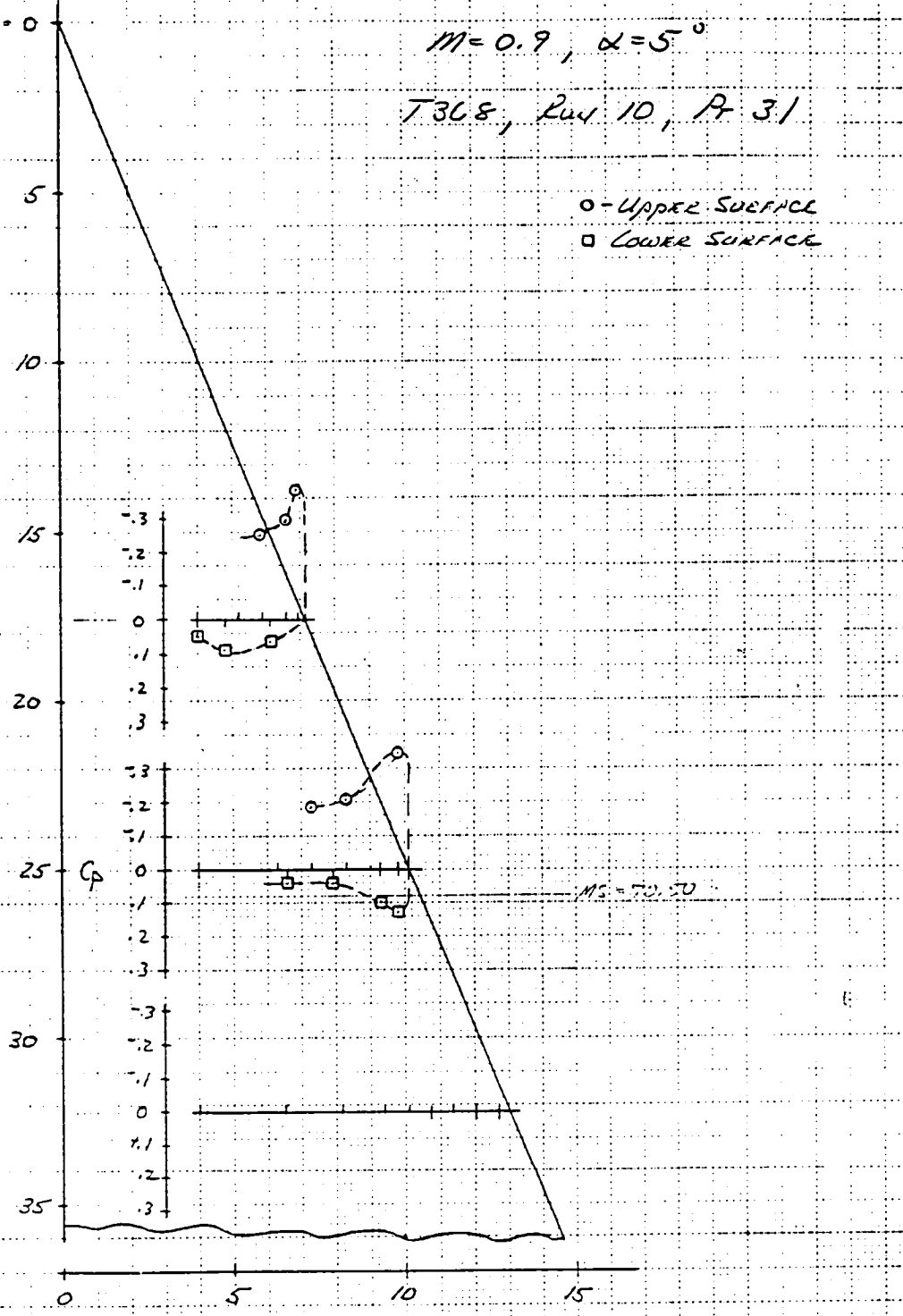
Figure 20e. Wing Static Pressure Distributions, M = 0.9, α = 0.5 deg

61
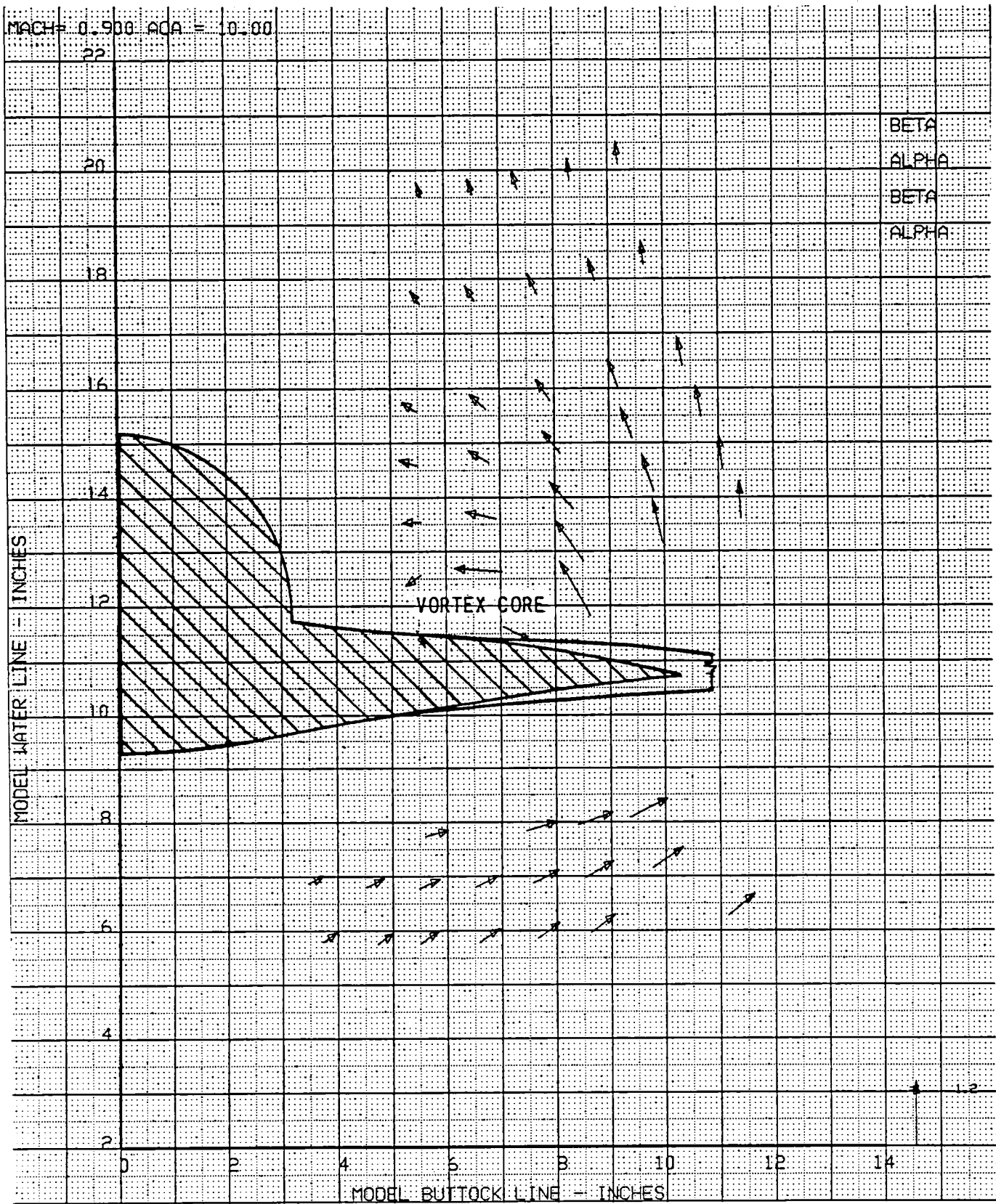
Figure 21a. Local Flowfield, MSTA = 70.50; Mach Number = 0.9; Angle of Attack = 10.0 deg
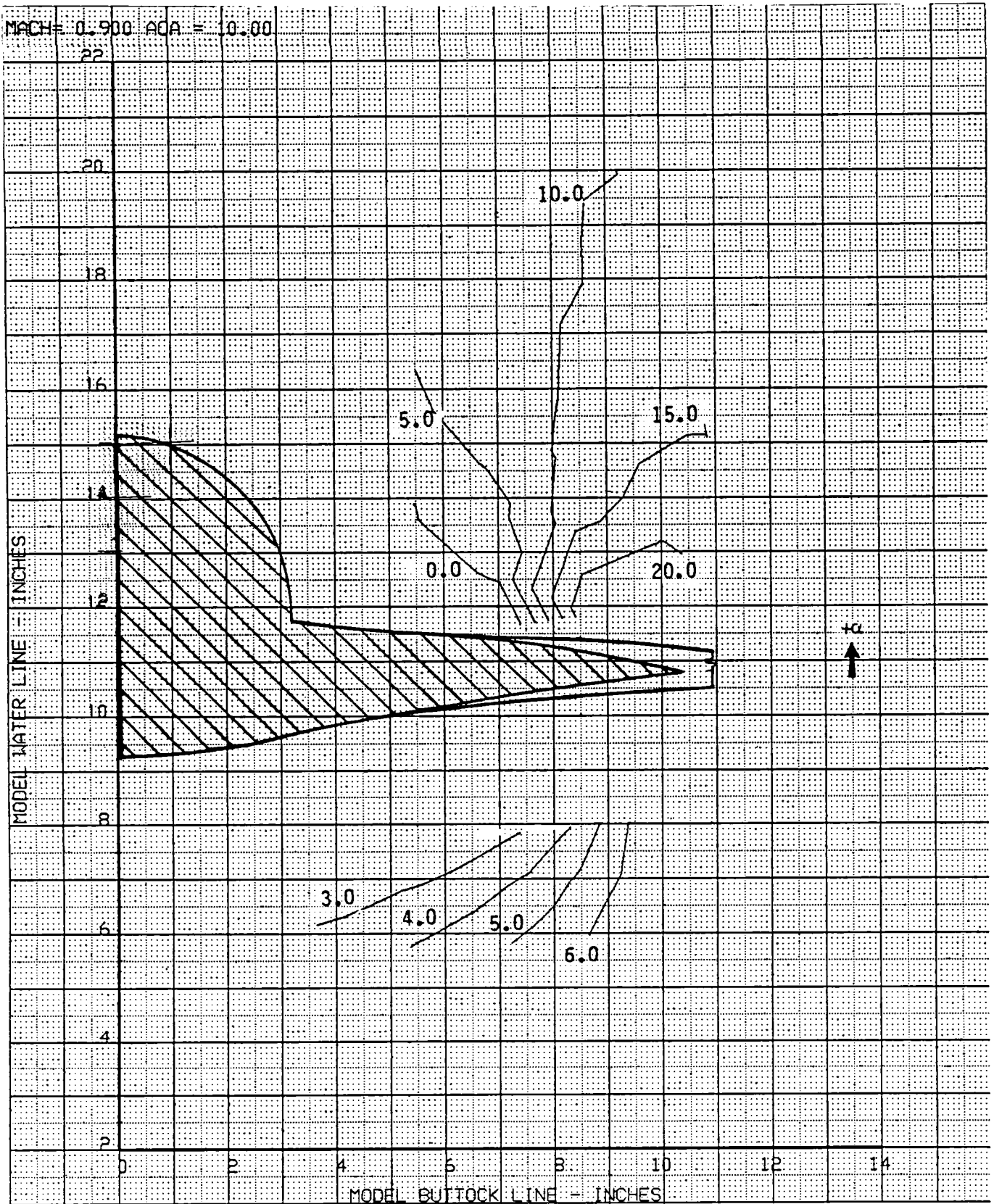
Figure 21b. Local Angle of Attack, Mach Number = 0.9; Angle of Attack = 10.0 deg

63
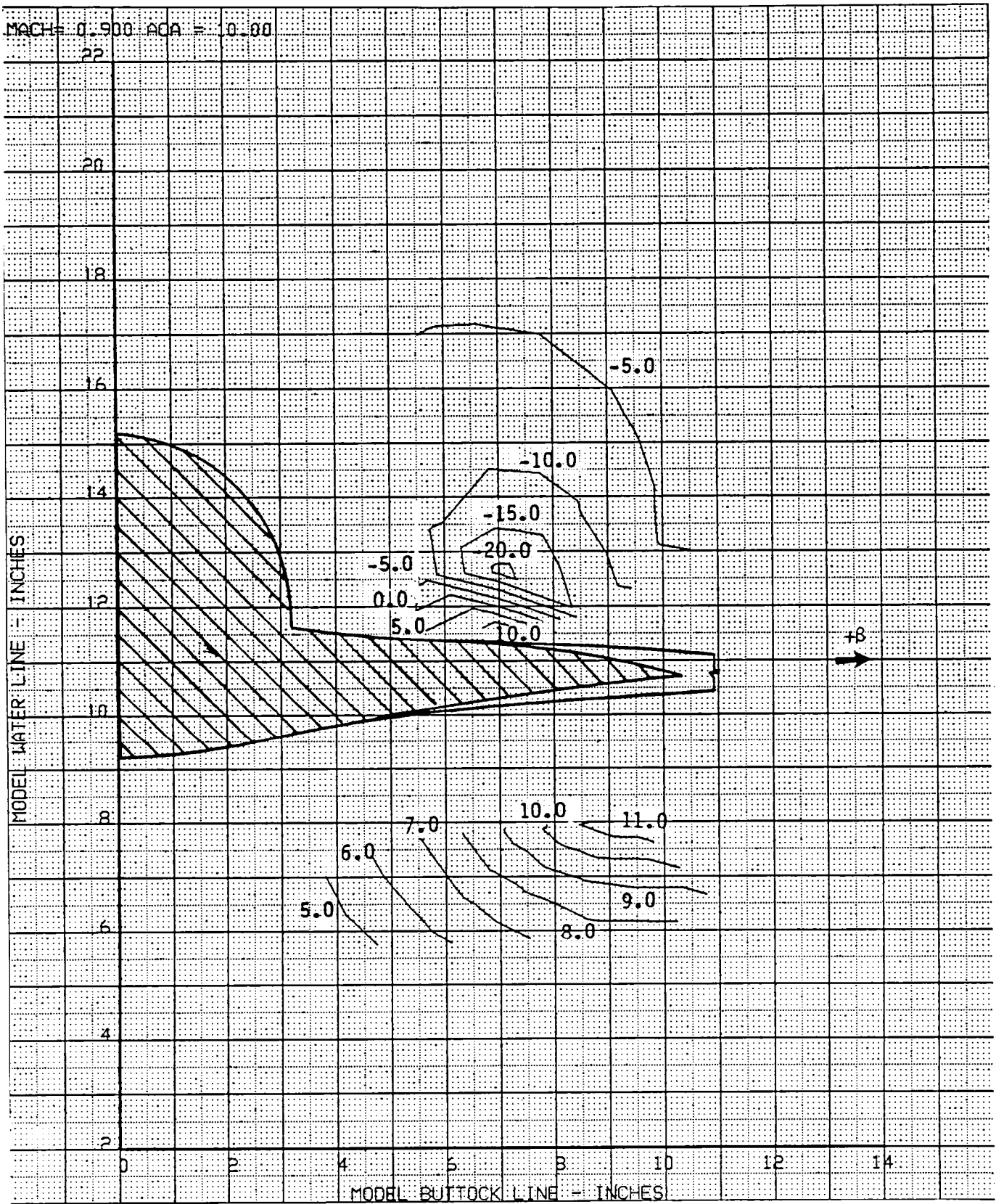
Figure 21c. Local Sideflow Angle, Mach Number = 0.9; Angle of Attack = 10.0 deg

64
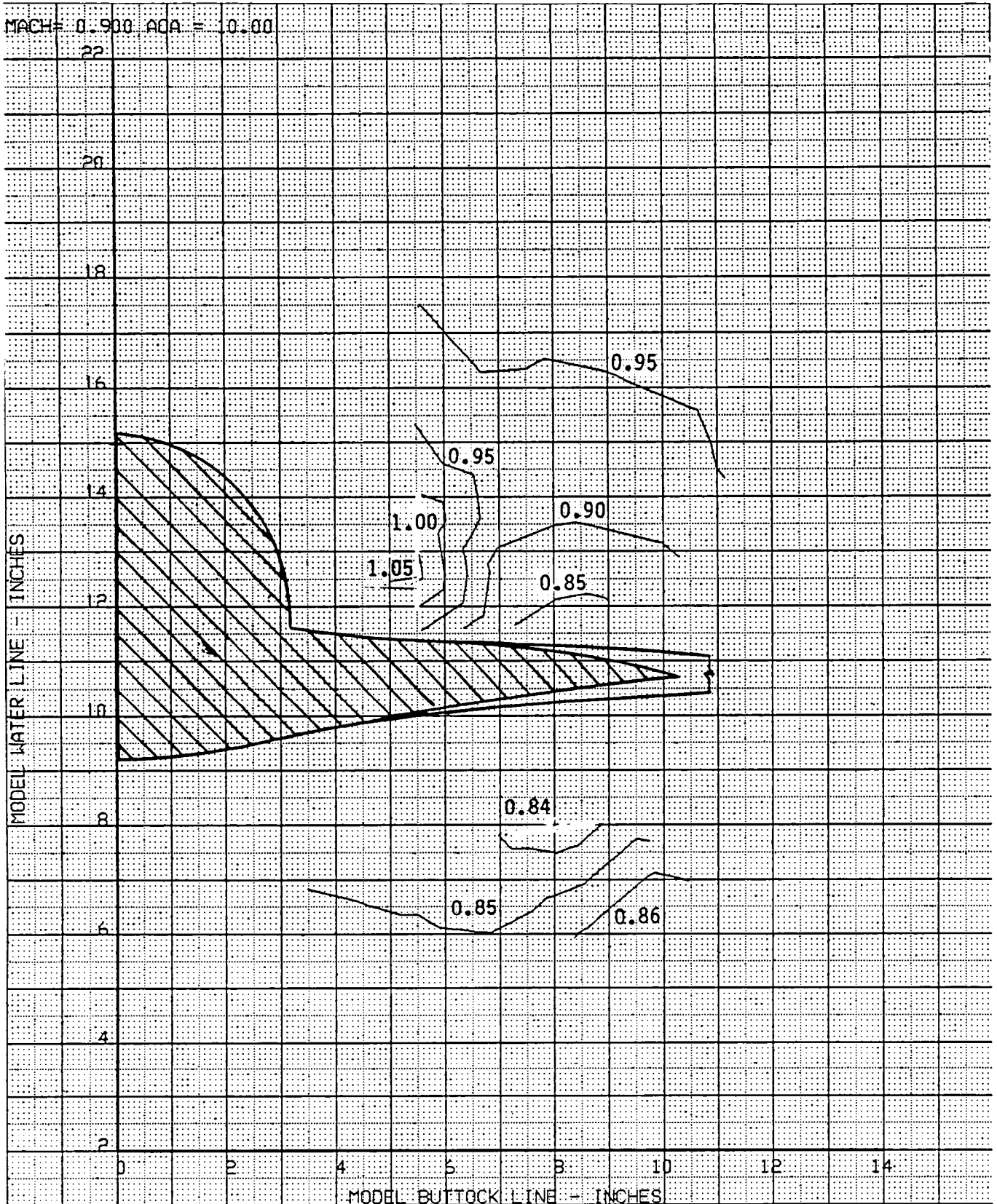
Figure 21d. Local Mach Number, Mach Number = 0.9; Angle of Attack = 10.0 deg

65
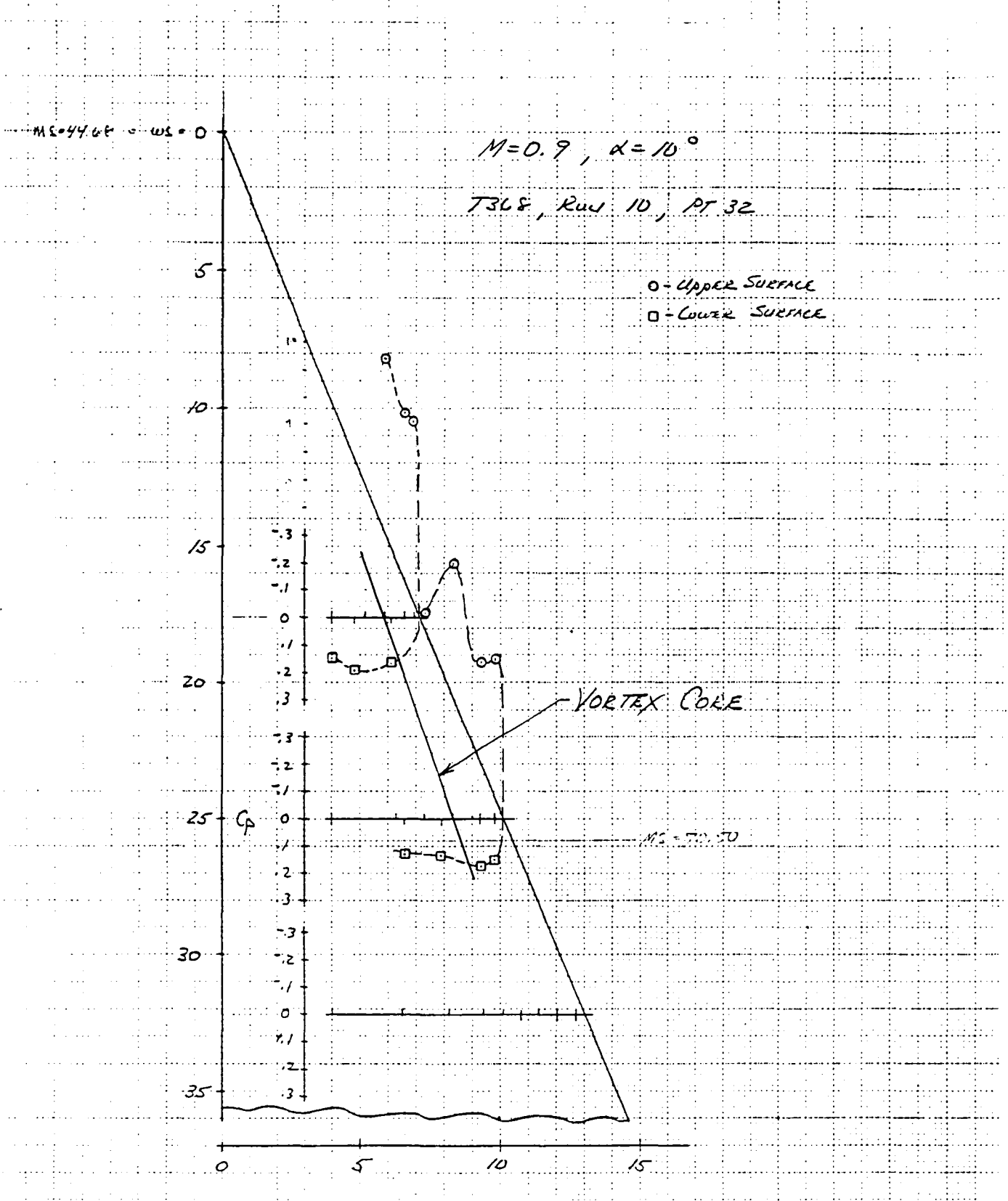
Figure 21e. Wing Static Pressure Distributions, M = 0.9, α = 10.0 deg
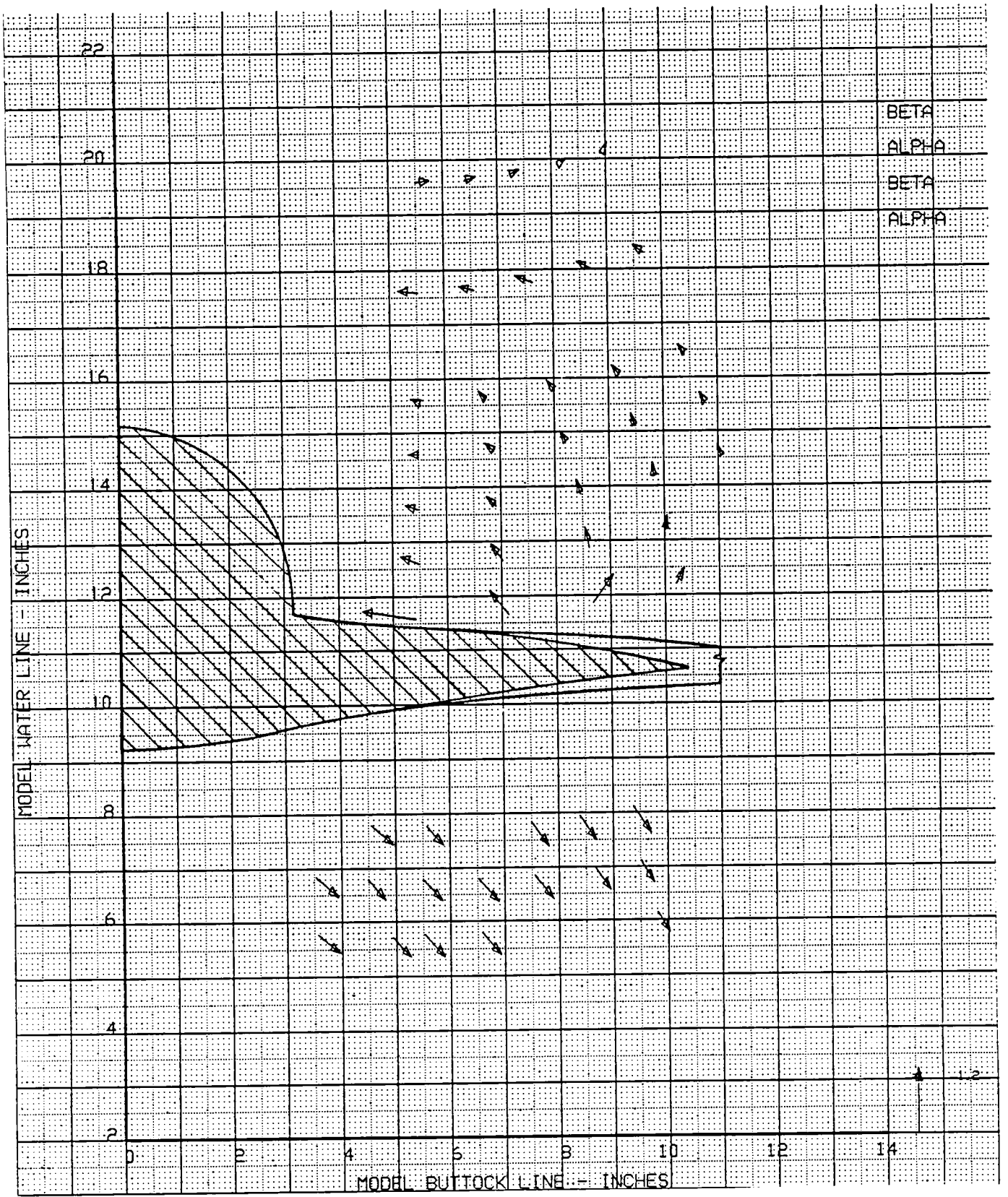
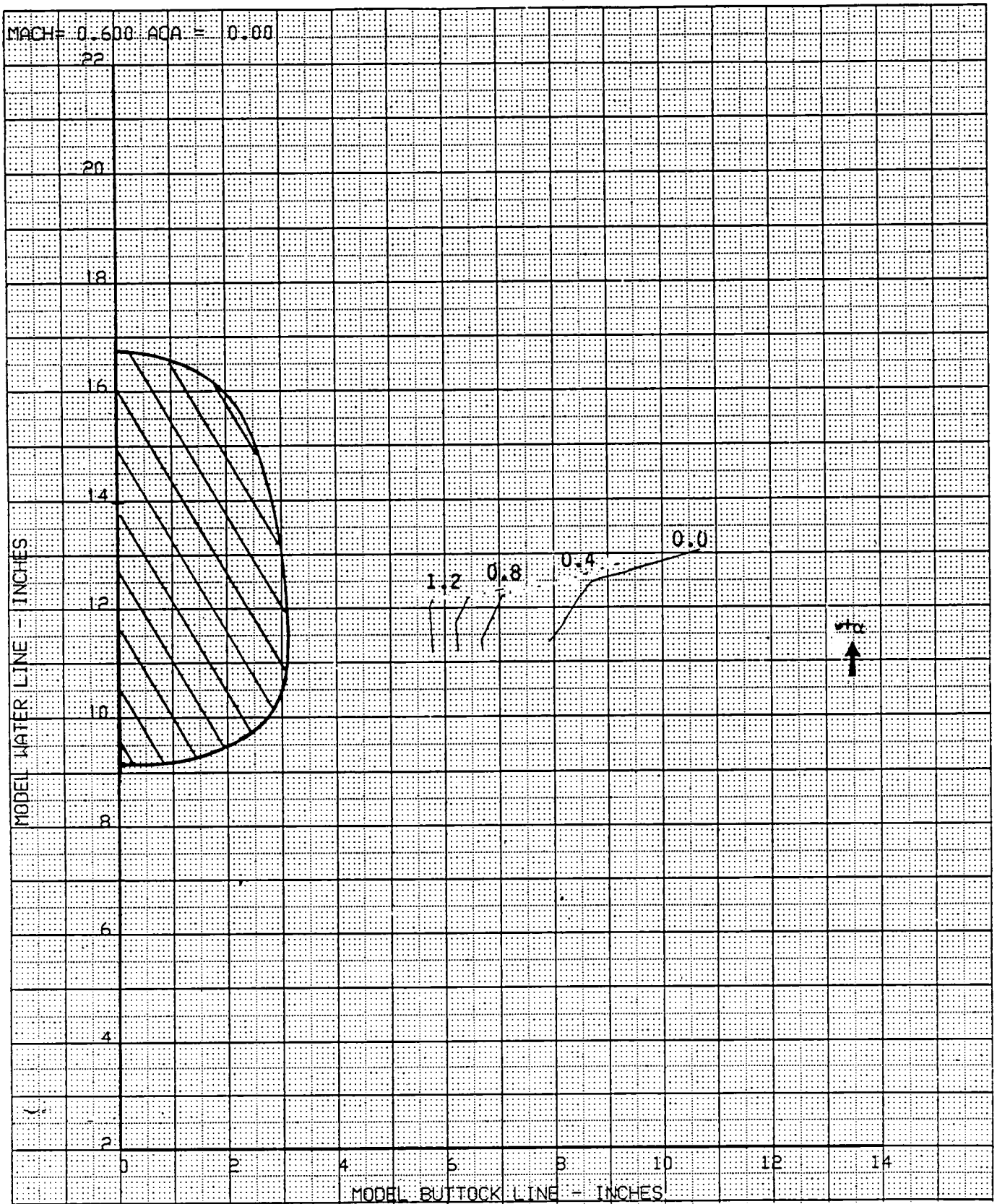*Figure 22a. Local Flowfield, MSTA = 70.50; Mach Number = 1.2; Angle of Attack = 0.0 deg*

67

Figure 22b. Local Angle of Attack, Mach Number = 1.2; Angle of Attack = 0.0 deg

68

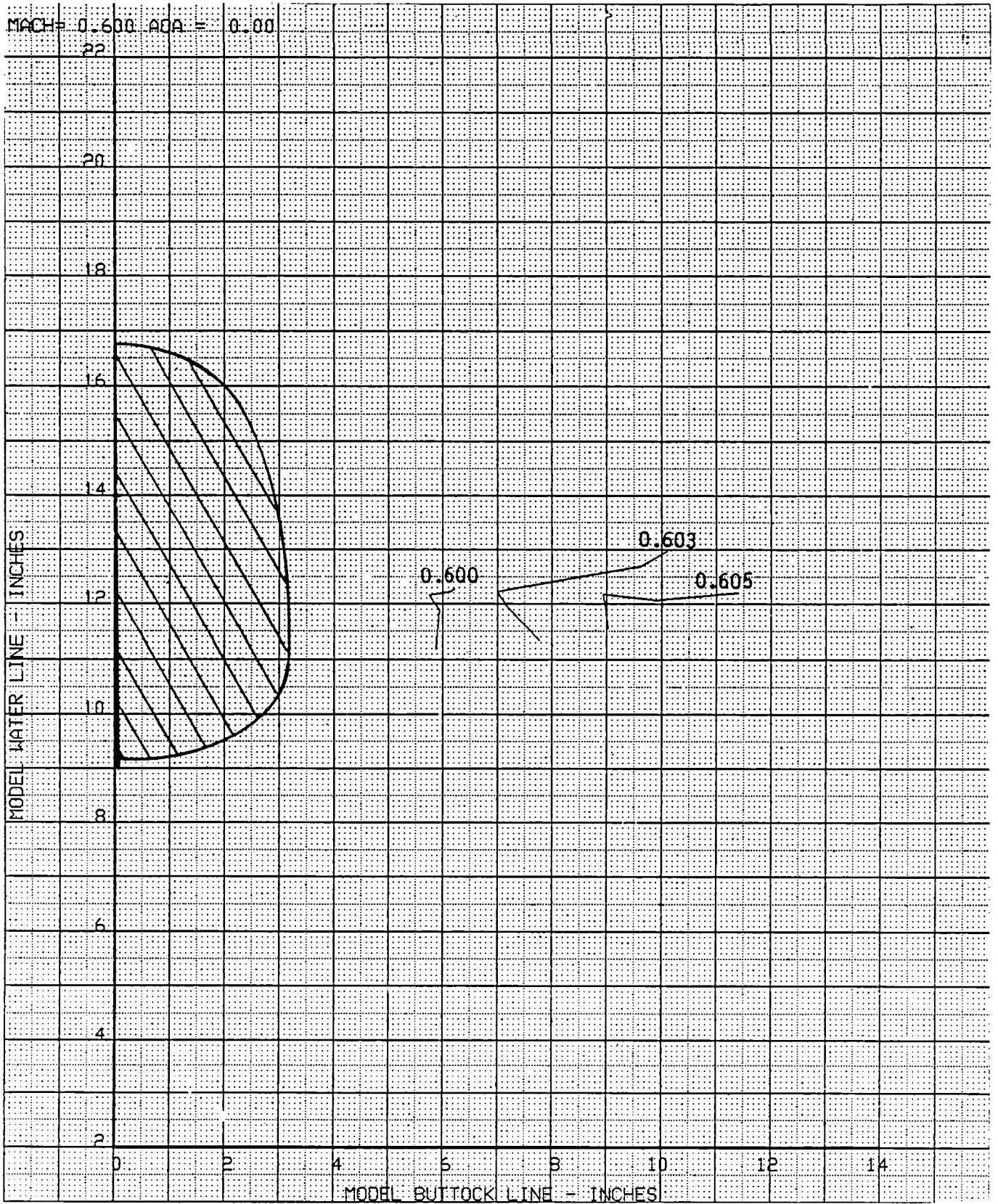*Figure 22c. Local Sideflow Angle, Mach Number = 1.2; Angle of Attack = 0.0 deg*

69

Figure 22d. Local Mach Number, Mach Number = 1.2; Angle of Attack = 0.0 deg

70

Figure 22e. Wing Static Pressure Distributions, M = 1.2, α = 0.0 deg

71

Figure 23a. Local Flowfield, MSTA = 70 50; Mach Number = 1.2; Angle of Attack = 5.0 deg

72
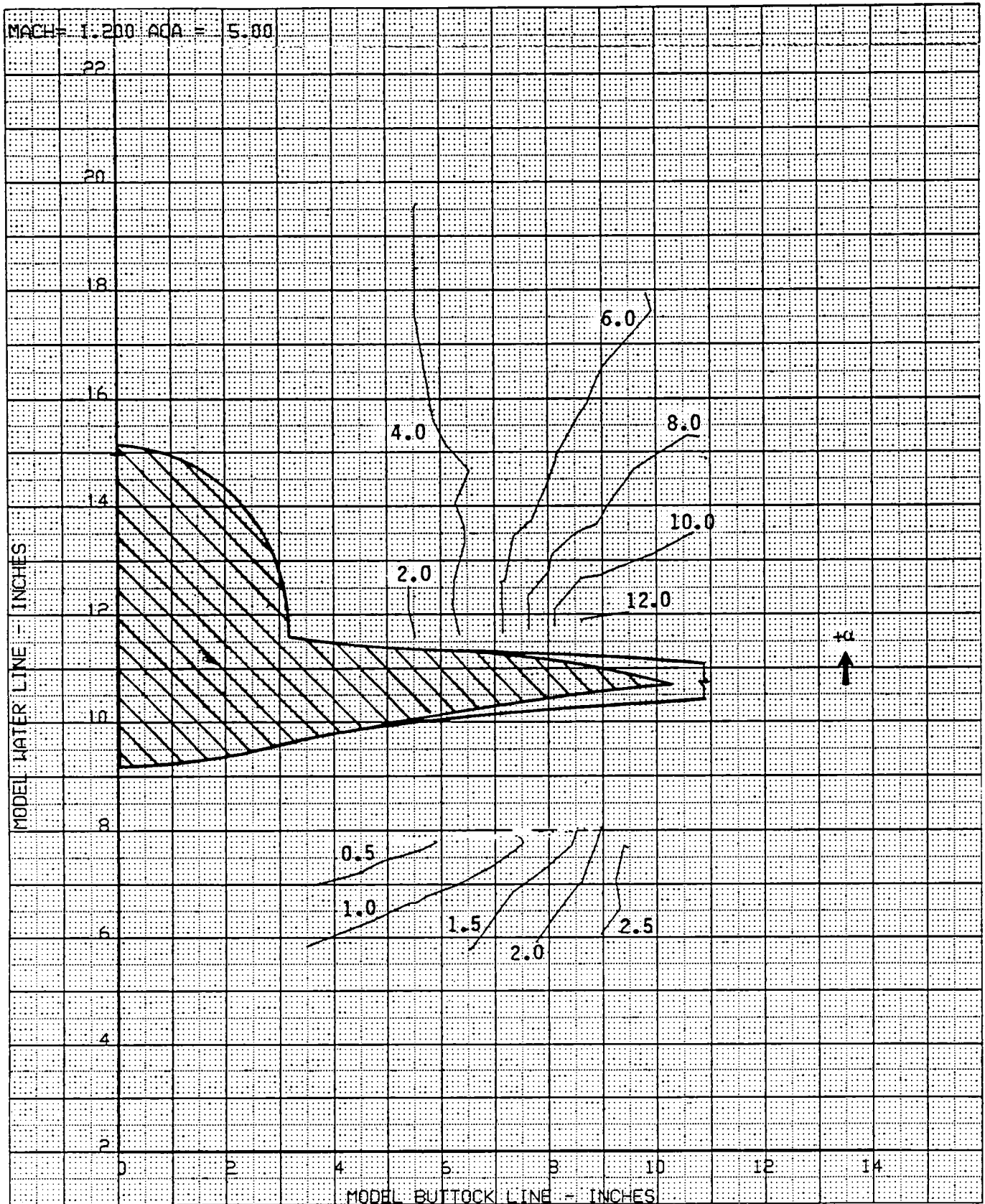
Figure 23b. Local Angle of Attack, Mach Number = 1.2; Angle of Attack = 5.0 deg

73
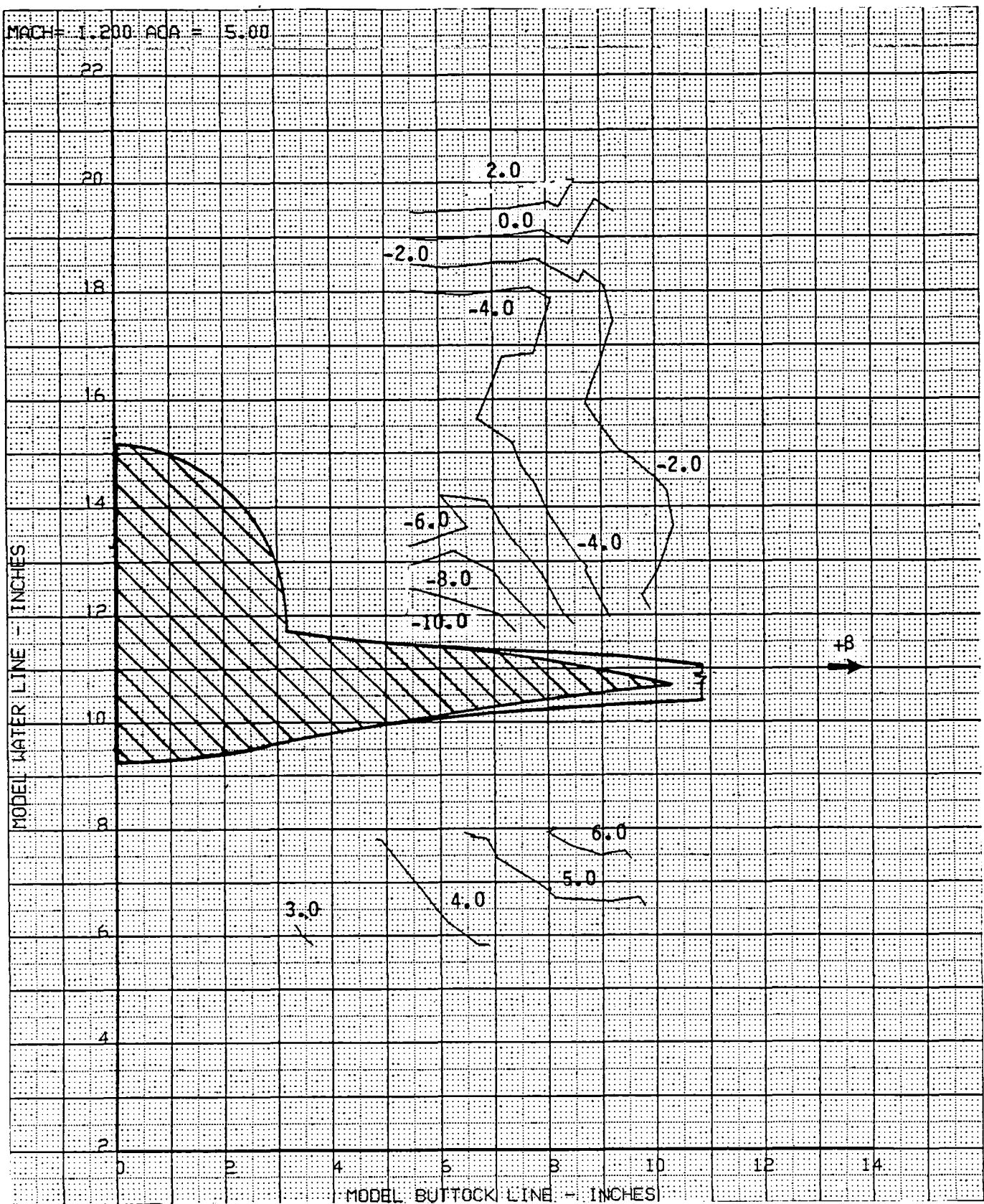
Figure 23c. Local Sideflow Angle, Mach Number = 1.2; Angle of Attack = 5.0 deg
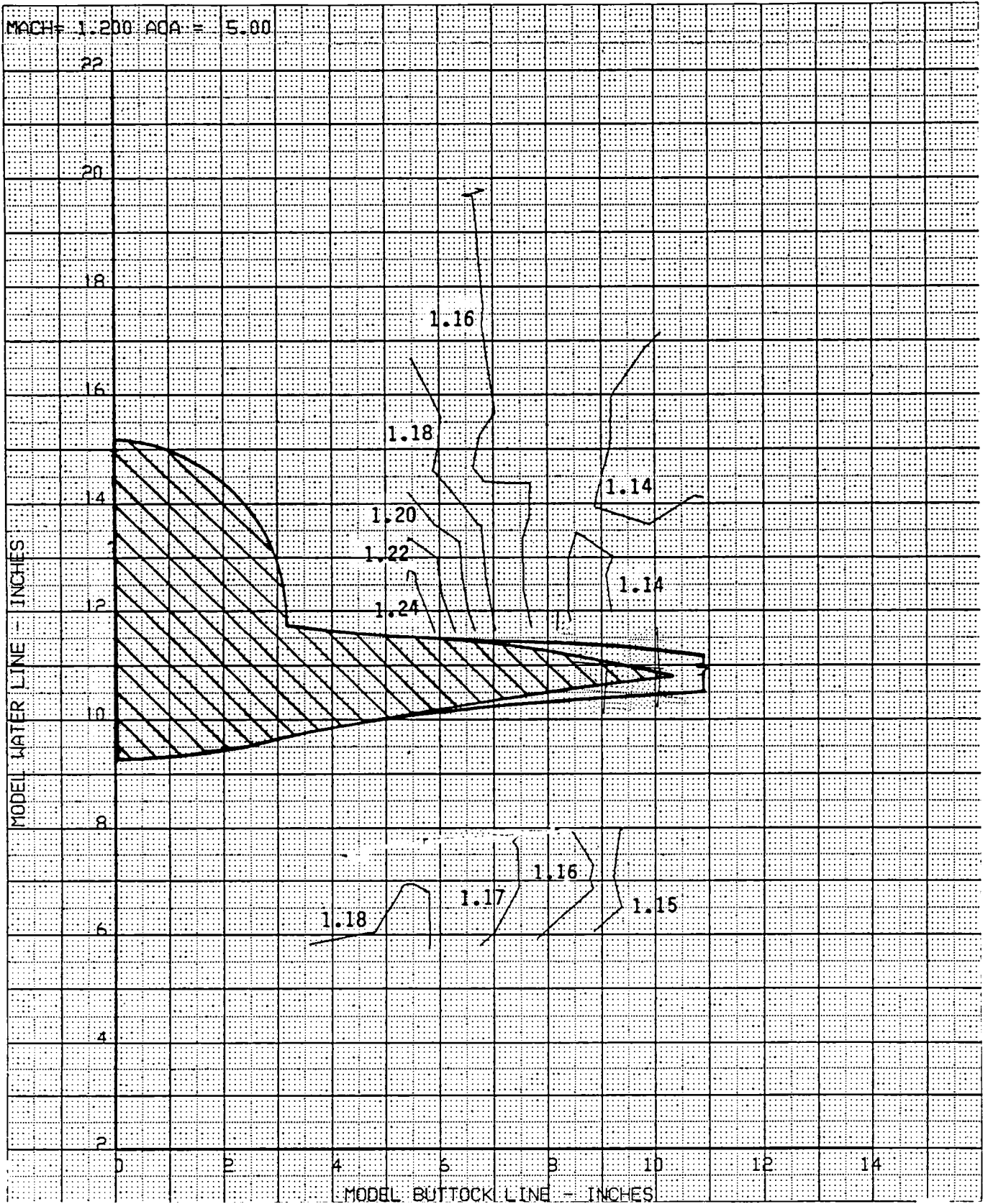
Figure 23d. Local Mach Number, Mach Number = 1.2; Angle of Attack = 5.0 deg

75
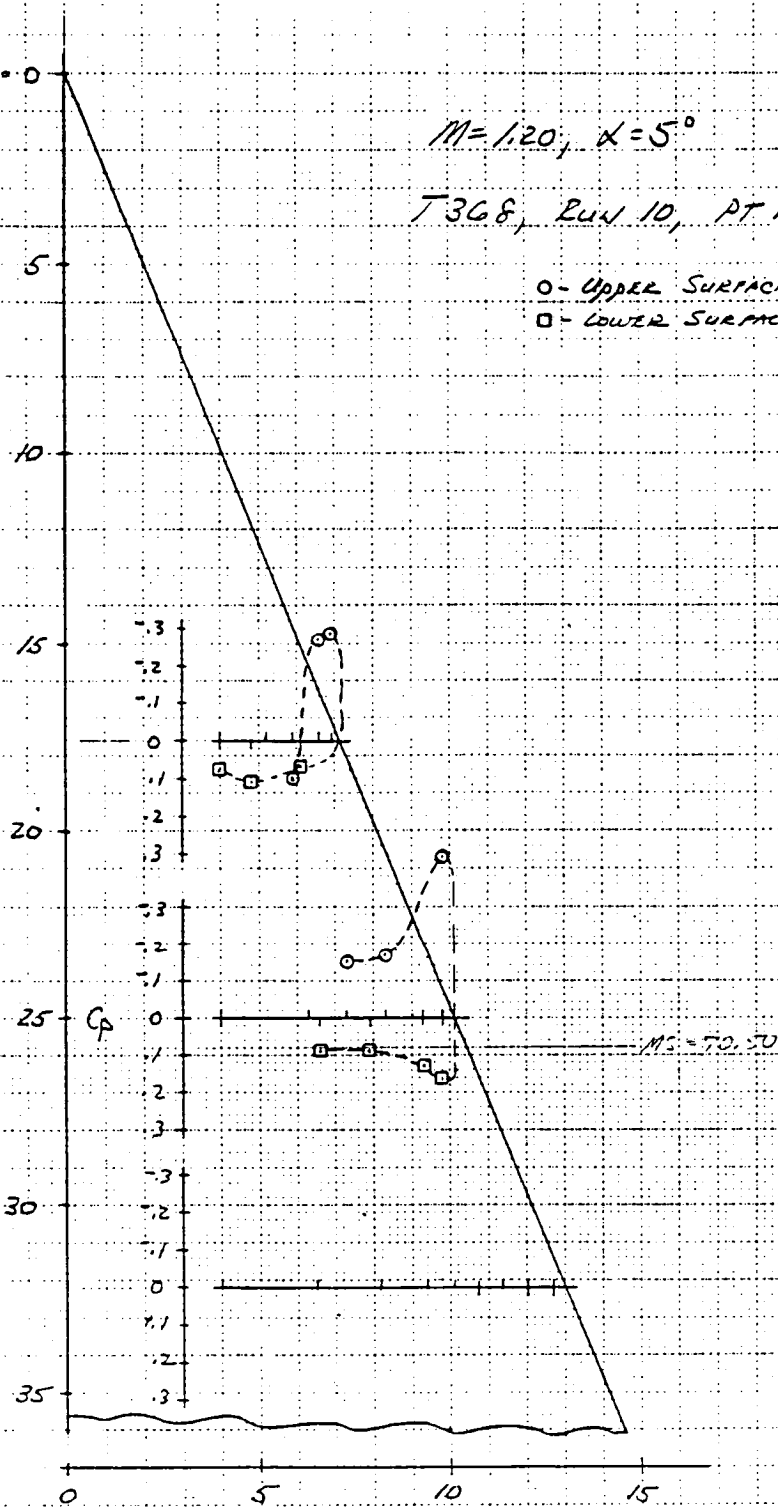
Figure 23e. Wing Static Pressure Distributions, M = 1.2, α = 5.0 deg

Figure 24a. Local Flowfield, MSTA = 70.50; Mach Number = 1.2; Angle of Attack = 7.5 deg

77
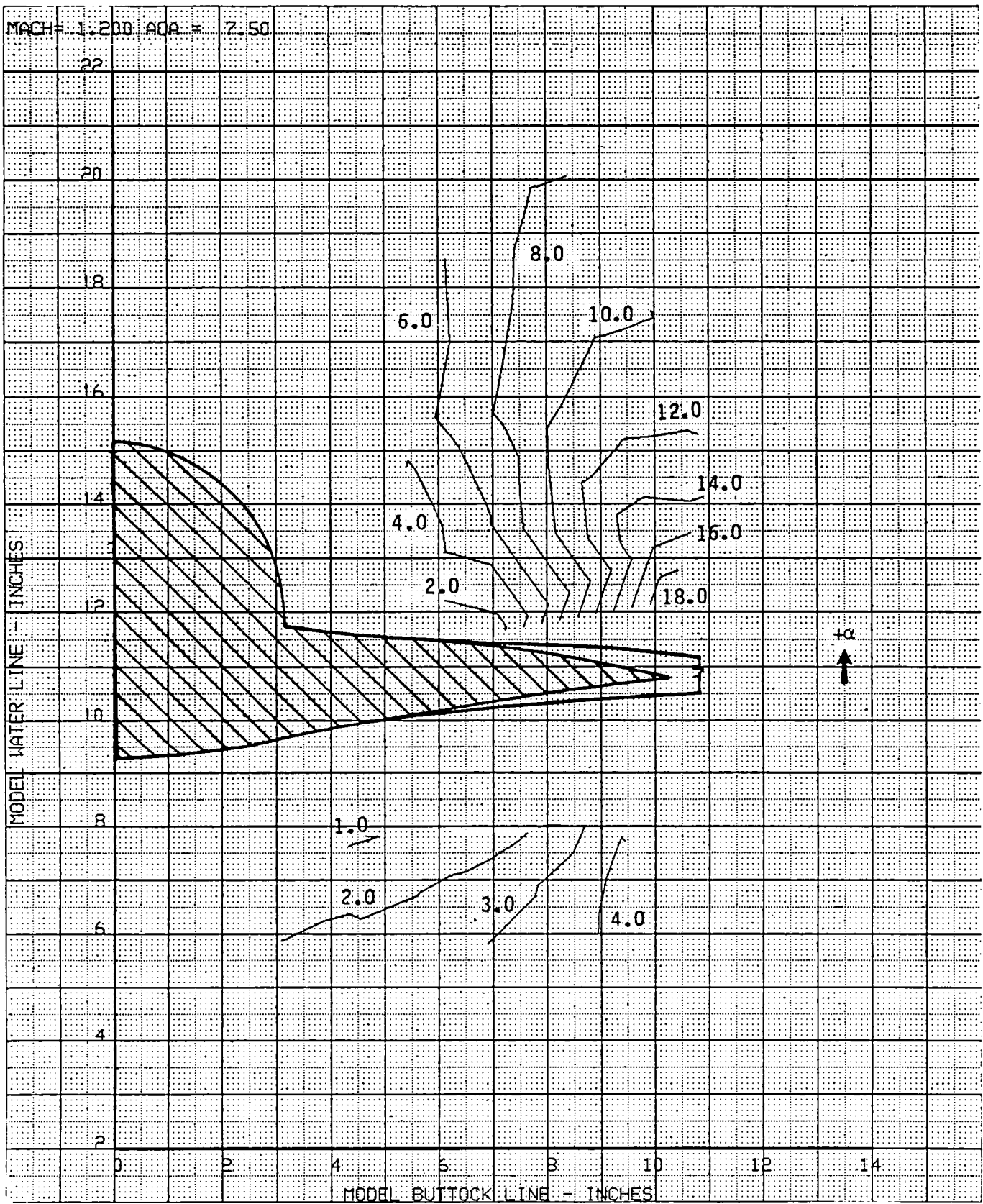
Figure 24b. Local Angle of Attack, Mach Number = 1.2; Angle of Attack = 7.5 deg

78

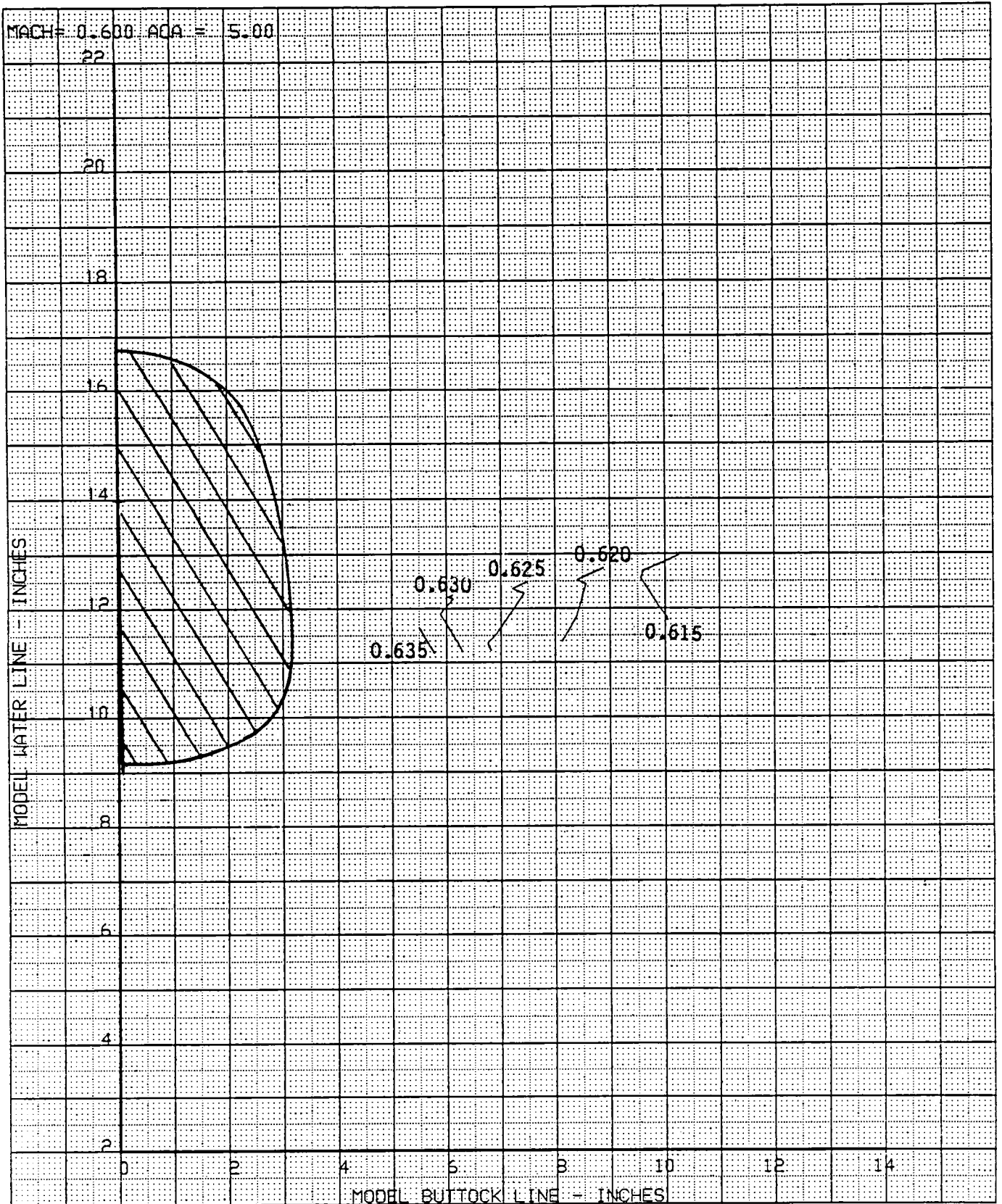*Figure 24c. Local Sideflow Angle, Mach Number = 1.2; Angle of Attack = 7.5 deg*

79

MACH = 1.200 AOA = 7.50

Figure 24d. Local Mach Number, Mach Number = 1.2; Angle of Attack = 7.5 deg

80

Figure 24e. Wing Static Pressure Distributions, M = 1.2, α = 7.5 deg
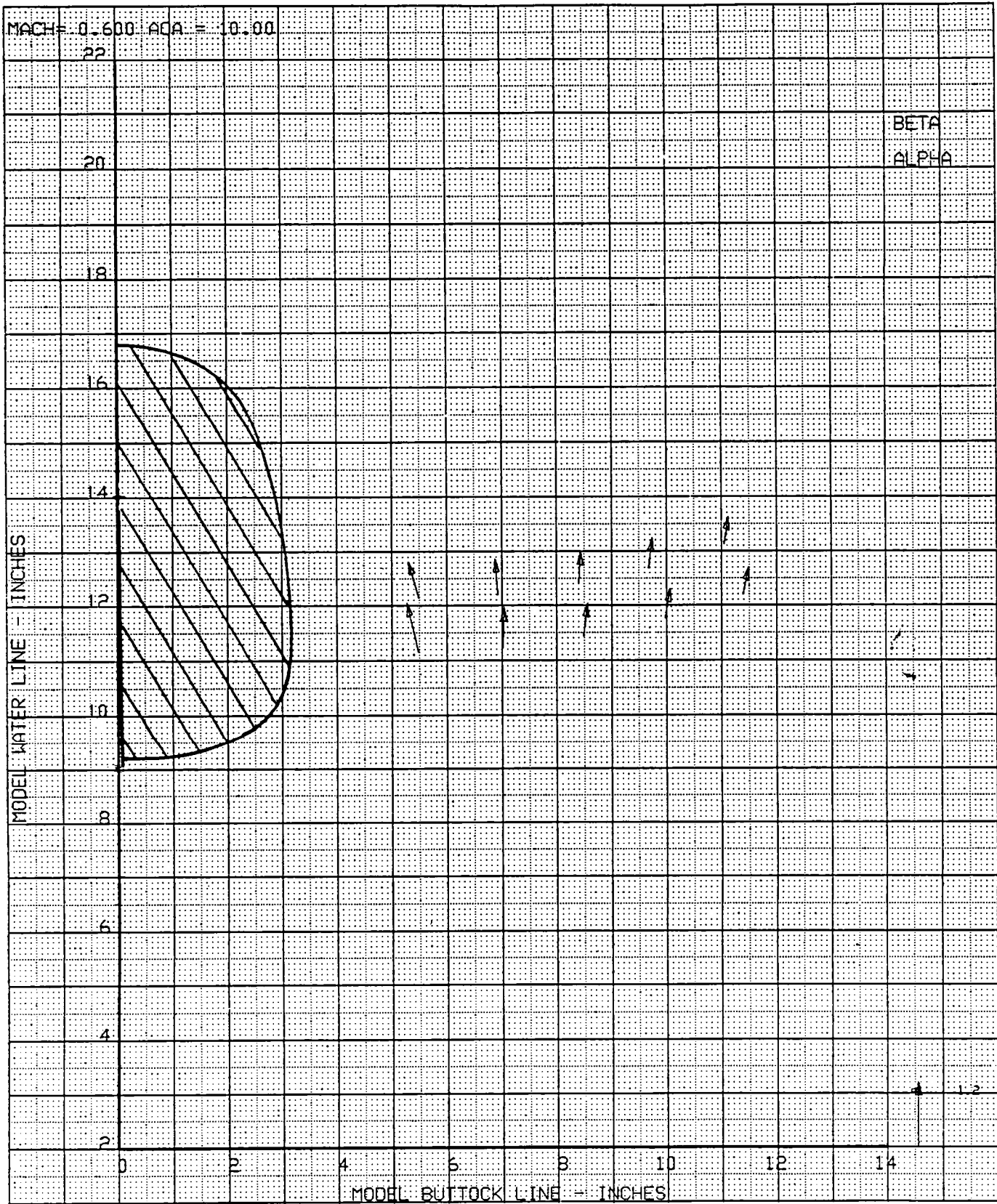
81
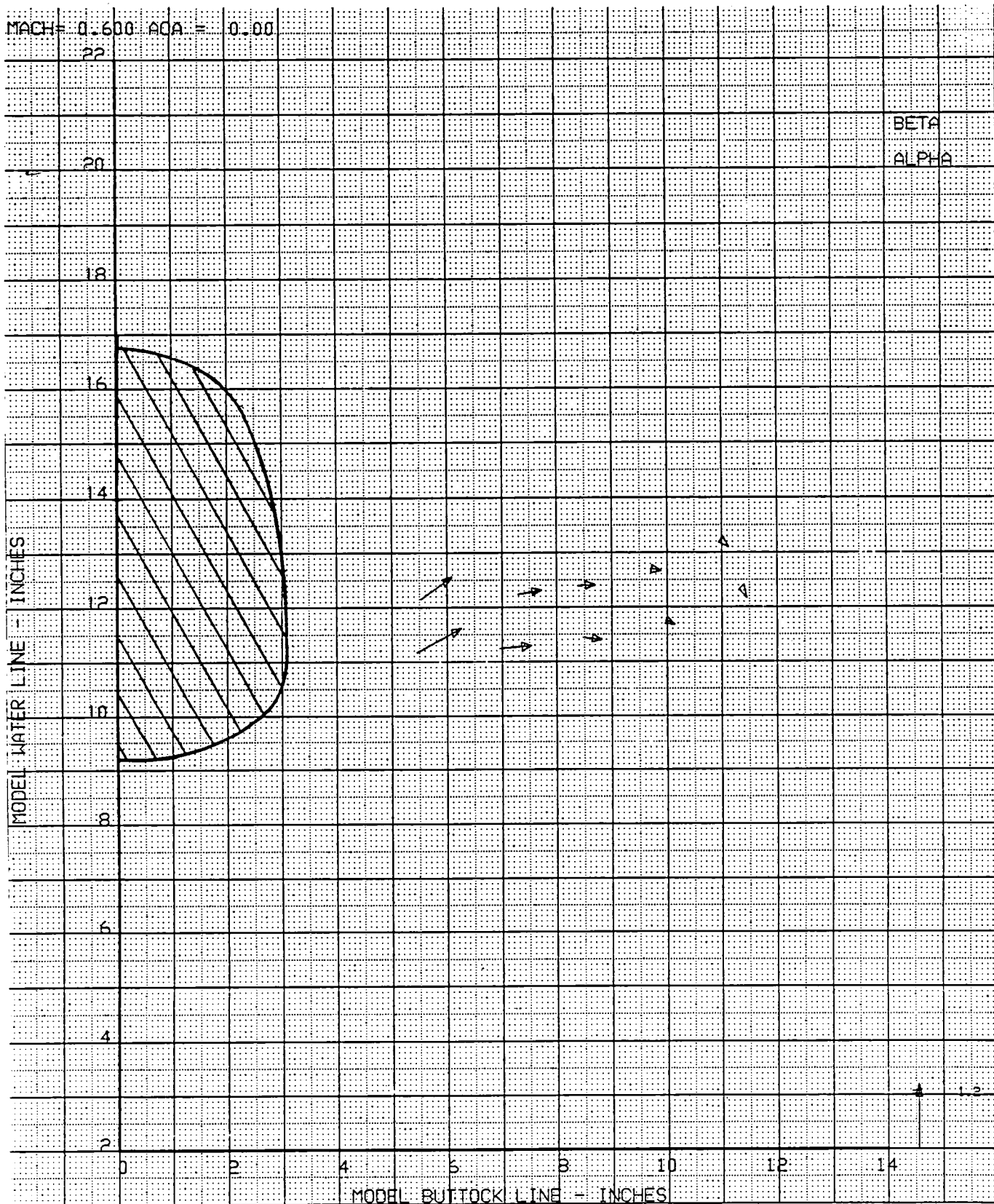
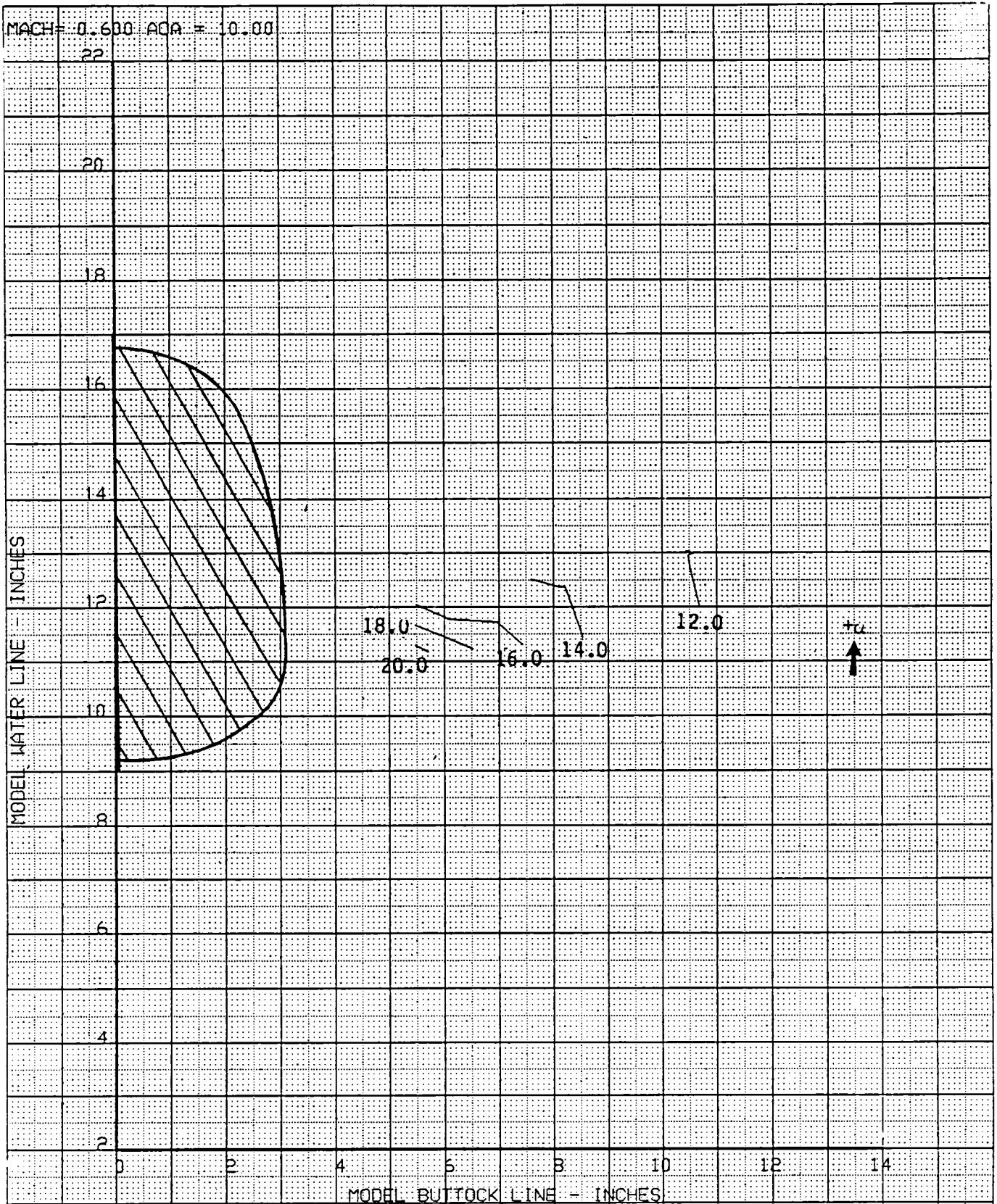*Figure 25a. Local Flowfield, MSTA = 50.50; Mach Number = 0.6; Angle of Attack = 0.0 deg*

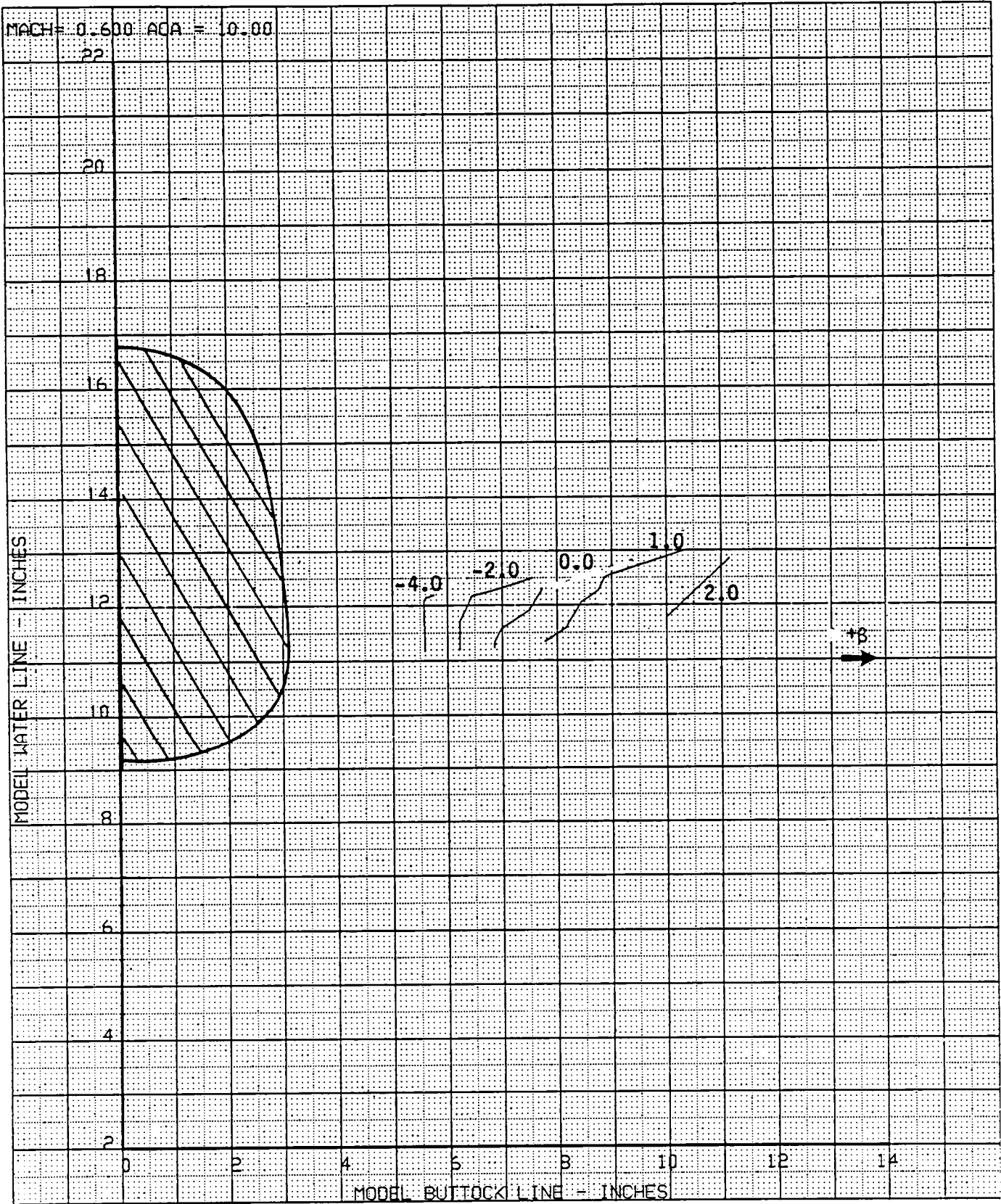*Figure 25b. Local Angle of Attack, Mach Number = 0.6; Angle of Attack = 0.0 deg*

83
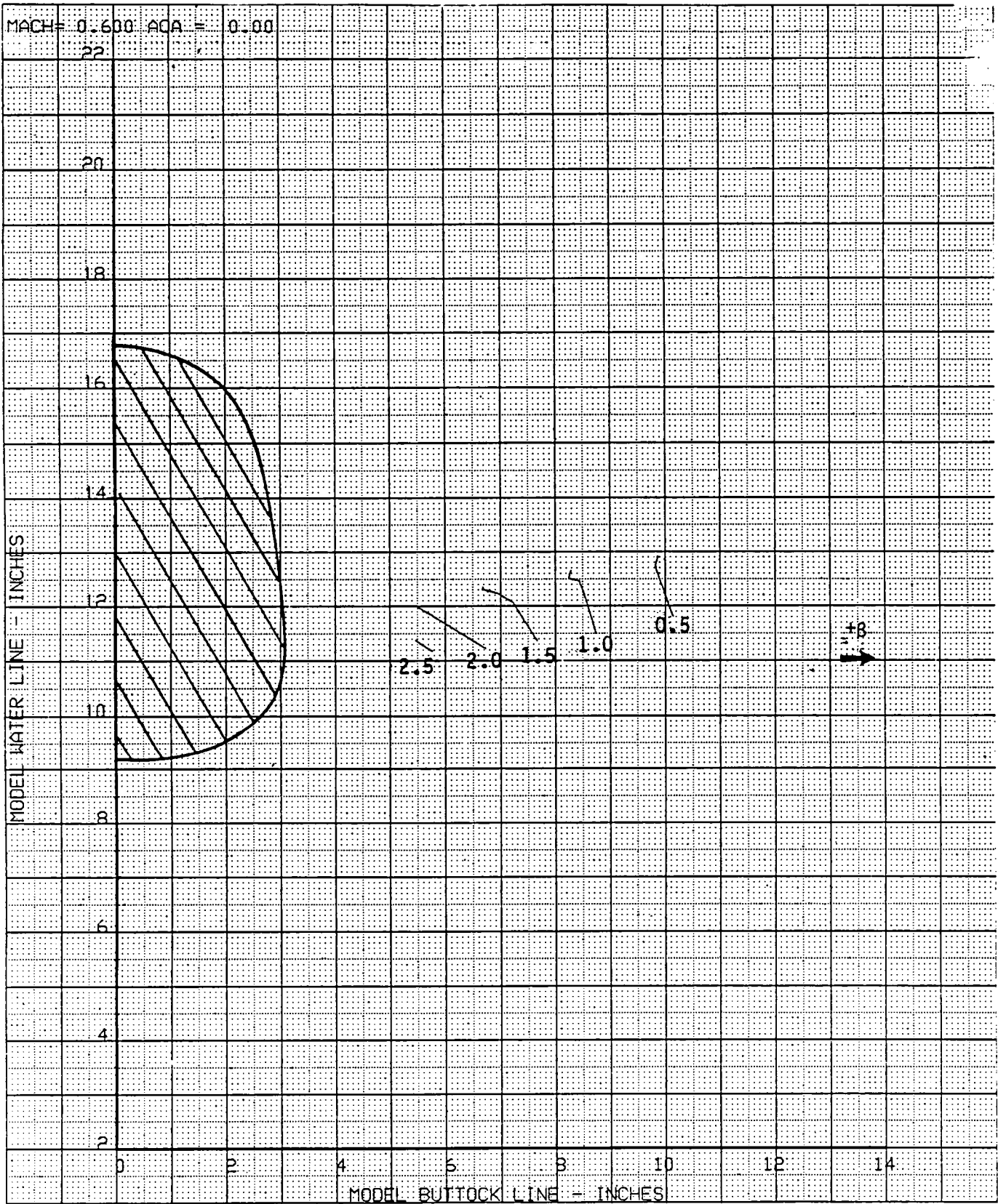
Figure 25c. Local Sideflow Angle, Mach Number = 0.6; Angle of Attack = 0.0 deg

84

Figure 25d. Local Mach Number, Mach Number = 0.6; Angle of Attack = 0.0 deg

85
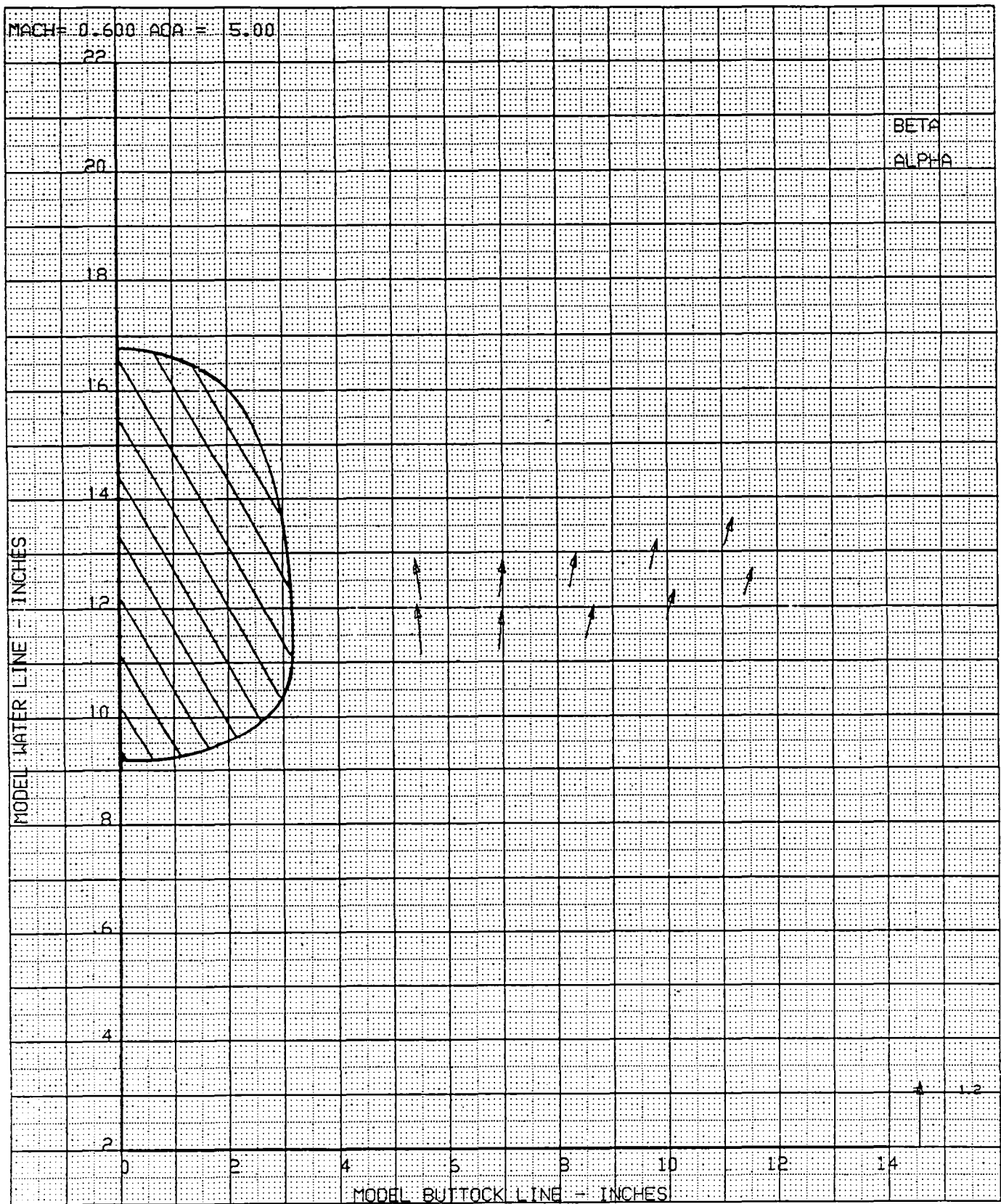
Figure 26a. Local Flowfield, MSTA = 50.50; Mach Number = 0.6; Angle of Attack = 5.0 deg
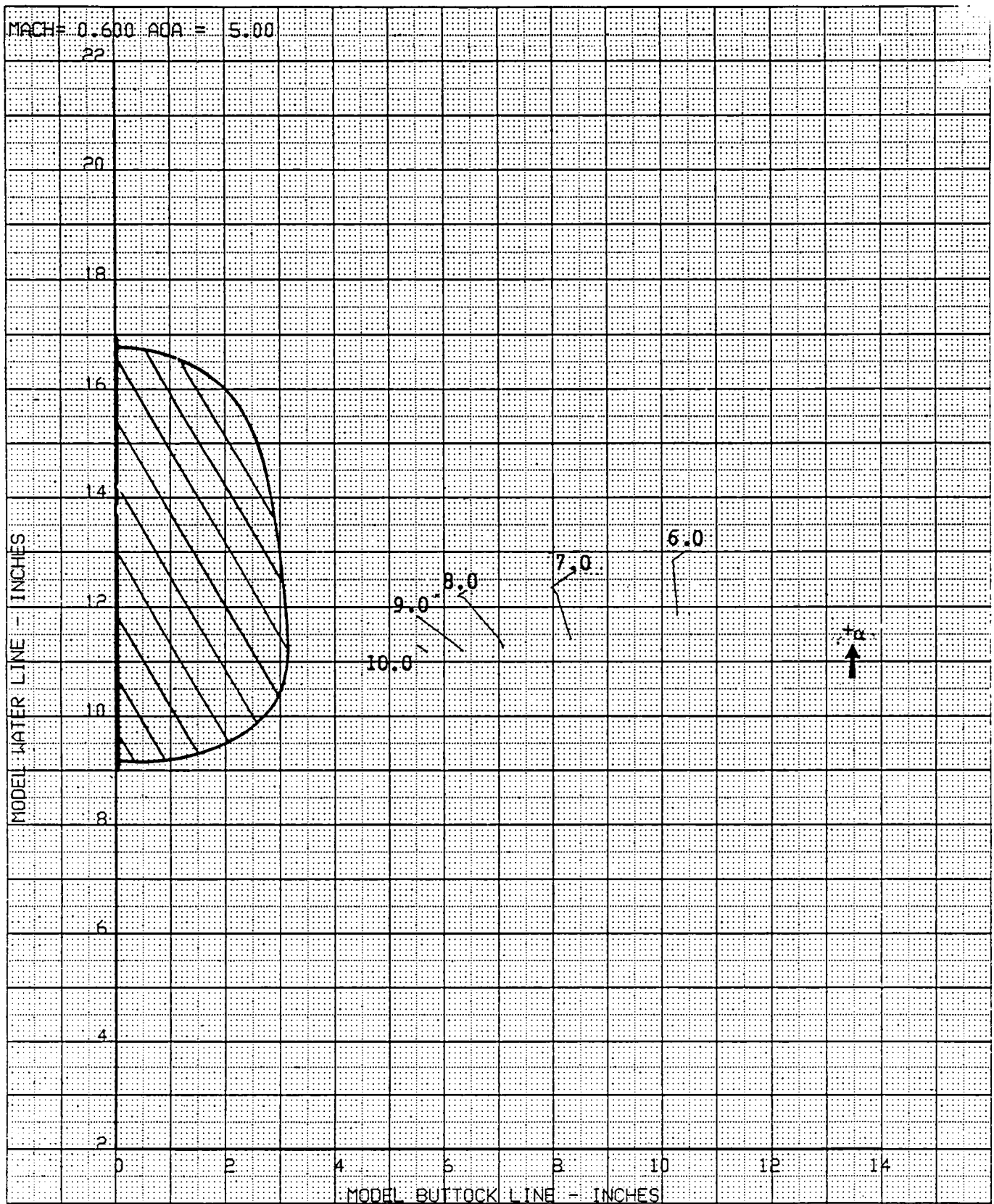
Figure 26b. Local Angle of Attack, Mach Number = 0.6; Angle of Attack = 5.0 deg

87
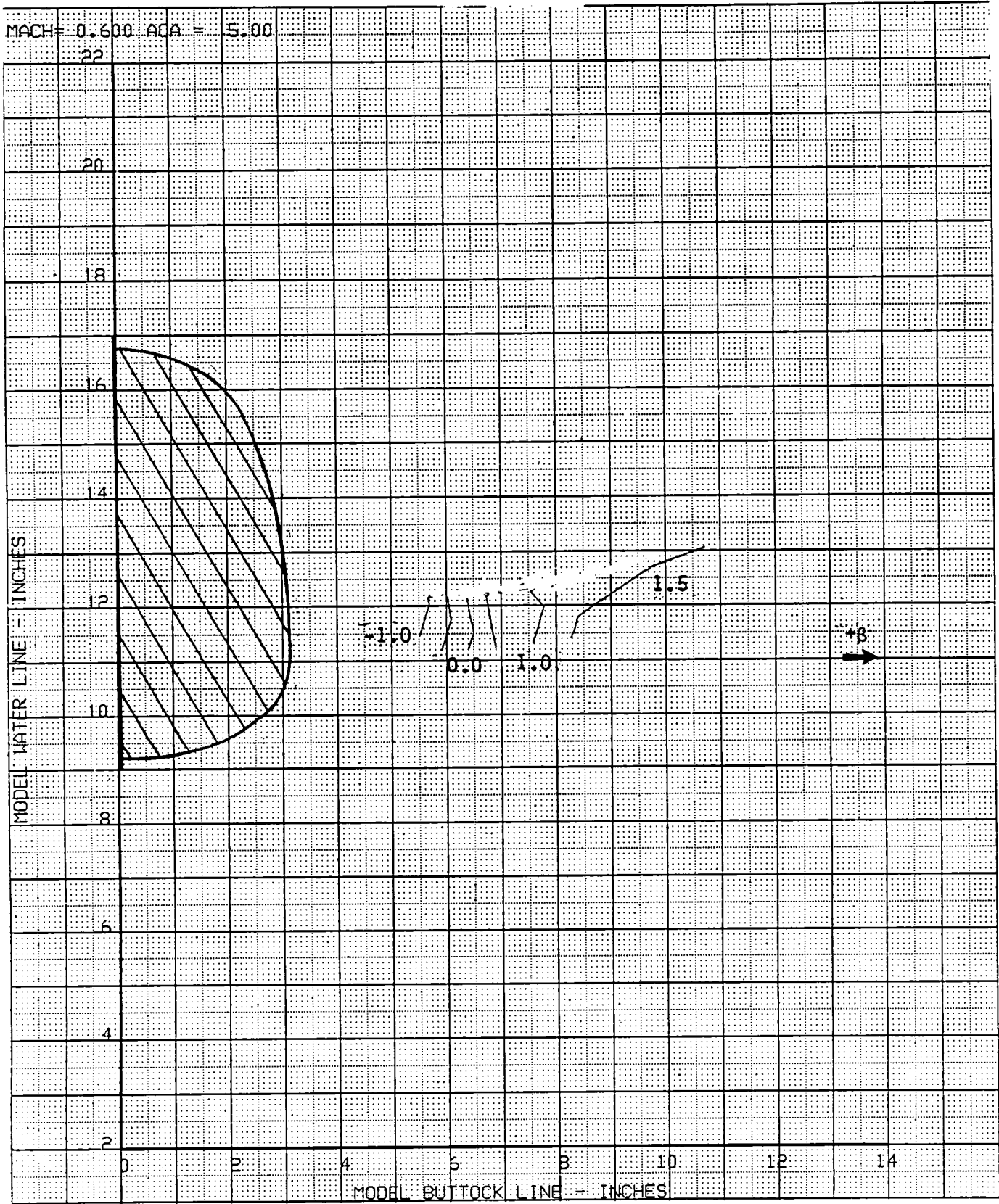
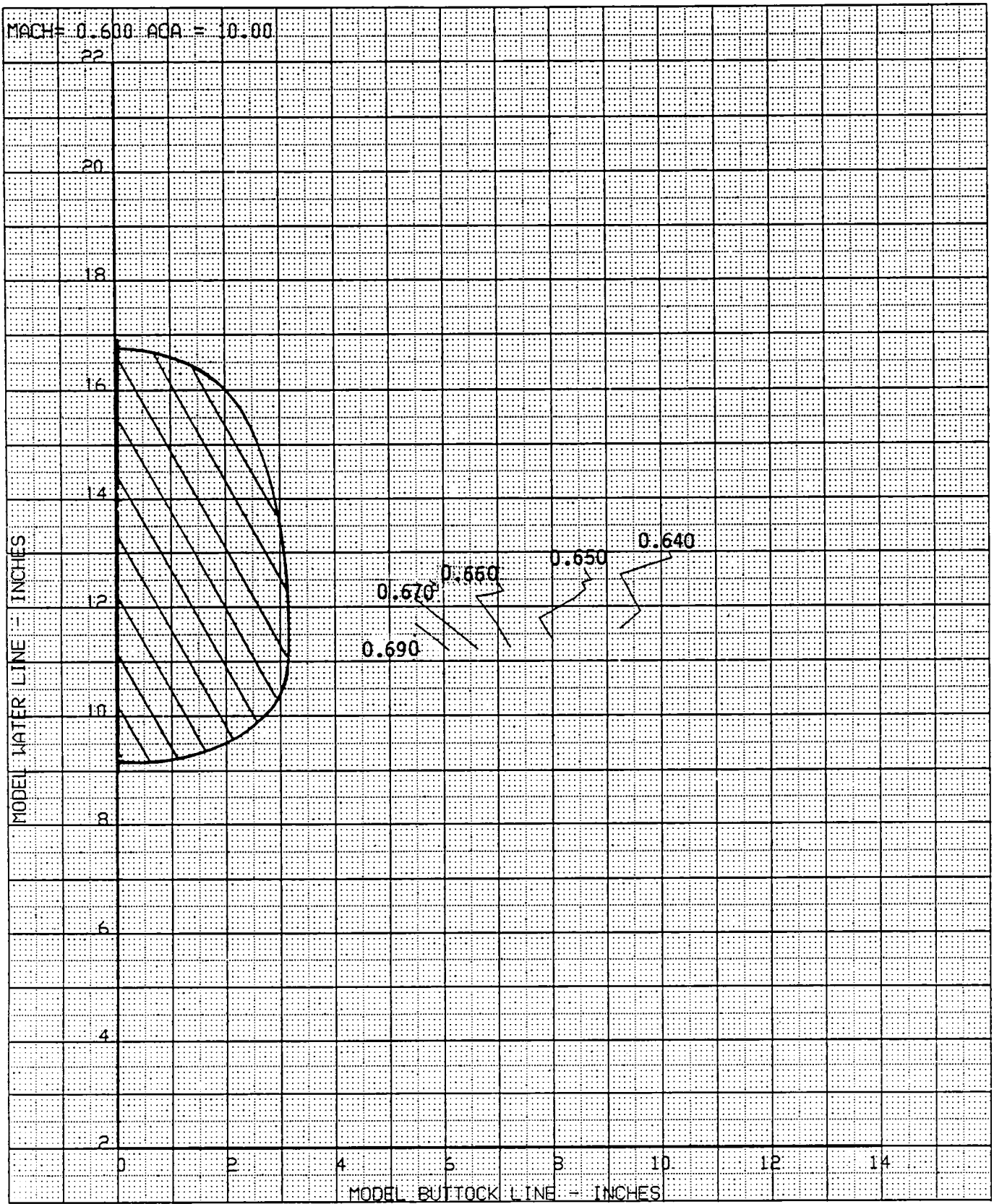*Figure 26c. Local Sideflow Angle, Mach Number = 0.6; Angle of Attack = 5.0 deg*

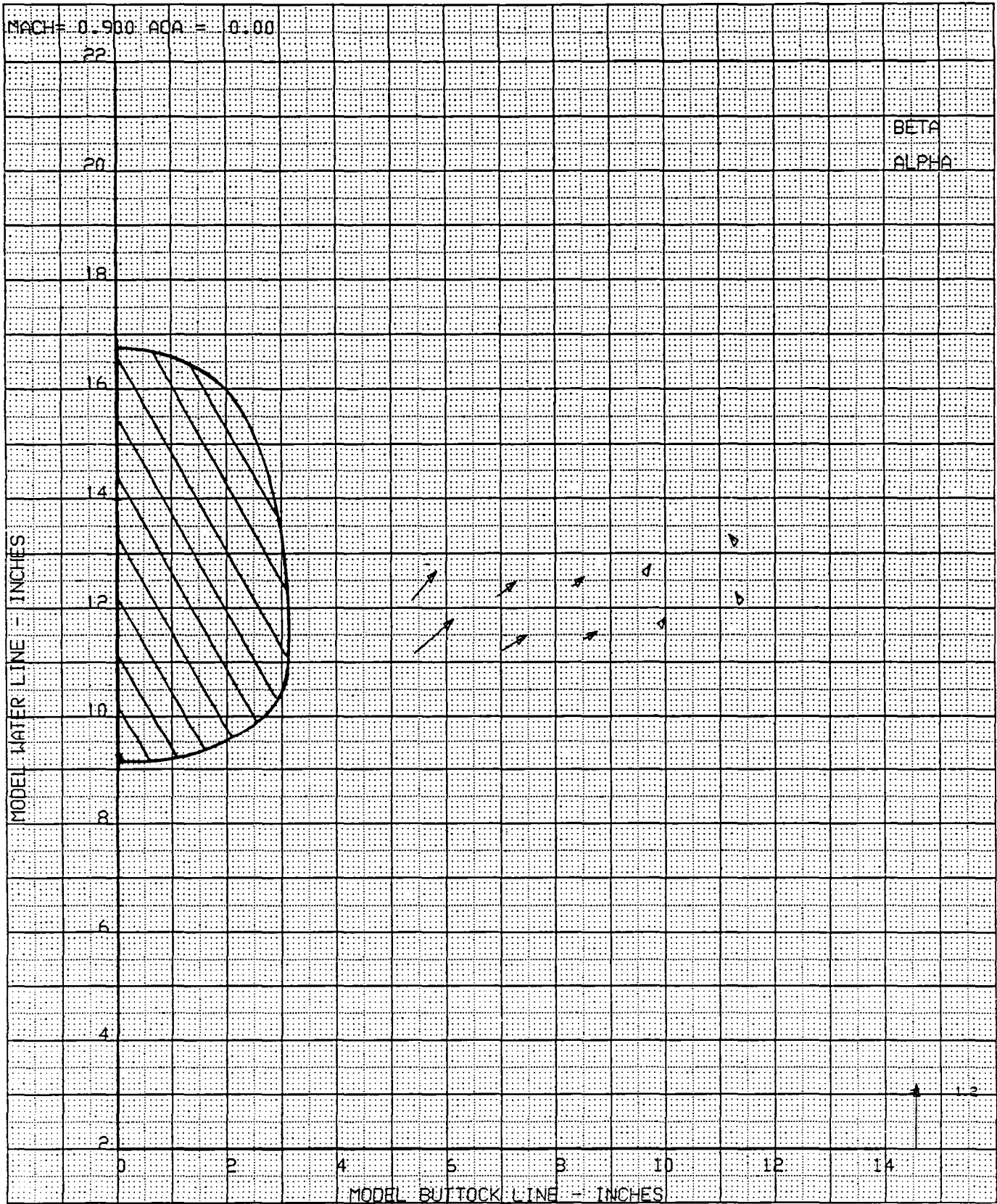Figure 26d. Local Mach Number, Mach Number = 0.6; Angle of Attack = 5.0 deg

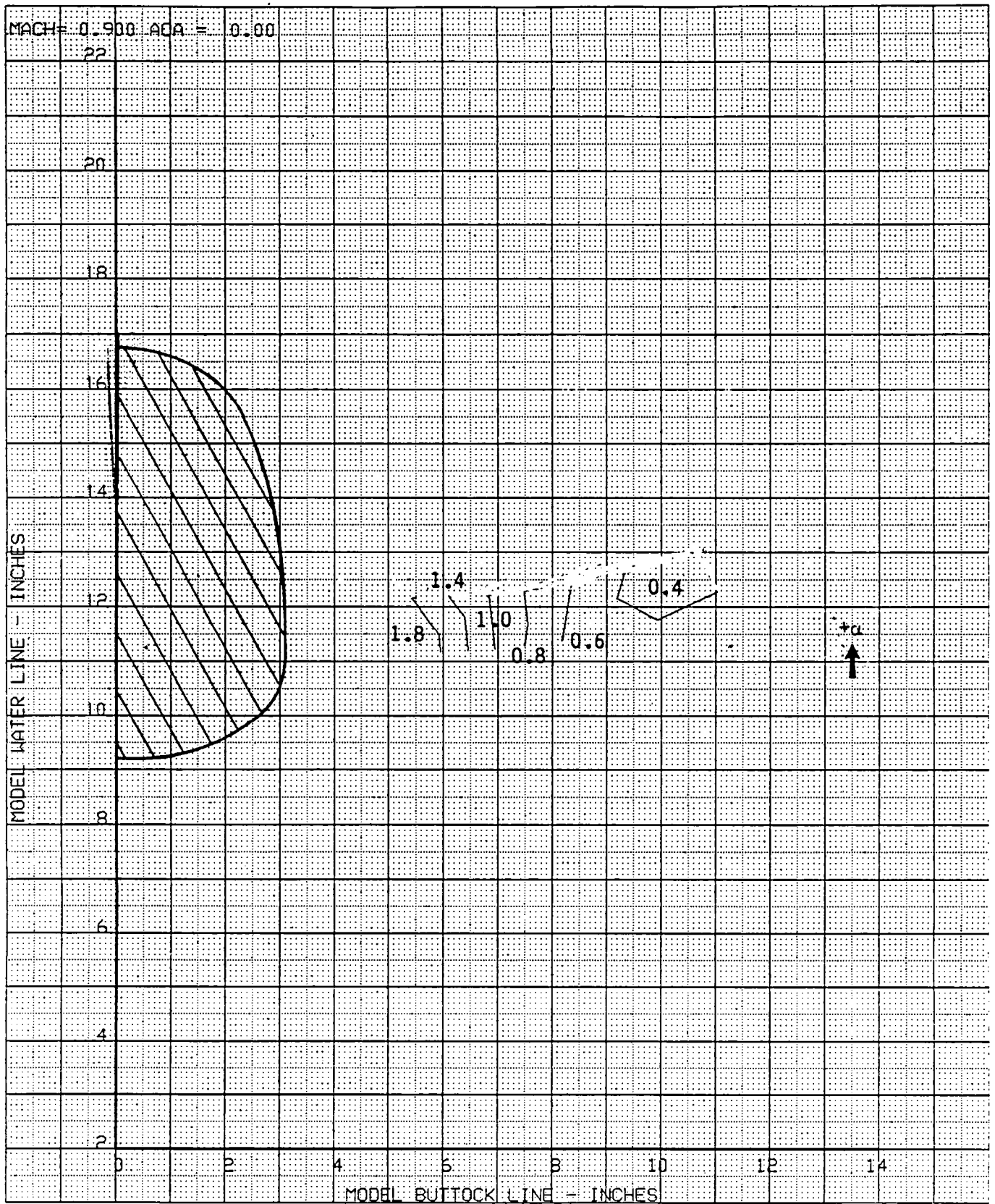*Figure 27a. Local Flowfield, MSTA = 50.50; Mach Number = 0.6; Angle of Attack = 10.0 deg*

90

MACH = 0.600 AOA = 10.00

MODEL WATER LINE - INCHES

MODEL BUTTOCK LINE - INCHES

Figure 27b. Local Angle of Attack, Mach Number = 0.6; Angle of Attack = 10.0 deg

91

Figure 27c. Local Sideflow Angle, Mach Number = 0.6; Angle of Attack = 10.0 deg

92

Figure 27d. Local Mach Number, Mach Number = 0.6; Angle of Attack = 10.0

93

Figure 28a. Local Flowfield, MSTA = 50.50; Mach Number = 0.9; Angle of Attack = 0.0 deg

94

Figure 28b. Local Angle of Attack, Mach Number = 0.9; Angle of Attack = 0.0 deg
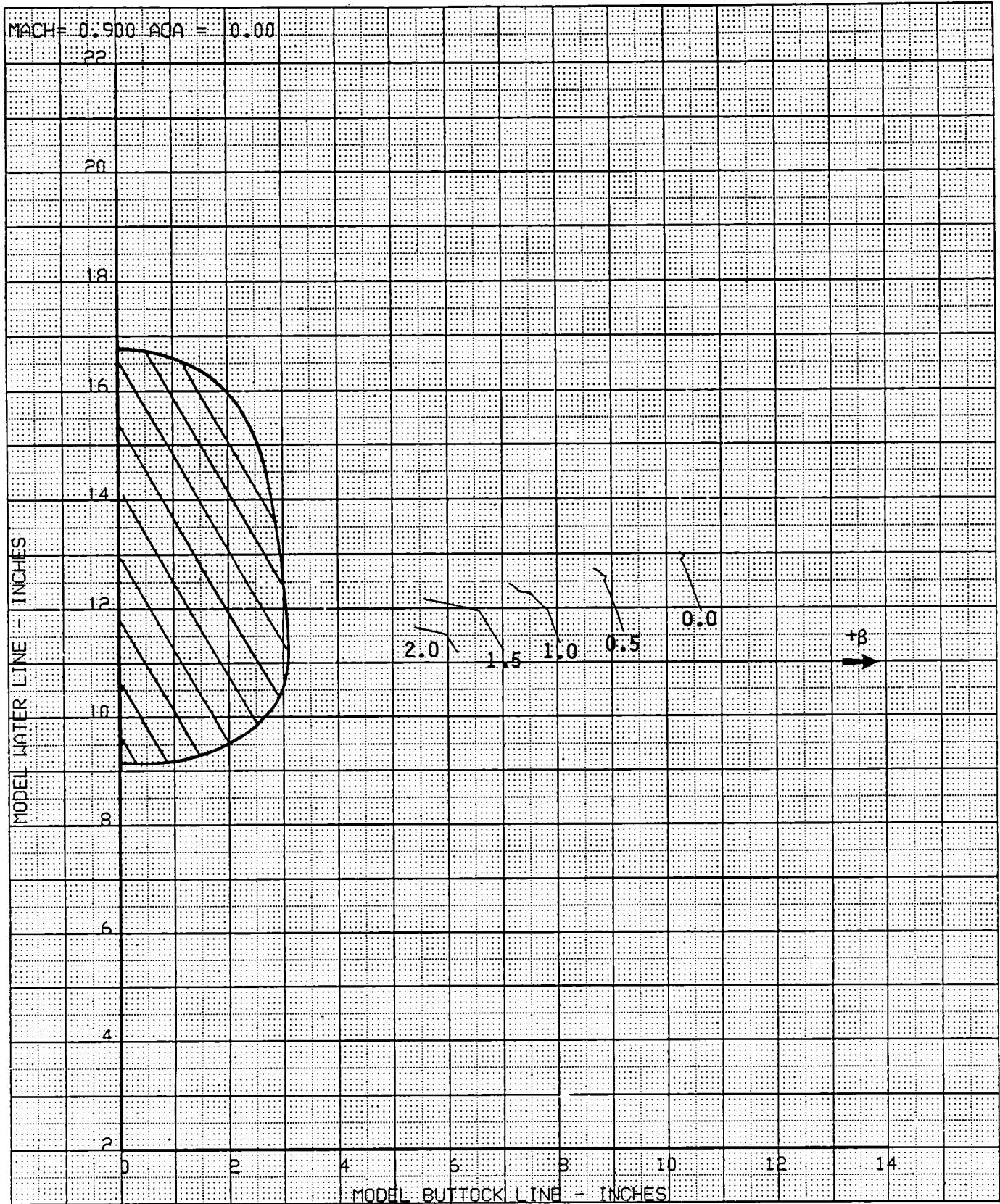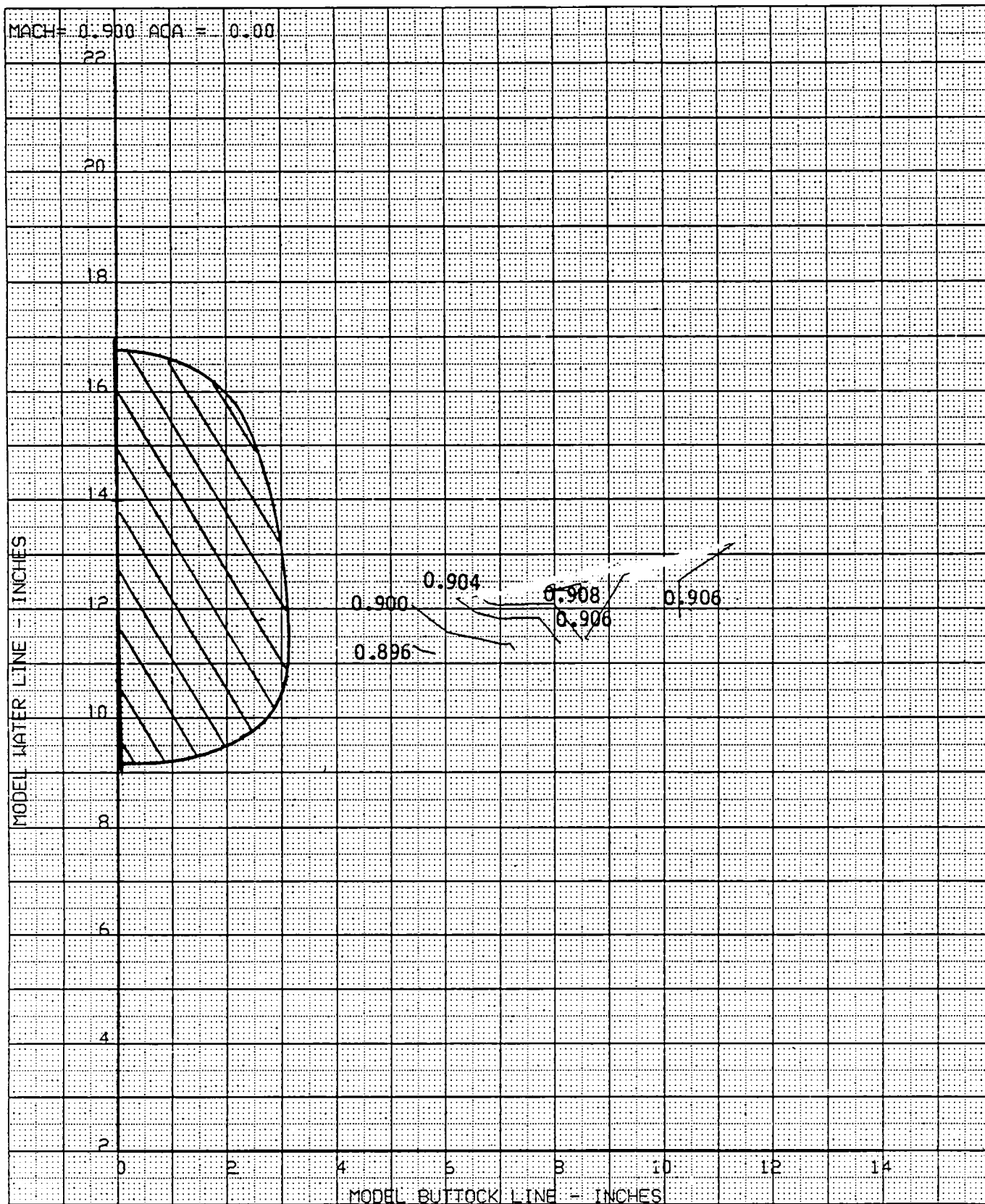
95

Figure 28c. Local Sideflow Angle, Mach Number = 0.9, Angle of Attack = 0.0 deg

96

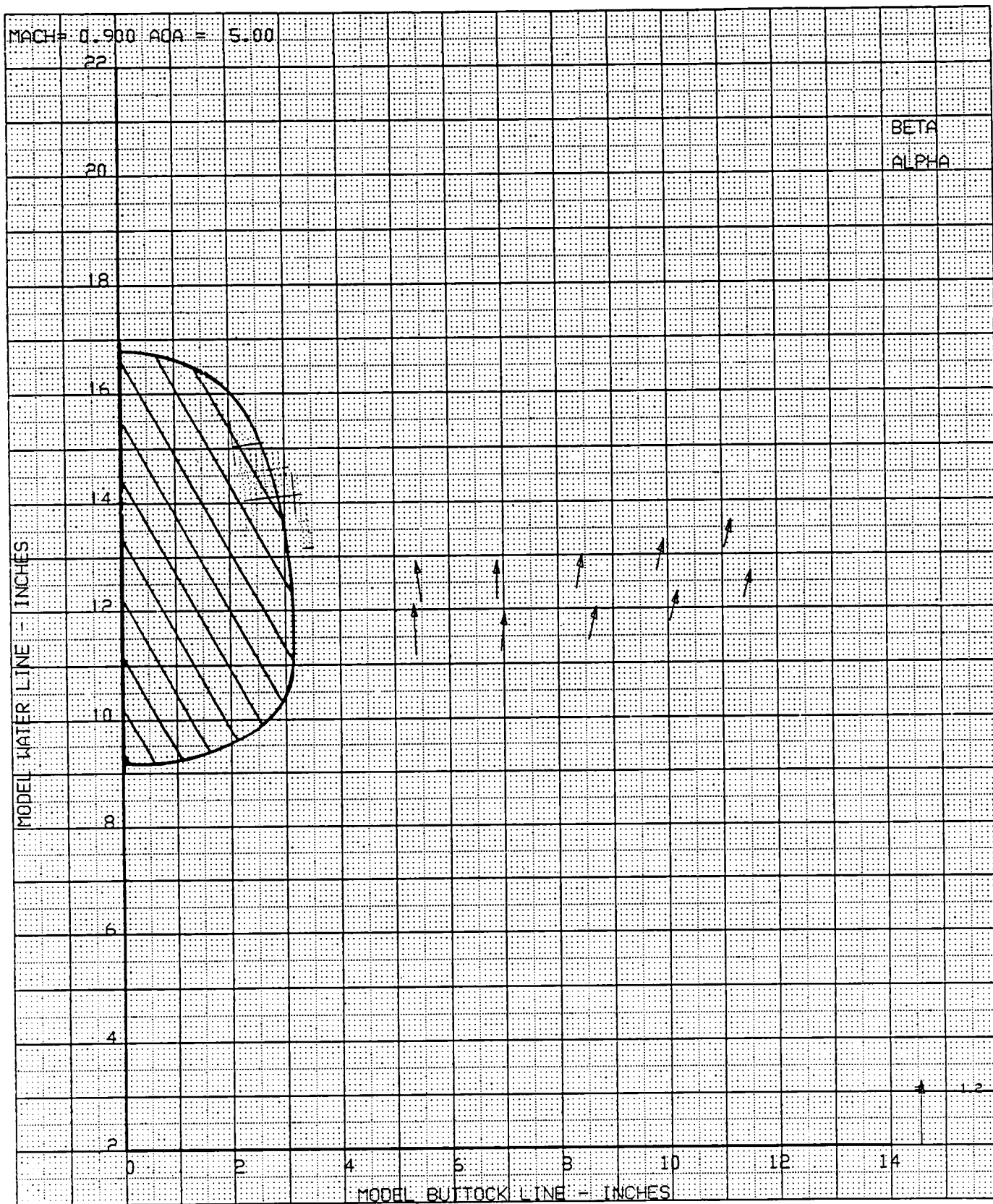*Figure 28d. Local Mach Number, Mach Number = 0.9; Angle of Attack = 0.0 deg*

97

Figure 29a. Local Flowfield, MSTA = 50.50; Mach Number = 0.9; Angle of Attack = 5.0 deg
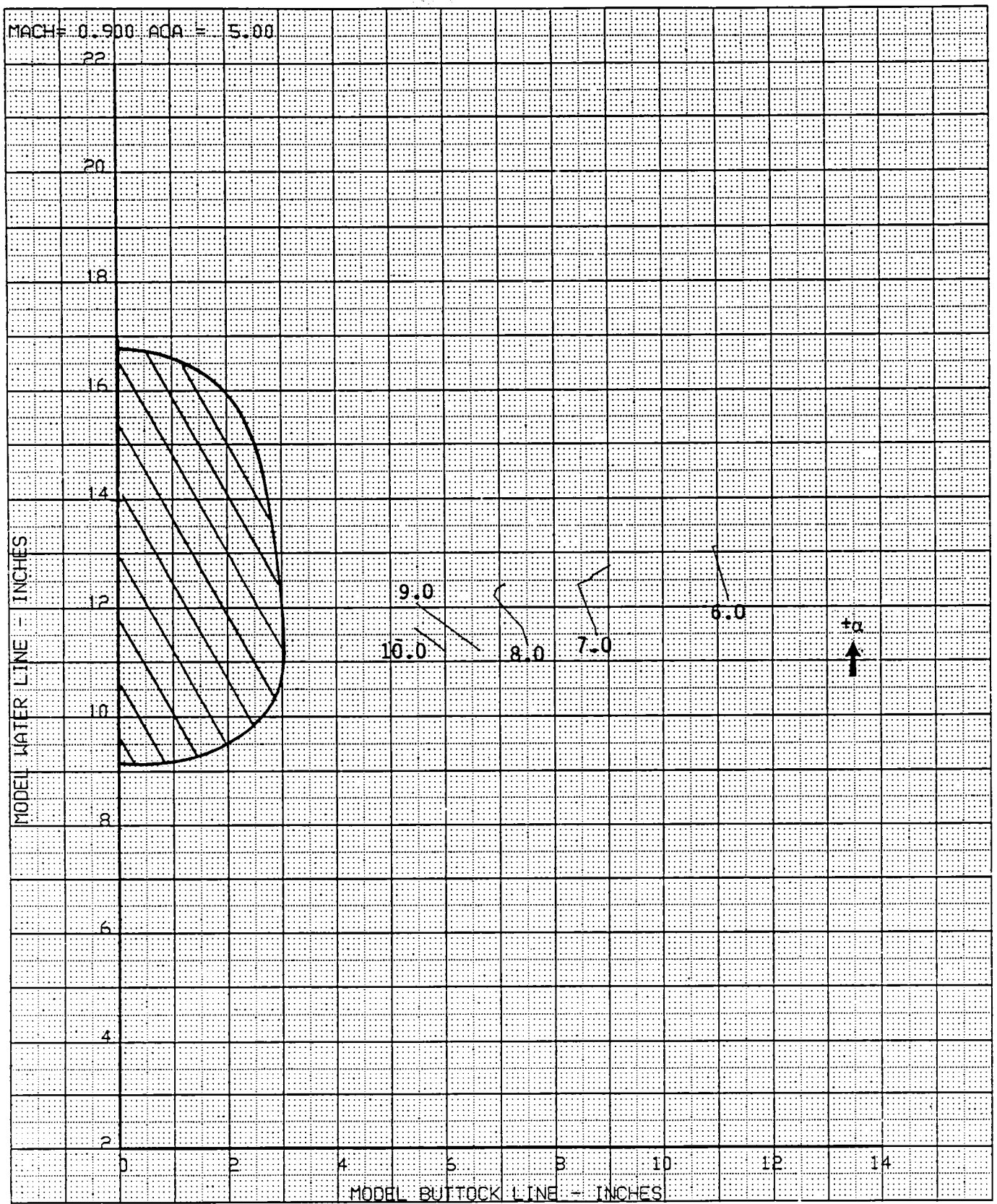
98

Figure 29b. Local Angle of Attack, Mach Number = 0.9; Angle of Attack = 5.0
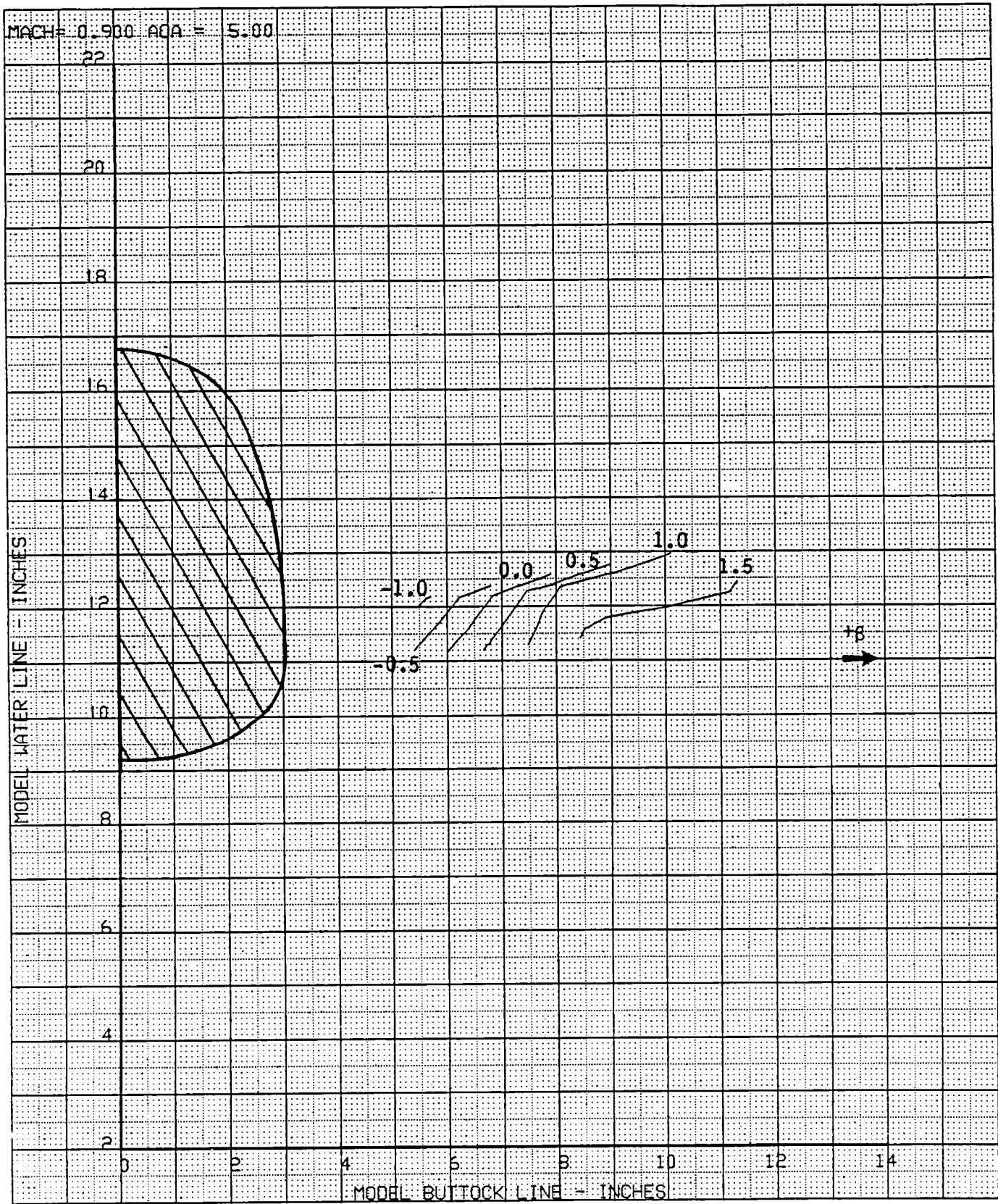
99

Figure 29c. Local Sideflow Angle, Mach Number = 0.9; Angle of Attack = 5.0 deg
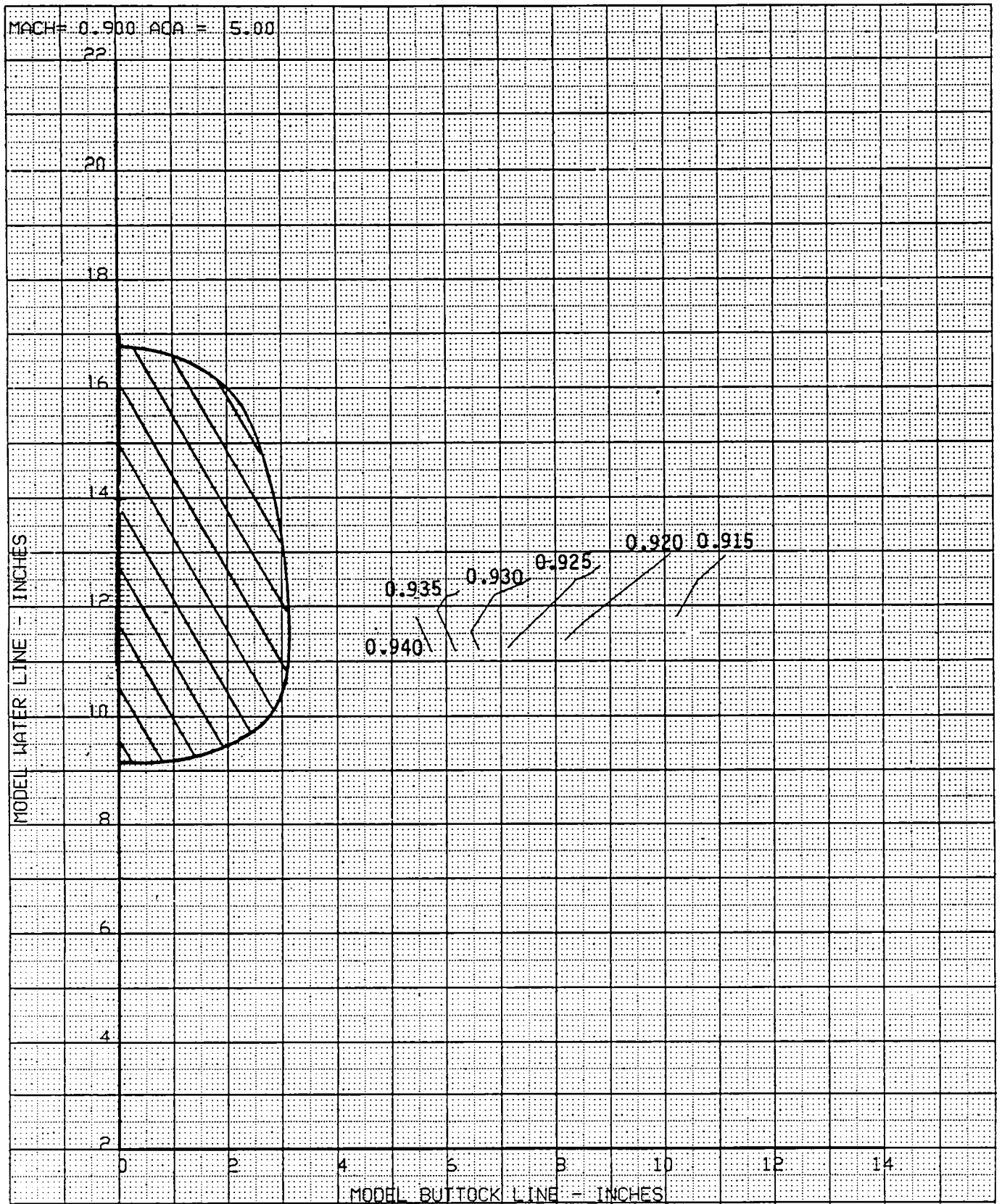
100

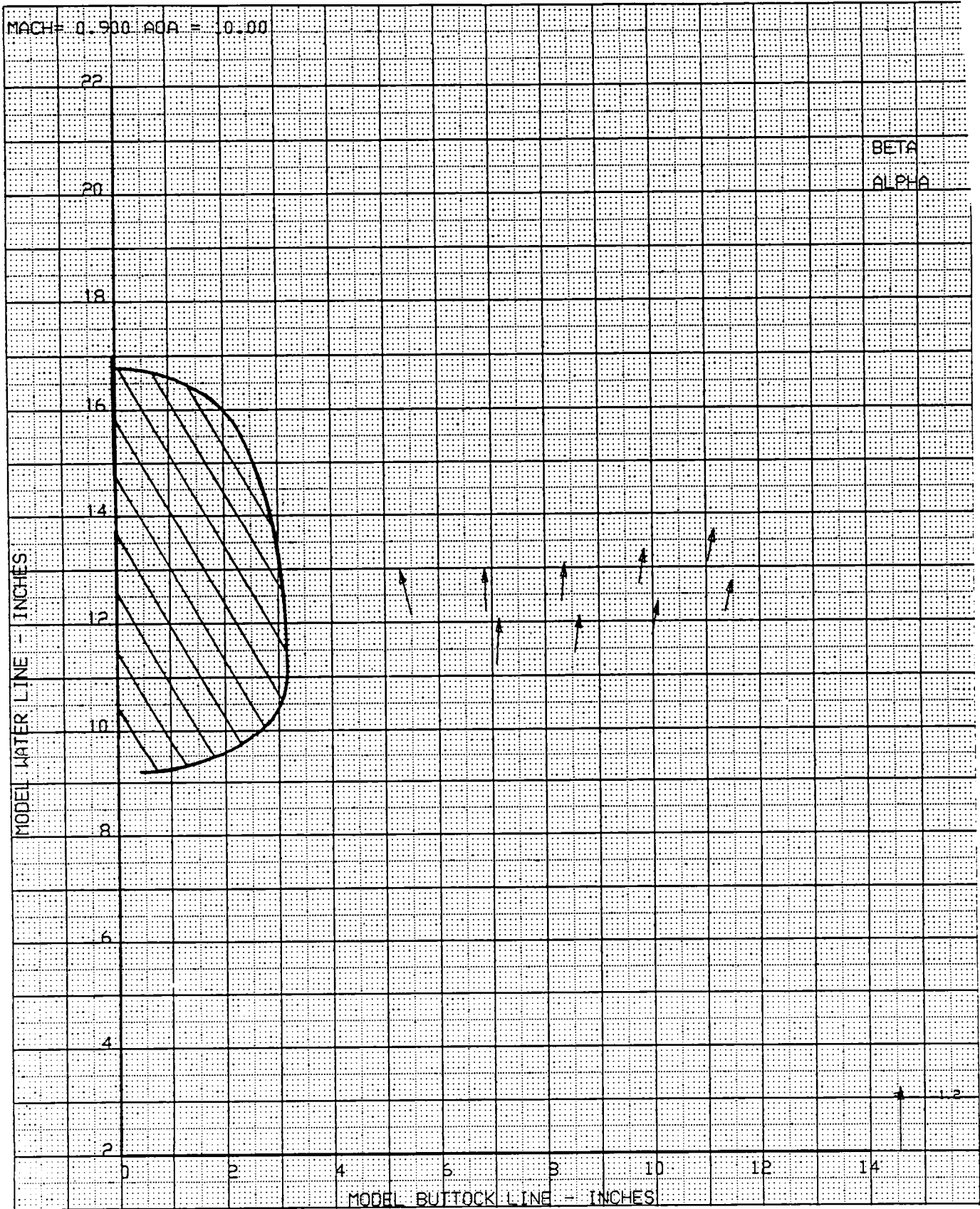*Figure 29d. Local Mach Number, Mach Number = 0.9; Angle of Attack = 5.0*

Figure 30a. Local Flowfield, MSTA = 50.50; Mach Number = 0.9; Angle of Attack = 10.0 deg
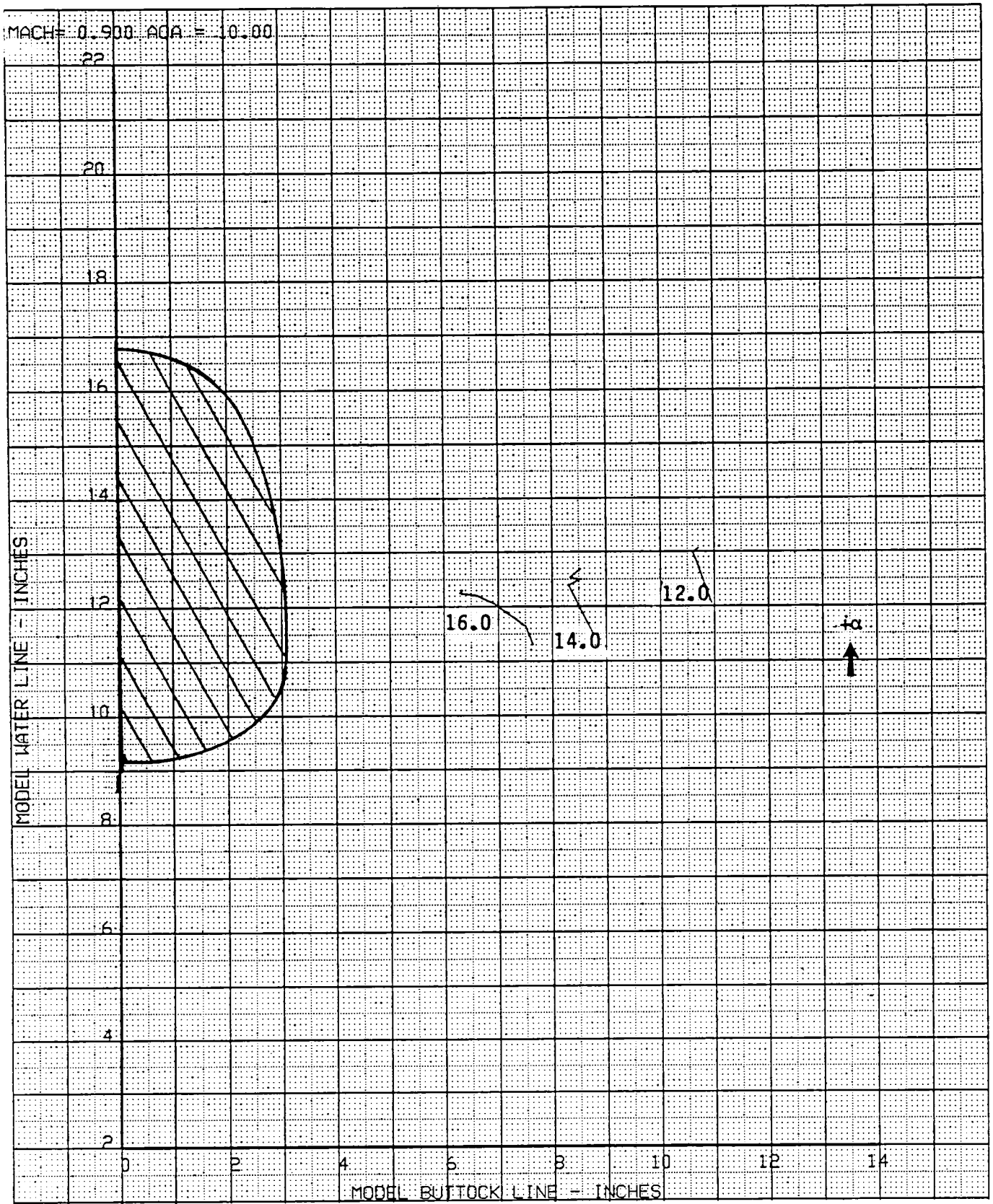
102

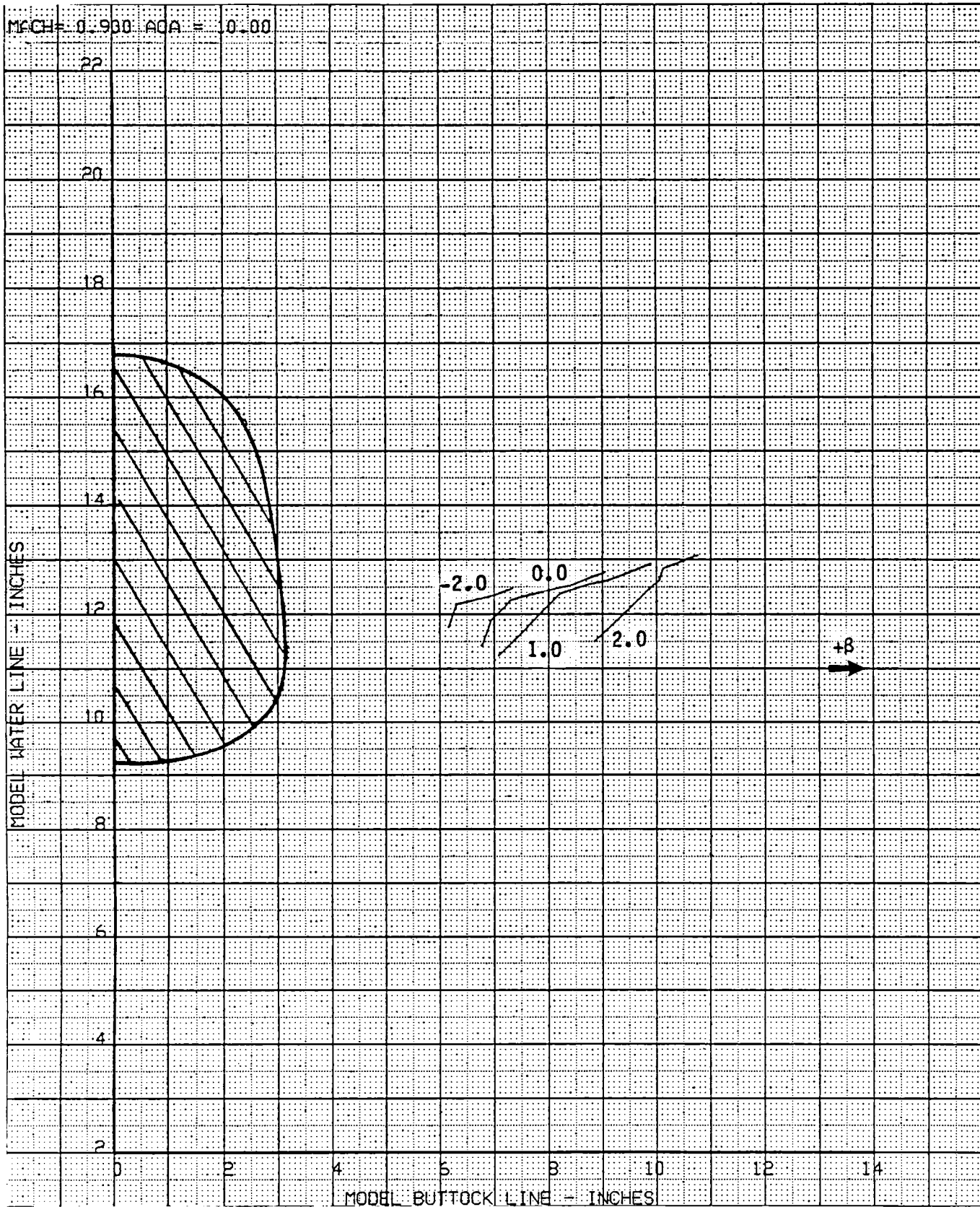*Figure 30b. Local Angle of Attack, Mach Number = 0.9; Angle of Attack = 10.0 deg*

Figure 30c. Local Sideflow Angle, Mach Number = 0.9; Angle of Attack = 10.0 deg
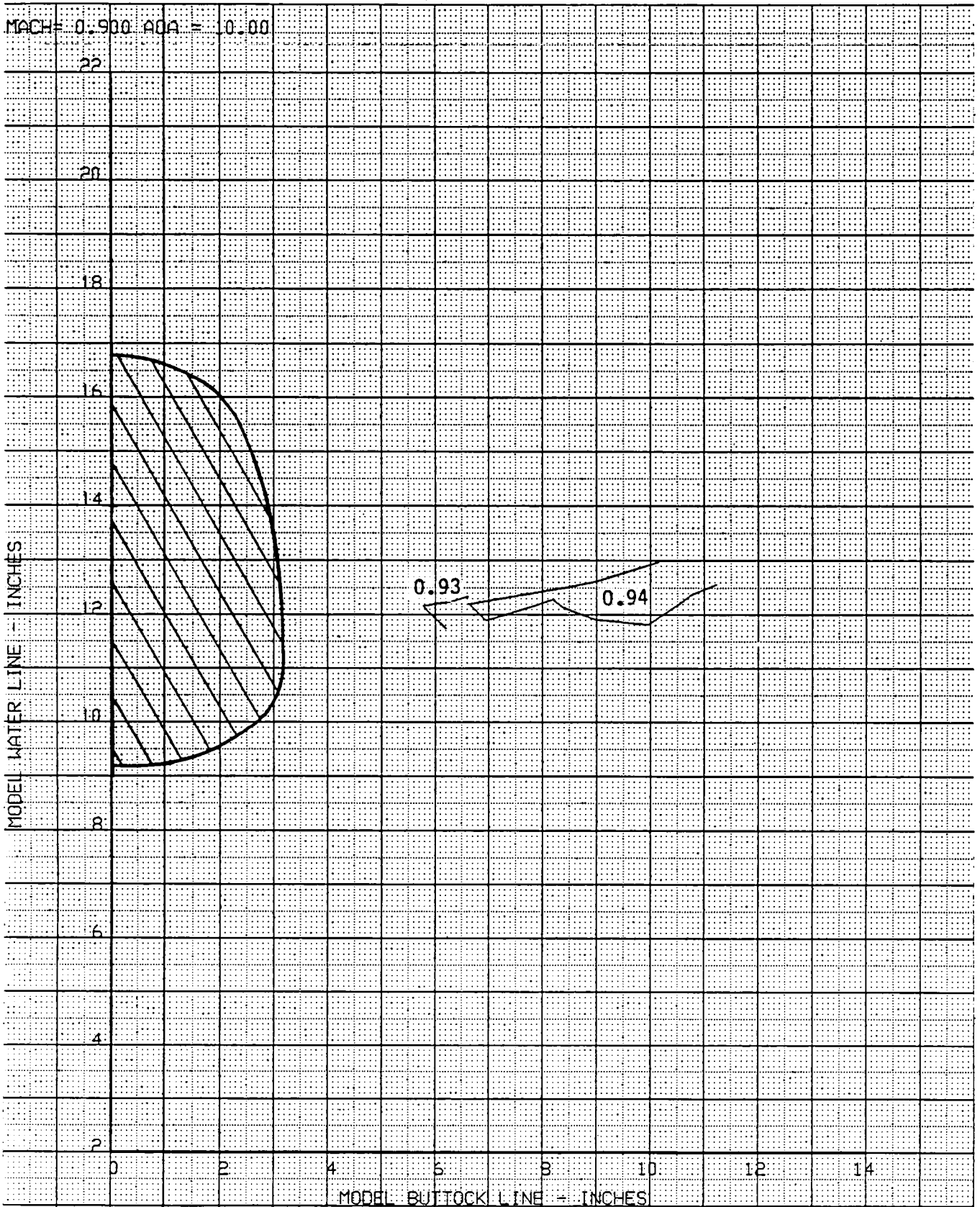
104

Figure 30d. Local Mach Number, Mach Number = 0.9; Angle of Attack = 10.0 deg

Figure 31a. Local Flowfield, MSTA = 50.50; Mach Number = 1.2; Angle of Attack = 0.0 deg

106

MACH= 1.200 AOA = 0.00

Figure 31b. Local Angle of Attack, Mach Number = 1.2; Angle of Attack = 0.0 deg

107

Figure 31c. Local Sideflow Angle, Mach Number = 1.2; Angle of Attack = 0.0 deg

Figure 31d. Local Mach Number, Mach Number = 1.2; Angle of Attack = 0.0 deg
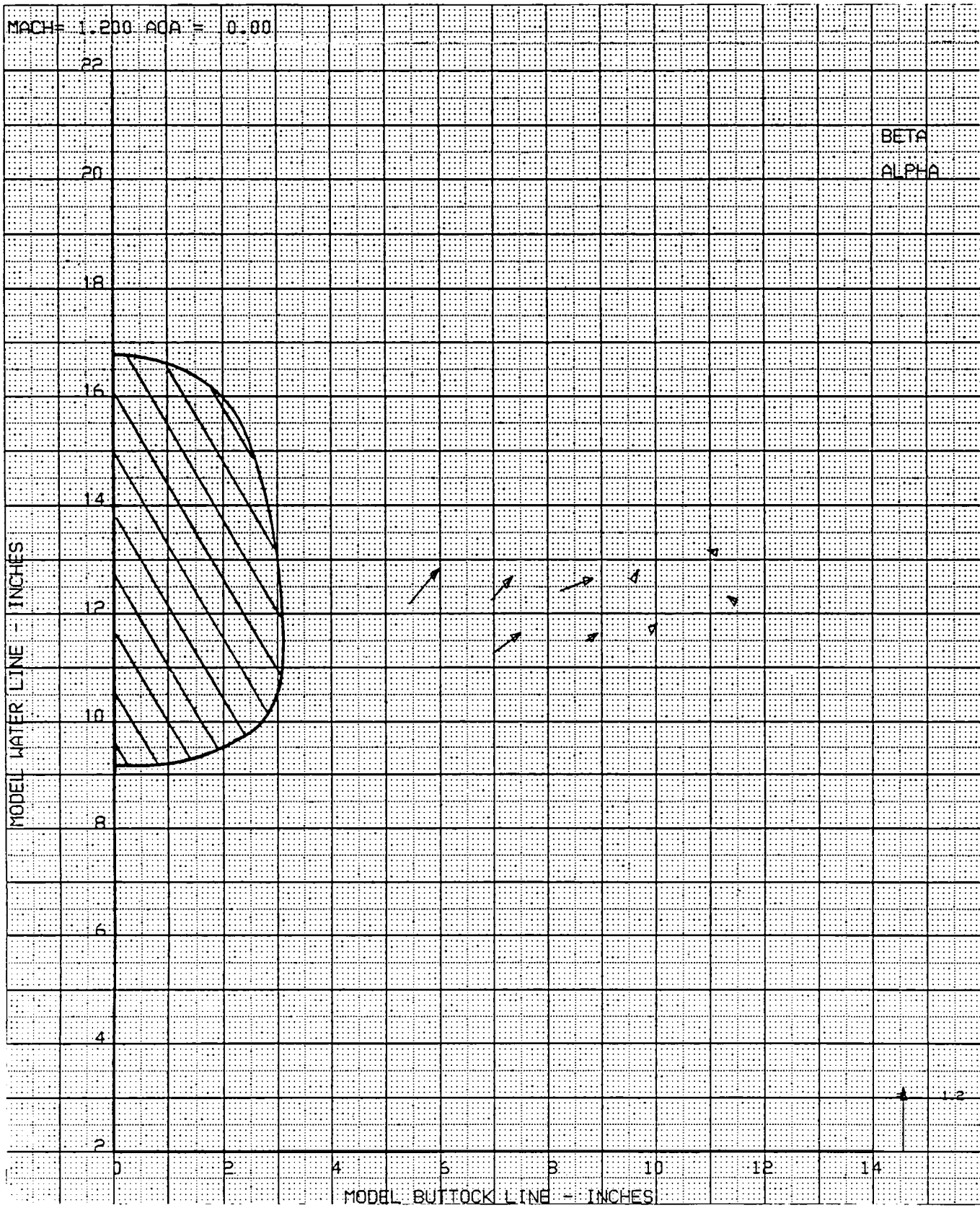
109

Figure 32a. Local Flowfield, MSTA = 50.50; Mach Number = 1.2; Angle of Attack = 5.0 deg
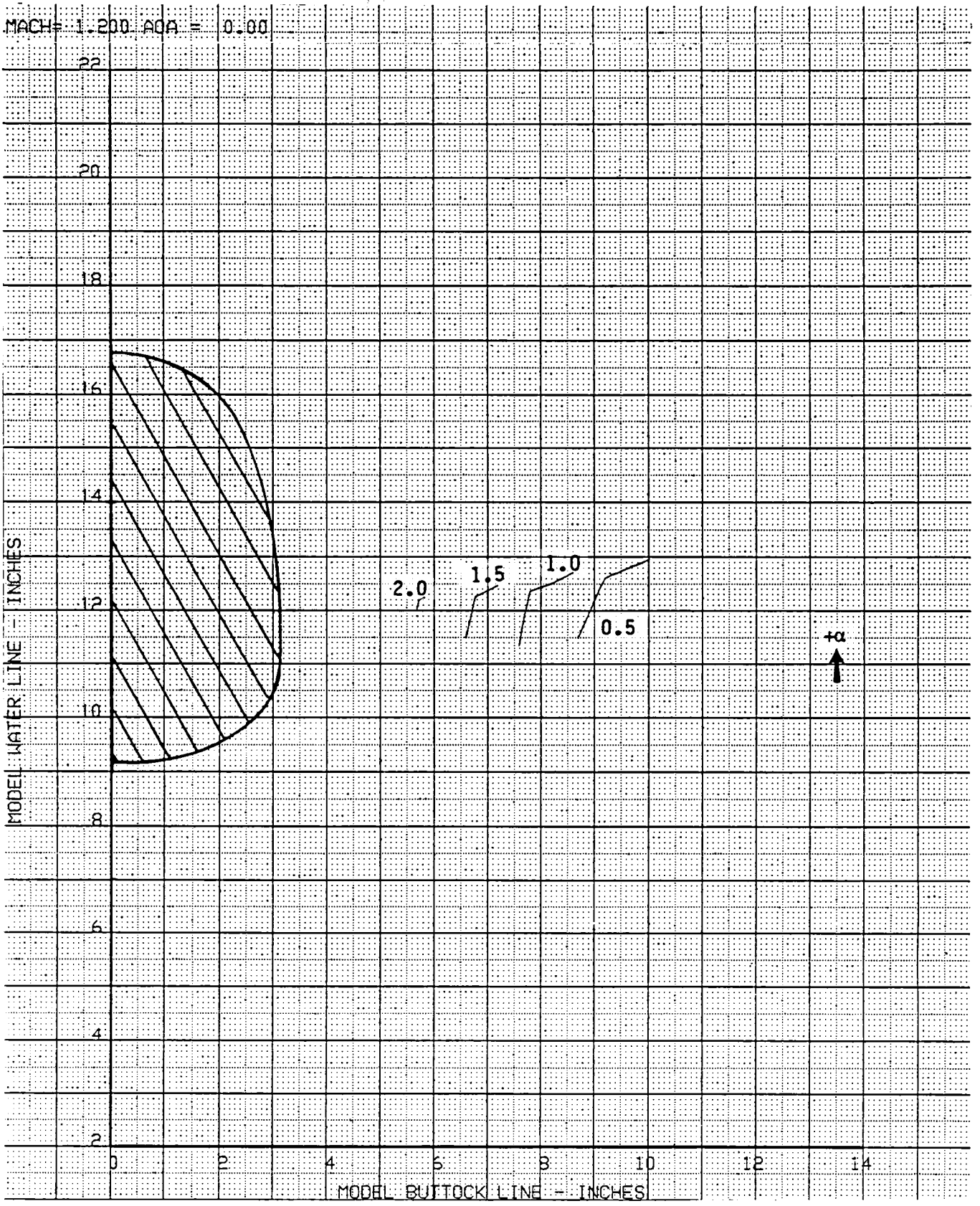
110
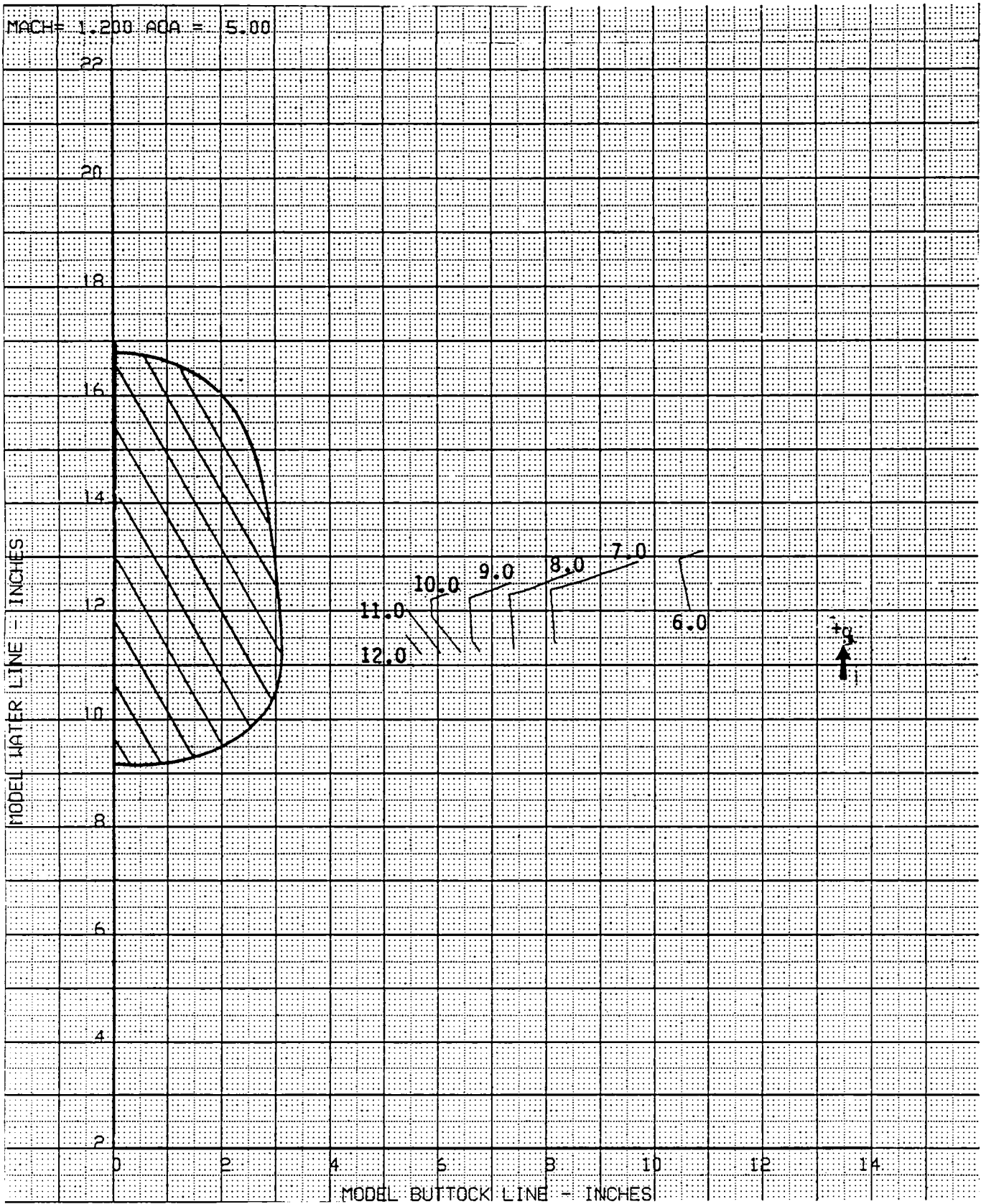
Figure 32b. Local Angle of Attack, Mach Number = 1.2; Angle of Attack = 5.0 deg
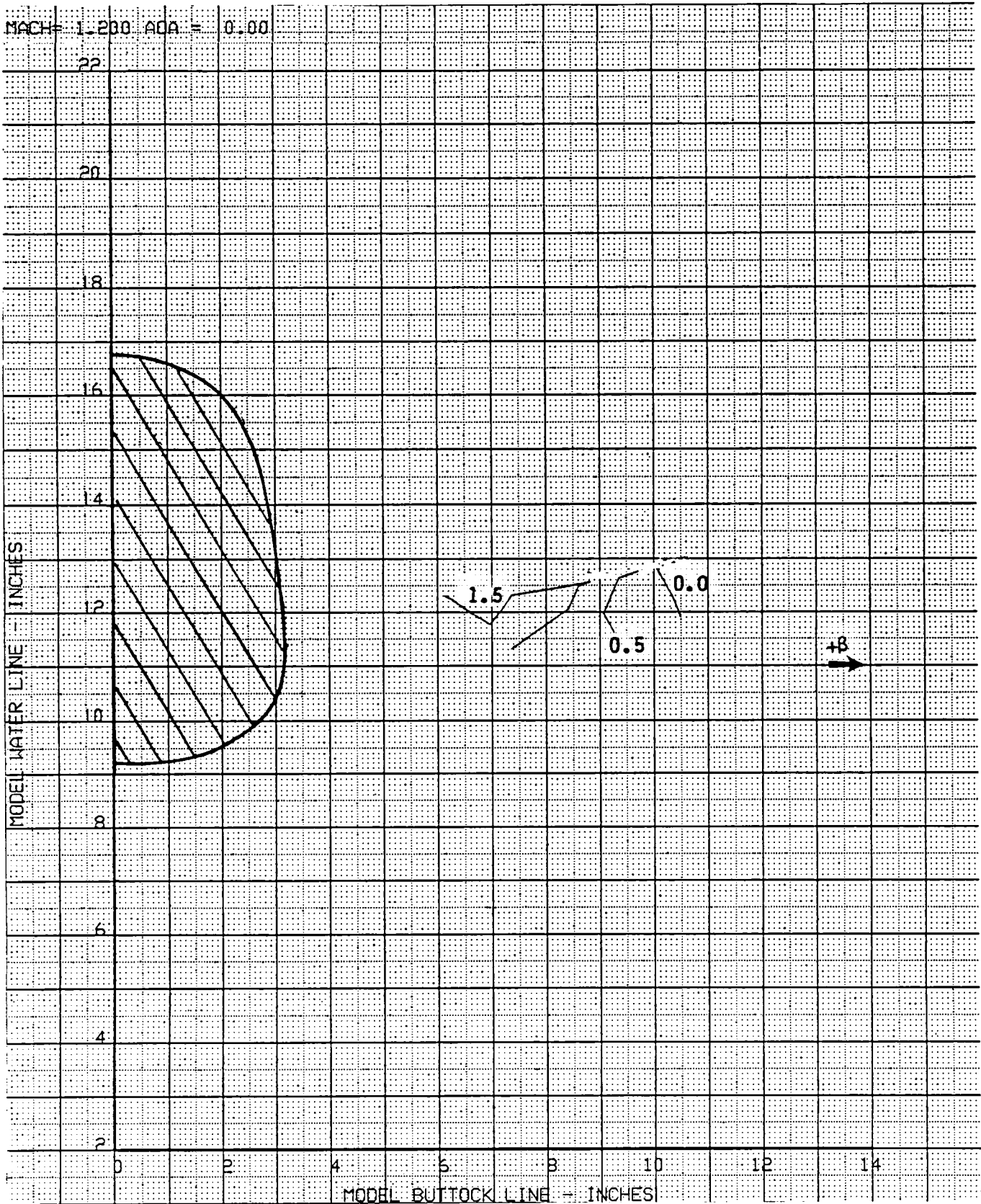
111

Figure 32c. Local Sideflow Angle, Mach Number = 1.2; Angle of Attack = 5.0 deg
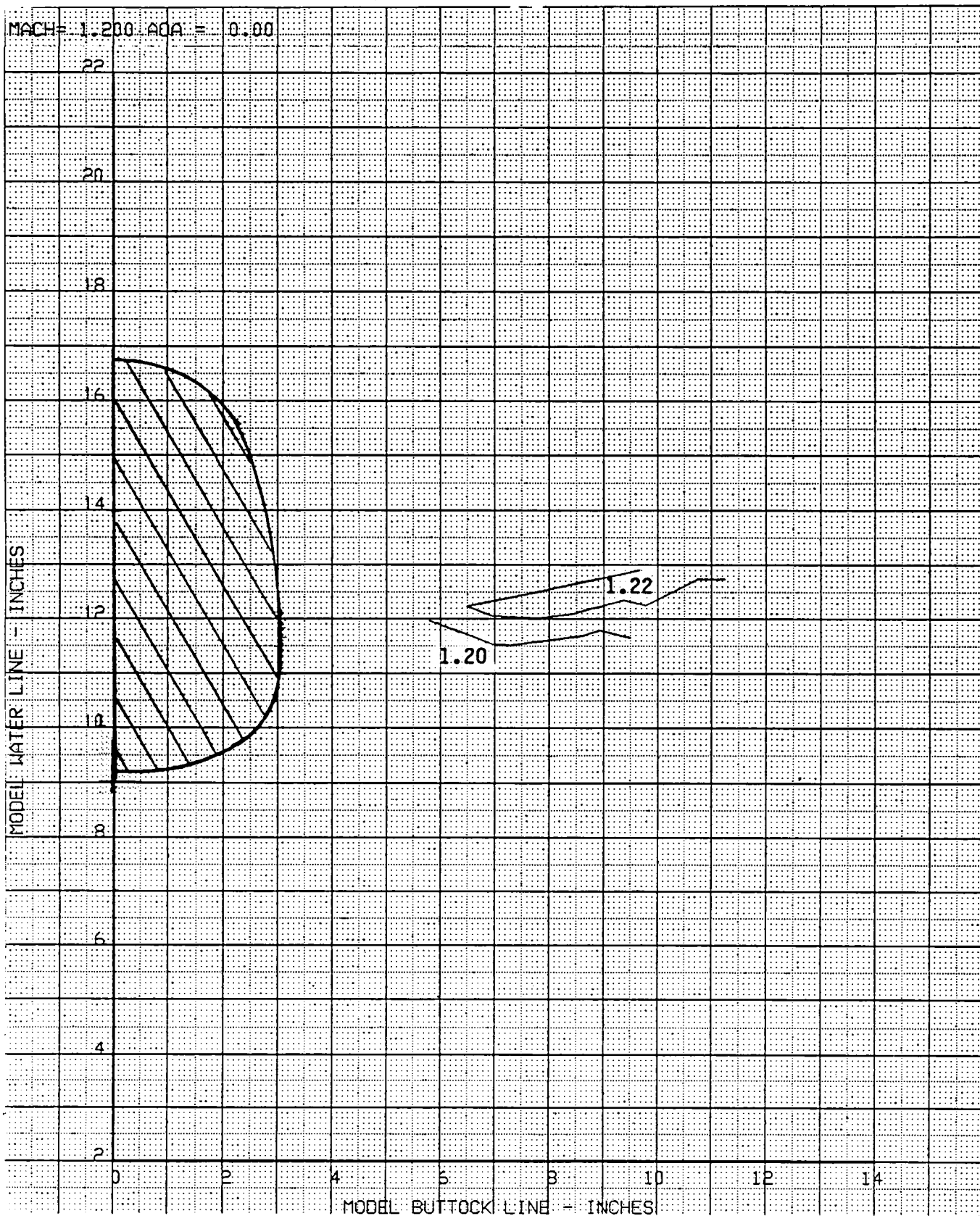
112
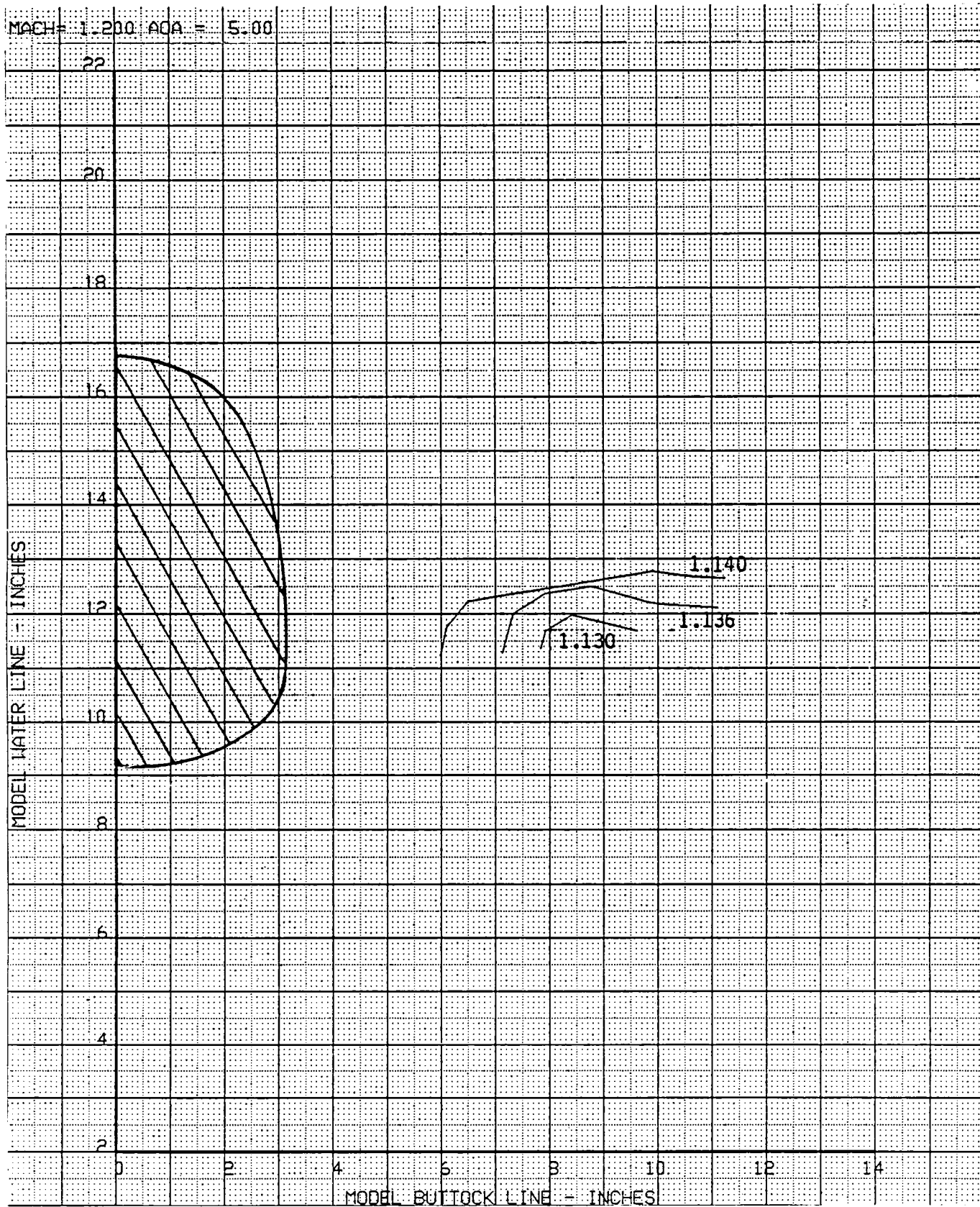
Figure 32d. Local Mach Number, Mach Number = 1.2; Angle of Attack = 5.0 deg

113

Figure 33a. Local Flowfield, MSTA = 50.50; Mach Number = 1.2; Angle of Attack = 7.5 deg

MACH= 1.200 AOA = 7.50

MODEL WATER LINE - INCHES

MODEL BUTTOCK LINE - INCHES

Figure 33b. Local Angle of Attack, Mach Number = 1.2; Angle of Attack = 7.5 deg

115

MACH = 1.200 AOA = 7.50

Figure 33c. Local Sideflow Angle, Mach Number = 1.2; Angle of Attack = 7.5 deg

116

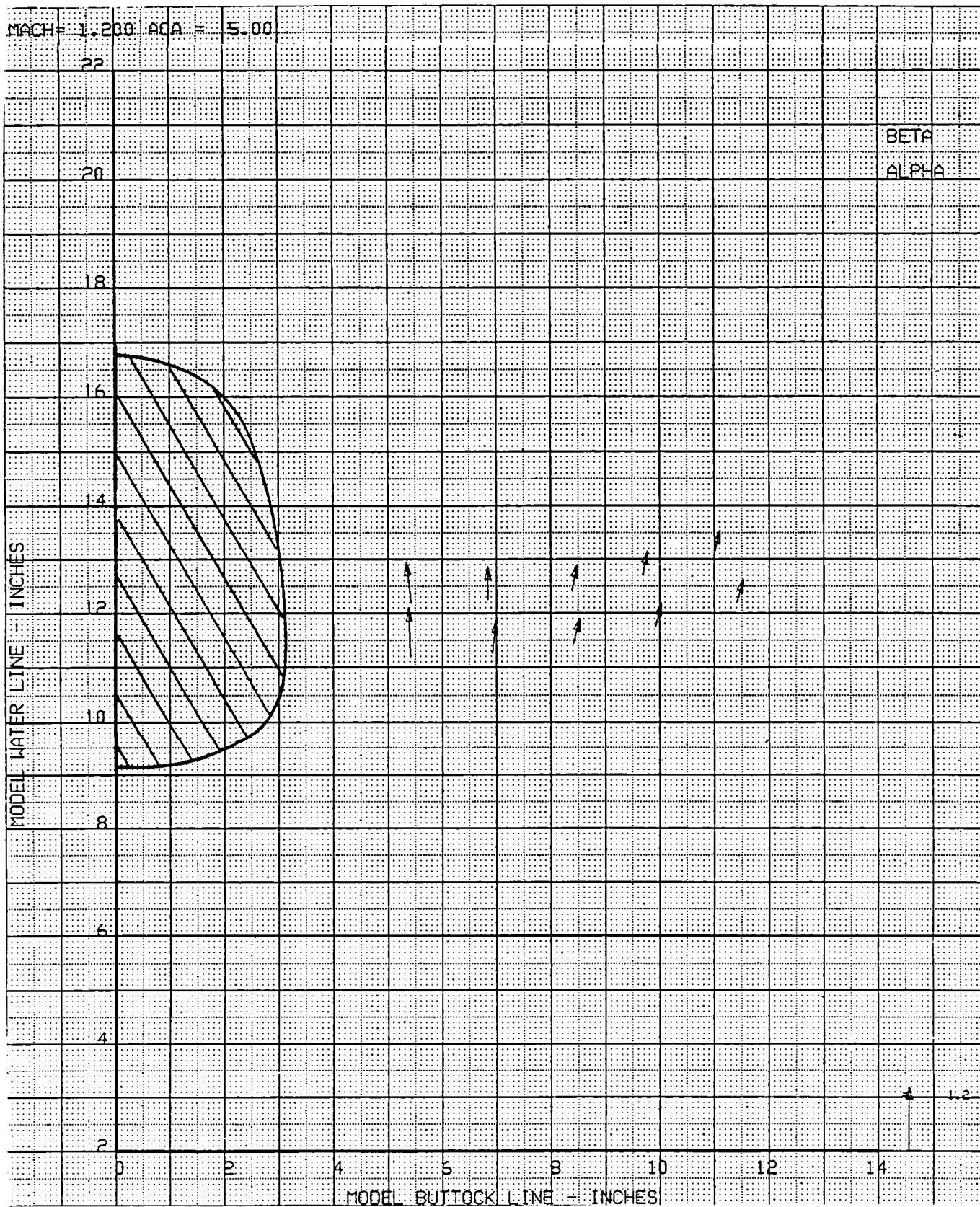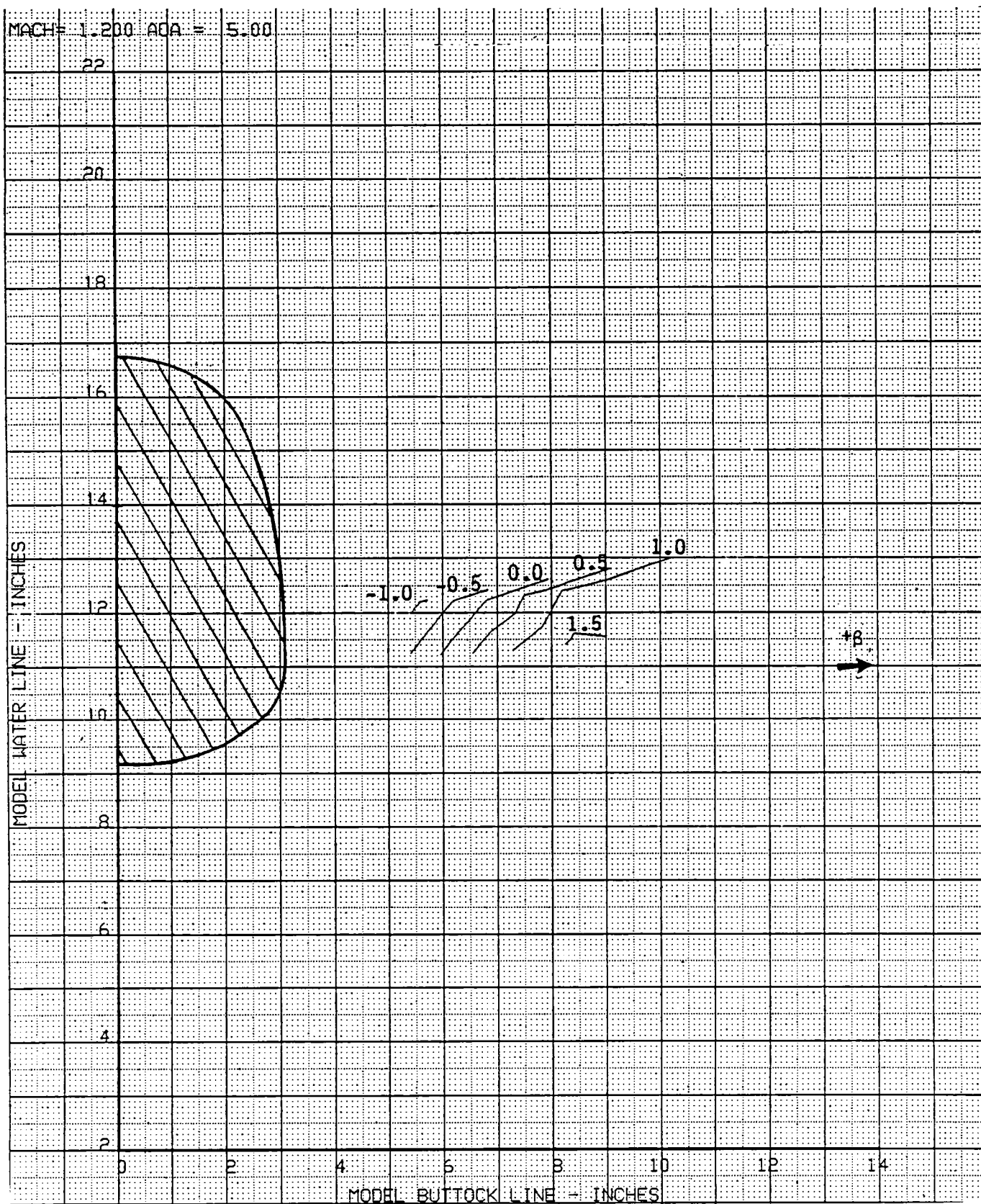*Figure 33d. Local Mach Number, Mach Number = 1.2; Angle of Attack = 7.5 deg*

117

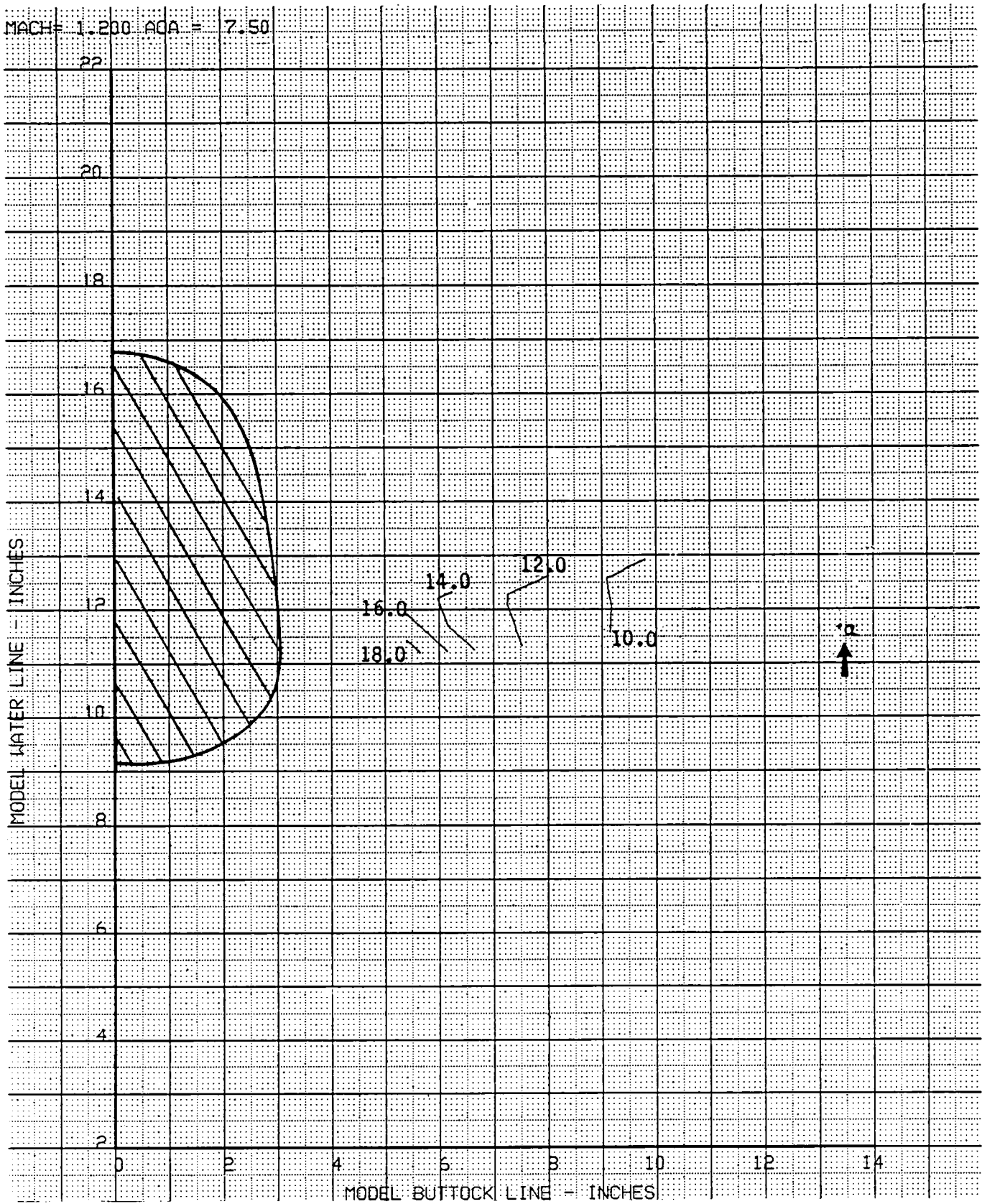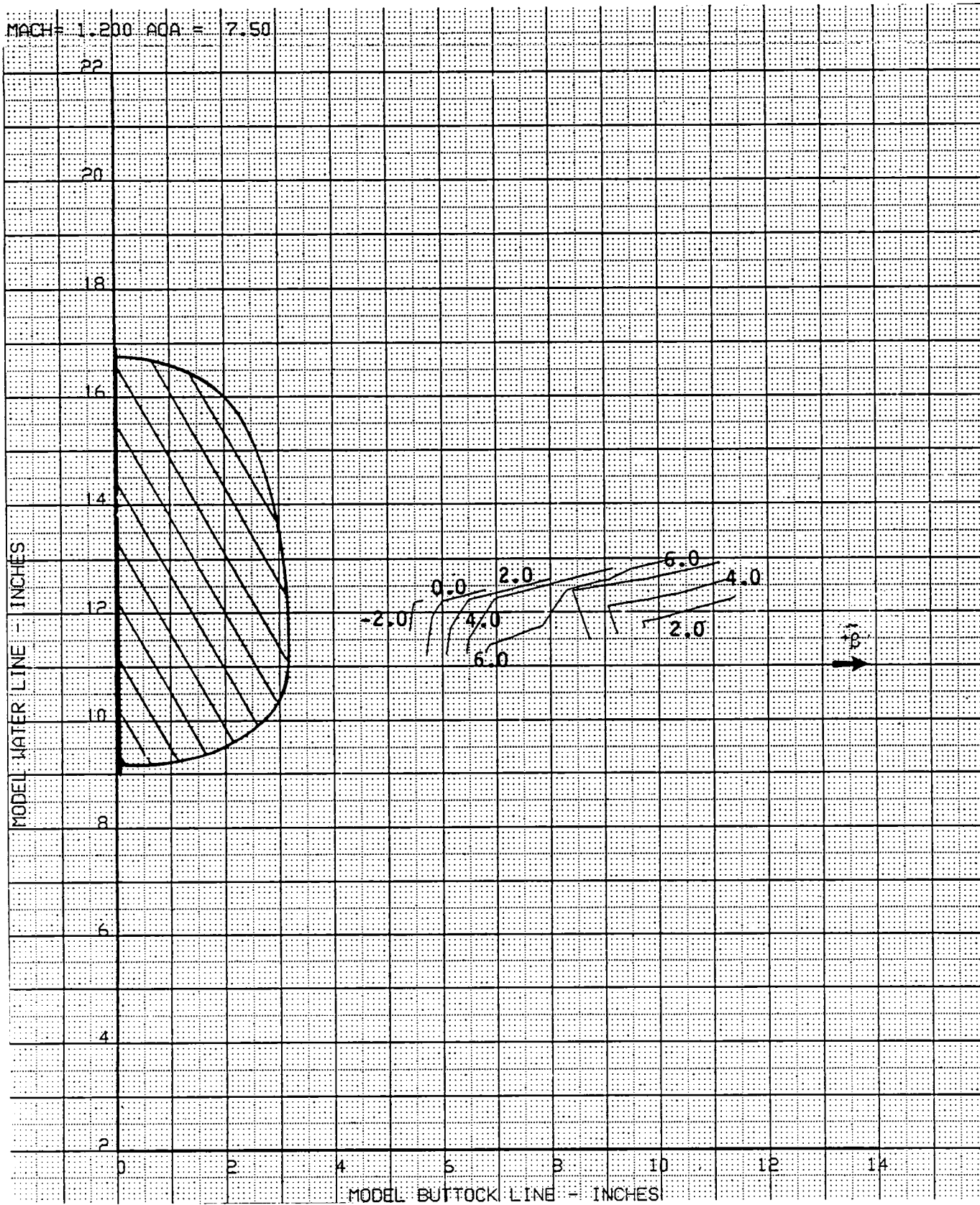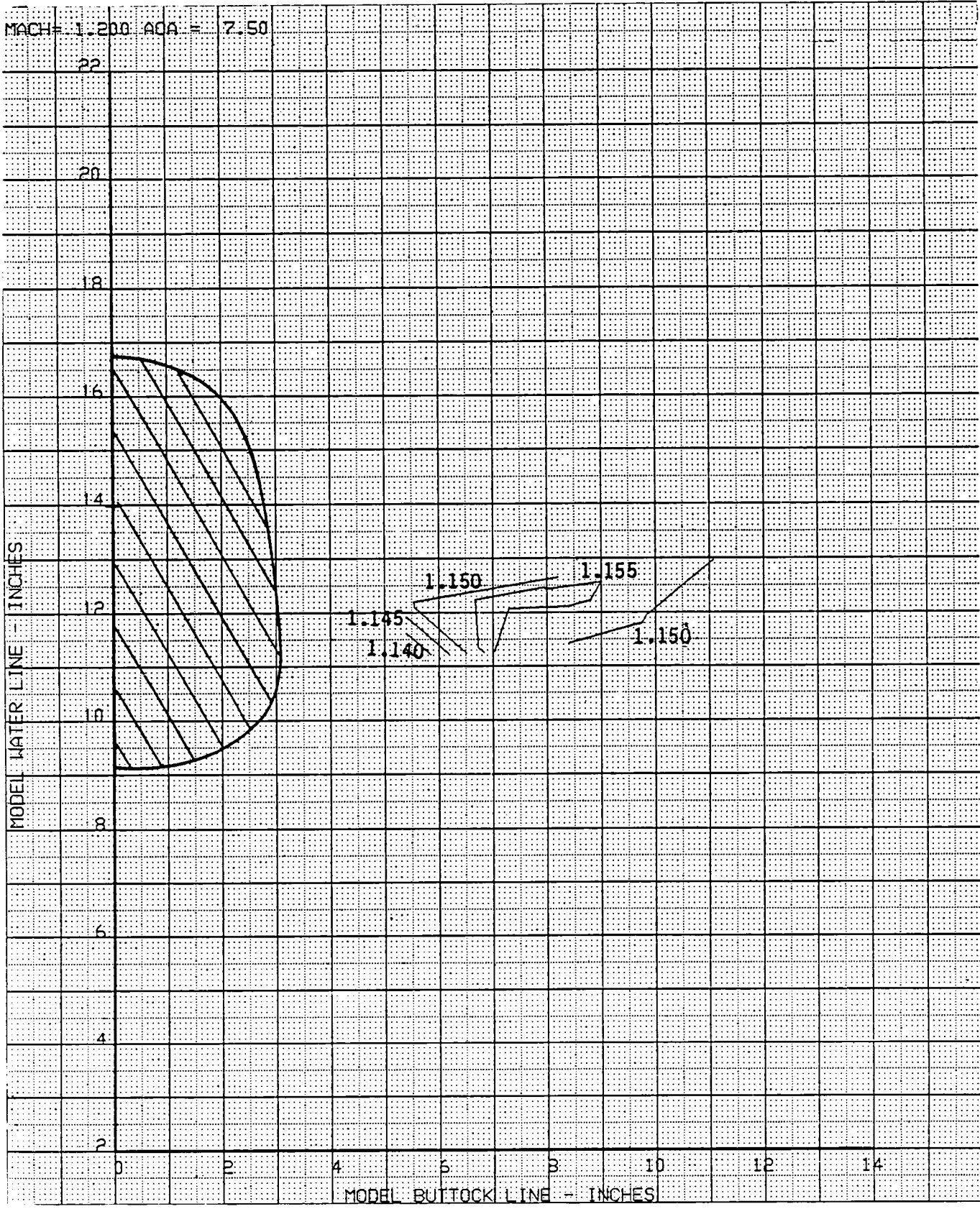| 1. Report No. NASA CR 172239	2. Government Accession No.	3. Recipient's Catalog No.
4. Title and Subtitle INLET FLOW FIELD INVESTIGATION, PART I - TRANSONIC FLOW FIELD SURVEY		5. Report Date January 1984
		6. Performing Organization Code L-7150
7. Author(s) J. A. Yetter, V. Salemann, M. B. Sussman		8. Performing Organization Report No. D180-27738-1
9. Performing Organization Name and Address		10. Work Unit No.
		11. Contract or Grant No. NAS1-16612
12. Sponsoring Agency Name and Address NATIONAL AERONAUTICS AND SPACE ADMINISTRATION WASHINGTON, D.C. 20546		13. Type of Report and Period Covered Contract Report
		14. Sponsoring Agency Code

15. Supplementary Notes

LANGLEY TECHNICAL MONITOR: S. F. Yaros
Final Report - Part I

16. Abstract

A wind tunnel investigation has been conducted to determine the local inlet flow field characteristics of an advanced tactical supersonic cruise airplane. The study was undertaken to establish a data base for the development and validation of analytical codes directed at the analysis of inlet flow fields for advanced supersonic airplanes. Testing was conducted at the NASA-Langley 16-foot Transonic Tunnel at freestream Mach numbers of 0.6 to 1.20 and angles of attack from 0.0 to 10.0 degrees. Inlet flow field surveys were made at locations representative of wing (upper and lower surface) and forebody mounted inlet concepts. Results are presented in the form of local inlet flow field angle of attack, sideflow anlge, and Mach number contours. Wing surface pressure distributions supplement the flow field data.

17. Key Words (Suggested by Author(s)) Inlet flow field Forebody flow field Flow field survey Transonic flow		18. Distribution Statement Unclassified - Unlimited Subject Category 02
19. Security Classif. (of this report) Unclassified	20. Security Classif. (of this page) Unclassified	21. No. of Pages 127	22. Price*

NASA-C-168 (Rev. 10-75)

NASA Contractor Report 172239
Distribution List
NAS1-16612

	No. Copies
NASA Langley Research Center Hampton, VA 23665 Attn: Research Information Office, Mail Stop 151A Dr. Steven F. Yaros, Mail Stop 280	2 64
NASA Ames Research Center Moffett Field, CA 94035 Attn: Library, Mail Stop 202-3	1
Dryden Flight Research Facility P. O. Box 273 Edwards, CA 93523 Attn: Library	1
NASA Goddard Space Flight Center Greenbelt, MD 20771 Attn: Library	1
NASA Lyndon B. Johnson Space Center 2101 Webster Seabrook Road Houston, TX 77058 Attn: JM6/Library	1
NASA Marshall Space Flight Center Marshall Space Flight Center, AL 35812 Attn: Library, Mail Stop AS24L	1
Jet Propulsion Laboratory 4800 Oak Grove Drive Pasadena, CA 91103 Attn: 111-113/Library	1
NASA Lewis Research Center 21000 Brookpark Road Cleveland, OH 44135 Attn: Library, Mail Stop 60-3	1
NASA John F. Kennedy Space Center Kennedy Space Center, FL 32899 Attn: Library, NWSI-D	1
National Aeronautics and Space Administration Washington, DC 20546 Attn: RJH-2	1
NASA Scientific and Technical Information Facility 6571 Elkridge Landing Road Linthicum Heights, MD 21090	25 plus original